

PERFORMANCE ASSESSMENT OF CEMENT-BASED MATERIALS BLENDED WITH MICRONIZED SAND: MICROSTRUCTURE, DURABILITY AND SUSTAINABILITY

Proefschrift

ter verkrijging van de graad van doctor
aan de Technische Universiteit Delft,
op gezag van de Rector Magnificus prof. ir. K.C.A.M. Luyben,
voorzitter van het College voor Promoties,
in het openbaar te verdedigen op donderdag 20 juni 2013 om 10.00 uur
door

Ying WANG

Master of Engineering aan de Beijing Jiaotong University, P.R. China.
geboren te Tianjin, P.R. China.

Dit proefschrift is goedgekeurd door de promotoren:

Prof. dr. ir. K. van Breugel

Prof. dr. ir. E. M. Haas

Copromotor Dr. G. Ye

Samenstelling promotiecommissie:

Rector Magnificus,	voorzitter
Prof. dr. ir. K. van Breugel,	Technische Universiteit Delft, promotor
Prof. dr. ir. E. M. Haas,	Technische Universiteit Delft, promotor
Dr. G. Ye,	Technische Universiteit Delft, copromotor
Prof. dr. J-E. Jonassen,	Luleå Tekniska Universitet, Sweden
Prof. dr. G. de Schutter,	Universiteit Gent, België
Prof. R. Gao,	Beijing Jiaotong University, P. R. China
Prof. dr. ir. R.B. Polder,	TNO
Prof. dr. ir. H.E.J.G. Schlangen,	Technische Universiteit Delft, reservelid

ISBN . 97890-6562-322-5

Keywords: cement-based material, micronized sand, microstructure, transport properties, service life, sustainability, CO₂ footprint.

Printed by VSSD, the Netherlands

Cover design: Ying Wang and VSSD

Copyright © 2013 by Ying Wang

All right reserved. No part of the material protected by this copyright notice may be reproduced or utilized in any form or by any means, electronic or mechanical, including photocopying, recording or by any information storage and retrieval system, without written permission from the author.

Table of Contents

List of Symbols	v
List of Abbreviations	ix
Chapter 1	1
1.1 General	1
1.2 Objective and Limitation of the Thesis	2
1.3 Outline of the Research	2
Chapter 2	5
2.1 Introduction	5
2.2 Different Types of Fillers	5
2.3 Quartz Sand	6
2.4 Micronized Sand	7
2.5 Effects of Micronized Sand on Cement Paste	8
2.5.1 Dilution effect	9
2.5.2 Filler effect	10
2.5.3 Nucleation effect	10
2.6 Pore Structure	11
2.7 Transport Properties	12
2.7.1 Permeability	13
2.7.2 Diffusivity	14
2.8 Sustainability	15
2.8.1 Global warming potential - CO ₂ emission	16
2.8.2 Durability and sustainability	17
2.9 Summary	17
Chapter 3	19
3.1 Introduction	19
3.1.1 Pores in cement paste	19
3.1.2 Definition of pore structure parameters	19
3.1.3 Microstructure of cement paste blended with micronized sand	21
3.2 Materials and Methods	22
3.2.1 Materials	22
3.2.2 Methodology for characterizing the microstructure	24
3.2.3 Sample preparation	27
3.3 Results and Discussions	29
3.3.1 Effect of micronized sand on the hydration process	29
3.3.2 Effects of micronized sand on the pore structure of cement paste	30
3.3.3 Observation of microstructure	34
3.3.4 The thickness of the interfacial zone between micronized sand and hydration products	35
3.4 Summary	39
Chapter 4	41

4.1	Introduction	41
4.2	Water Permeability	41
4.2.1	Darcy's law	41
4.2.2	Material and method used to determine k_w	42
4.2.3	Results and discussions	45
4.3	Diffusivity	51
4.3.1	Mechanism	51
4.3.2	Material and method	52
4.3.3	Results and discussions	54
4.4	Summary	56
	Chapter 5	57
5.1	Introduction	57
5.2	HYMOSTRUC3D Simulation—incorporating micronized sand	58
5.2.1	HYMOSTRUC	58
5.2.2	Extensions and modifications of HYMOSTRUC3D	59
5.2.3	Short summary	67
5.3	Simulation Results and Validation	67
5.3.1	Input parameters	67
5.3.2	Simulation results	67
5.3.3	Summary	73
5.4	Studies Based on the Simulated Microstructure of Cement Paste Incorporating Micronized Sand	73
5.4.1	Connectivity of pores calculated based on the simulated microstructure	73
5.4.2	Water permeability coefficients calculated from the simulated microstructure	75
5.4.3	Short summary	76
5.5	Summary	76
	Chapter 6	77
6.1	Introduction	77
6.2	Optimum Packing Systems	77
6.2.1	Packing model	78
6.2.2	Optimum packing	80
6.3	Properties of Ternary Mixtures from Simulation	83
6.3.1	Binary mixed materials	83
6.3.2	Ternary mixed materials	83
6.4	Experiments Validation	84
6.5	Summary	86
	Chapter 7	87
7.1	Introduction	87
7.2	Service Life Prediction according to DuraCrete	88
7.3	Value Determination of Parameters in DuraCrete Model	89
7.3.1	Chloride content C_s^d and C_i	90
7.3.2	Correction factor k	90
7.3.3	Aging factor n	91
7.3.4	Reference diffusivity D_0	92
7.3.5	Design value of critical chloride content C_{cr}^d	93

7.4 Service Life Prediction by Using DuraCrete Model	94
7.4.1 Chloride penetration profiles	94
7.4.2 Cover layer thickness modification	95
7.5 Cost Evaluation	97
7.6 Summary	99
Chapter 8	101
8.1 Introduction	101
8.2 Life Cycle Assessment	103
8.3 Step 1: Determination of Goal and Scope	104
8.3.1 Goal and scope	104
8.3.2 Impact categories	104
8.4 Step 2: Inventory Analysis	105
8.5 Step 3: Impact Assessment	107
8.6 Step 4: Interpretation	110
8.7 Summary	112
Chapter 9	115
9.1 Mixture Design, Cost and Sustainability Aspect	115
9.2 Service Life and CO ₂ Footprint	115
9.3 Cost and Service Life	119
9.4 Summary	121
Chapter 10	123
10.1 Retrospection	123
10.2 Conclusions	125
10.3 Further Research	126
Bibliography	129
Summary	137
Samenvatting	141
Acknowledgements	145
Curriculum Vitae	147

List of Symbols

Roman

A	[m ²]	cross-sectional area of the sample
A_{C_s}	[-]	a regression parameter describing the relation between the chloride surface concentration and water to binder ratio
a_{ij}	[-]	represented the loosening effect
b_{ij}	[-]	represented the wall effect
b_{MS}, n_{MS}	[-]	Rosin-Rammler constants of micronized sand particle
C	[-]	connectivity of pores
$C(x,t)$	[-]	the chloride content % at depth x (mm) at time t
C_{cr}	[-]	the critical chloride concentration, in % by mass of binder
C_i	[-]	the initial chloride content, % by mass of binder
C_s^d	[-]	the design value of surface chloride content, in % by mass of binder
C_x	[mol/m ³]	the concentration at a distance x from the reference point
D	[m ² /s]	the diffusion coefficient of the material
d	[m]	pore access diameter
D_0	[m ² /s]	the reference diffusivity after reference time t_0
d_{cr}	[-]	critical pore size
D_{nssm}	[m ² /s]	non-steady-state chloride migration coefficient
dq/dt	[m ³ /s]	rate of flow of water
dr	[mm]	change in the pore radii
dV	[mm ³]	a volume increment of the pore volume
$D_v(r)$	[-]	pore size distribution function
erf	[-]	Gauss error function
F_i	[-]	the influence of temperature of the hydration process
g	[m/s ²]	acceleration due to gravity

$G_{MS}(x)$	[-]	the under-size of micronized sand particles $<x$ μm
k	[-]	a correction factor in DuraCrete model
K_0	[-]	the basic rate factor of the boundary reaction
k_c	[-]	the curing condition factor
k_e	[-]	the environment factor
k_w	[m/s]	coefficient of permeability for water
L	[m]	thickness of the sample
n	[-]	the aging coefficient
p	[%]	total porosity
P	[MPa]	mercury injection pressure
t	[s]	time
T	[°C]	average value of the initial and final temperatures in the anolyte solution
t_0	[s]	the reference time in DuraCrete model
U	[V]	absolute value of the applied voltage
V_b	[-]	bulk volume of the material
V_p	[-]	total pore volume
x	[mm]	the position in the sample
x_d	[mm]	average value of the penetration depths
y_i	[-]	volume fraction retained in each size class i
β_1	[-]	an empirical constant
β_i	[-]	mono-sized packing density of grain i
γ	[-]	a correction factor in order to establish the physical consistency of the Rosin-Rammler function
Υ	[N/m]	surface tension of mercury
γ_i	[-]	packing density of mixture with one particle size class i ;
Δh	[m]	drop in hydraulic head through the sample
Δt	[s]	the interval time of the incremental volume collected
Δt_{j+1}	[-]	the time step
δ_{tr}	[μ]	the transition thickness
ΔV	[m ³]	the incremental volume
$\delta_{x,j}$	[-]	the thickness of the product layer at time t

$\Delta\delta_{in,x,j+1}$	[-]	the increase of the penetration depth in time step Δt_{j+1} ;
η	[Ns/m ²]	dynamic viscosity of the fluid
θ	[°]	contact angle between solid and mercury
κ	[m/s]	coefficient representing the intrinsic permeability of the material
λ	[-]	the factor depending on the rate-controlling mechanism, a boundary reaction ($\lambda=0$), or a diffusion controlled reaction ($\lambda=1$)
ρ	[kg/m ³]	density of the fluid
ρ_{MS}	[-]	the specific mass of the micronized sand
Ω_i	[-]	the various effects of water withdrawal of particles in the shell of a central cement particle
γ_{C_s}	[-]	partial factor for the surface chloride concentration
$\gamma_{C_{cr}}$	[-]	partial factor of the critical chloride concentration
$\gamma_{R_{cl}}$	[-]	the partial factor for the resistance with respect to chloride ingress

List of Abbreviations

BSE	backscattered electron
CH	calcium hydroxide
CO ₂	Carbon dioxide
C-S-H	calcium silicate hydrates
DOH	degree of hydration
EMC	energetically modified cement
ESEM	environmental scanning electron microscope
GWP	global warming potential
LCA	life cycle assessment
LPM	Linear Packing Model
LRFD	Load Resistance Factor Design
MIP	mercury intrusion porosimetry
MS	micronized sand
ODP	ozone layer depletion
OPC	ordinary Portland cement
PSD	particle size distribution
psd	pore size distribution
RCM	rapid chloride migration
SCC	self-compacting concrete
SEM	scanning electron microscope
SiO ₂	silicon dioxide
w/b	water to binder ratio
w/c	water to cement ratio
WBCVSD	World Business Council for Sustainable Development

Chapter 1

General Introduction

1.1 General

Concrete is recognized as the most important man-made construction material in the world. However, Portland cement material which is one of the constituents of the concrete is responsible for about 5-10% of the global CO₂ emission (Gibbs, P. et al. ; Meyer 2009). According to the Netherlands Environmental Assessment Agency, in the second half of 2008 half of the annual increase in global CO₂ emission is from fossil fuel use and from cement production. The cement industry is aware of the environmental problem of concrete because of the use of Portland cement. In addition, the natural resource of the main raw material limestone, of which cement is made, is being exhausted. The emission of CO₂ and the depletion of the raw material make it necessary to find alternatives to reduce the amount of Portland cement needed in the concrete industry. Attempts have been made to partially replace the cement content by pozzolanic or inert fillers. According to Moosberg-Bustnes (Gibbs, P. et al. ; Moosberg-Bustnes, Lagerblad et al. 2004), filler materials can affect the concrete in four ways:

- Filler effect. The added particles fill the intergranular voids between cement particles and thus improve the compactness of the concrete.
- Dilution effect. The added particles is diluting the cement-based mixture, influencing the average distance between cement particles and the water content available for cement hydration.
- Nucleation effect. The added particles enhance hydration by acting as nucleation sites and becoming an integrate part of the cement paste.
- Chemical effect. The particles react with a component in the cement, for example with calcium hydroxide, while forming hydration products.

In this study micronized sand is selected as the replacement material, which is produced by grinding of selected quartz sand with a high SiO₂ content. This material is considered as chemically inert filler, because it can not react with cement, water or hydration products. It can indirectly influence the hydration process and the microstructure of the cement paste.

Relevant properties of cement-based material blended with quartz sand have been studied by Ronin, Justnes and de Vries (Elfgren and Jonasson 2000; Justnes, Elfgren et al. 2005; De Vries 2008). This modified material could be highly interesting for the building industry. However, only a few properties of the material have been tested and discussed yet. The

transport properties, for instance, were not included, which is very important in view of the long-term performance of cement-based material.

1.2 Objective and Limitation of the Thesis

The objective of this research is to investigate the possibility of using micronized sand to replace Portland cement. The study focuses on the following aspects:

- The effects of micronized sand on the microstructure development and the transport properties of the cement paste will be explored, in order to evaluate the properties of cement-based materials blended with micronized sand.
- Numerical simulations of hydration and microstructure development of cement paste blended with micronized sand will be studied in order to optimize the use of micronized sand in cement paste are studied.
- The service life of the modified material will be evaluated based on the DuraCrete model. To maintain the proper performance of the structure is one of the biggest points of using material blended with micronized sand.
- The impact of the modified material on the environment will be considered from the sustainability point of view. The positive effect of using micronized sand in view of reducing the ecological footprint in the cement-based material will be investigated.

In this research, cement paste and concrete incorporating micronized sand were studied with the following restrictions:

- Portland cement with water-cement ratio (w/c) of 0.40 is used as reference material; in the samples blended with micronized sand, the water to binder ratio (w/b) is kept constant, as 0.40;
- The age of the samples is up to 90 days;
- Replacement percentages of micronized sand vary from 10 to 30%;
- No superplasticizer or other additives are considered in this study.

1.3 Outline of the Research

This thesis consists of 10 chapters. The overview of the research is shown in figure 1.1. The general introduction in the first chapter is followed by the literature review in the chapter 2, in which the fundamental knowledge and background of effects of fillers on the cement-based materials are studied. In chapter 3 and chapter 4, the experimental studies, regarding the microstructure and transport properties are presented and discussed in detail. The effects of micronized sand on

microstructure development are studied by means of mercury intrusion porosimetry (MIP) and scanning electron microscope measurements (SEM). Water permeability and chloride penetration (diffusion) measurements are carried out to determine the transport properties. Parameters, including particle size distribution, replacement percentage and fineness of fillers, will be taken into account. Apart from the experimental approaches, numerical simulations are dealt with in chapter 5 to chapter 7. The numerical simulation program HYMOSTRUC3D (van Breugel 1991; Koenders 1997; Ye 2003) will be modified and used to generate the microstructure of cement paste blended with micronized sand. Service life of structures made of concrete blended with micronized sand is predicted and discussed by using the results from rapid chloride migration (RCM) tests. In chapter 8, the impact of micronized sand on the environment is evaluated from the sustainability point of view. Categories, such as global warming, ozone depletion, acidification, photo-oxidant creation and eutrophication, are considered. In chapter 9, the mixture designs are considered from both economic and sustainability points of view. It gives perspectives for applying the modified material in practice. In the last chapter, the conclusions and further research are presented.

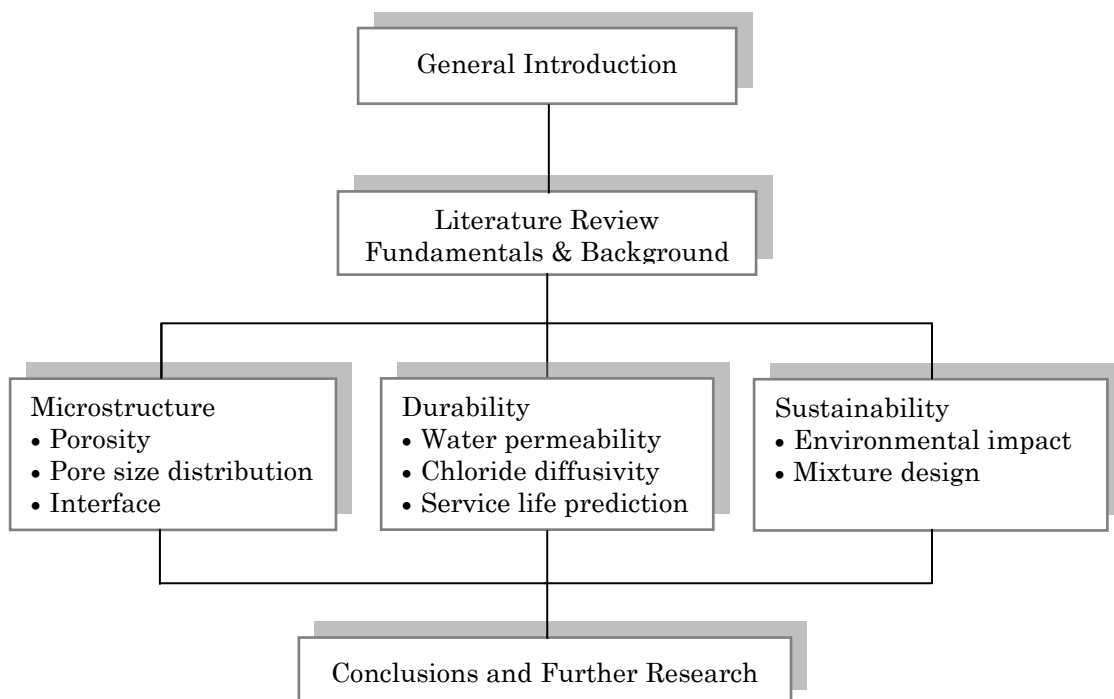


Figure 1.1. Overview of the thesis

Chapter 2

Literature Review: Effects of Fillers on Cement-based Material

2.1 Introduction

It has been studied that the production and use of Portland cement is responsible for about 5-10% of global total CO₂ emission (Meyer 2009). It is considered as a major concern in the concrete industry. Depending on the fineness of the cement and the water-cement ratio (w/c), the degree of hydration of cement in ordinary concrete mixtures is only about 60% to 80% (Bentz and Conway 2001). Since cement is an expensive material, to reduce the amount of cement and to make cement use efficiently in concrete are required in concrete industry (Bentz and Conway 2001). In order to make a more efficient use of the cement in the concrete, many pozzolanic and chemically inert mineral admixtures have been studied and used in the cement industry over the years. It is known that the fillers, such as fly ash, silica fume, limestone powder and blast furnace slag, have been used in cement industry for decades. These fillers have either physical or chemical effects on the material.

2.2 Different Types of Fillers

From many studies it has become evident that mineral admixtures, either chemically inert or reactive, modify the hydration kinetics of cement on the short and long term. In summary, the addition of admixtures can affect the concrete in four ways (Gibbs, P. et al. ; Moosberg-Bustnes, Lagerblad et al. 2004):

- Filler effect: the added particles fill the intergranular voids between cement particles and thus improve the compactness of the concrete.
- Dilution effect: the added particles is diluting the cement-based mixture, influencing the average distance between cement particles and the water content available for cement hydration.
- Heterogonous nucleation effect: the added particles enhance the hydration reaction by acting as nucleation sites, becoming an integrated part of cement paste.
- Chemical effect: particles react with a component in the cement, for example with calcium hydroxide, and thus form hydration product gel.

Table 2.1 shows the function and properties of different admixtures used in cement-based materials. Some admixtures, such as silica fume, are expensive. Other mineral admixtures, such as limestone powder, are facing the depletion of resources of the raw material, CaCO_3 . Another possibility is the use of fly ash. Although industry has claimed that fly ash is "neither toxic nor poisonous," this is a point of debate. Fly ash contains trace concentrations of heavy metals and other substances that are known to be detrimental to human health. Early strength of Portland cement containing up to 70% blast furnace slag is reduced. There is no perfect filler material. In recent decades, many efforts have been made to look for a material that is economical, environment-friendly and can reach, or even exceed, the properties of normal concrete.

Table 2.1. Properties of different types of admixtures (Neville 2006).

	<i>Fly ash</i>	<i>Silica fume</i>	<i>Limestone powder</i>	<i>Blast furnace slag</i>
Chemical composition	Silicon dioxide (SiO_2), aluminium oxide (Al_2O_3) and iron oxide (Fe_2O_3).	a fine-grain, thin, and very high surface area silica	calcium carbonate (CaCO_3)	Calcium oxide (CaO); Silicon dioxide (SiO_2); Aluminum oxide (Al_2O_3); Magnesium oxide (MgO)
Function	As a pozzolanic ingredient.	A very effective pozzolanic material.	Acting as inert filler and a nucleation site for cement.	As a pozzolanic ingredient.
Replacement Percentage	Up to 50%	6.5-8%	Up to 35%	Up to 90%

2.3 Quartz Sand

Quartz sand has been chosen as admixture and studied recently. It is the most abundant mineral in the Earth's crust; therefore, the use of this material will not cause a depletion of resources. This material is considered chemically inert and it plays a role as filler. Some aspects of the use of quartz sand have been studied in cement industry (Ronin, Jonasson et al. 1997; Johansson, Larsson et al. 1999; Justnes, Elfgren et al. 2005; Justnes, Dahl et al. 2007).

Inter-grinding of cement with quartz

One material, named as energetically modified cement (EMC), had been developed by V. Ronin and his colleagues at LuLeå University of Tech. (Sweden) in 1994 (Jonasson, Ronin et al. 1996; Johansson, Larsson et al. 1999; Elfgren and Jonasson 2000). EMC is produced by high intensive grinding/activation of OPC together with different types of fillers. The choices of fillers are not only quartz sand, but also silica fume, blast furnace slag and fly ash (Elfgren and Jonasson 2000). The grinding

process results in a reduction in size of both cement and filler particles. The increase of the cement surface leads to the improved binding capacity of OPC. The added filler acts as grinding media that increases the grinding effectiveness. The grinding process is shown schematically in figure 2.1.

Over more than 10 years' research, the properties and performance of concrete based on EMC have been studied and tested. Results show that with up to 50% of quartz sand as cement replacement in the binder, EMC concrete can perform similarly as normal concrete with regard to the setting time, workability and compressive strength. Service life properties of concrete structure are better for EMC than that for 100% OPC because of the densification of the microstructure (Elfgren and Jonasson 2000).

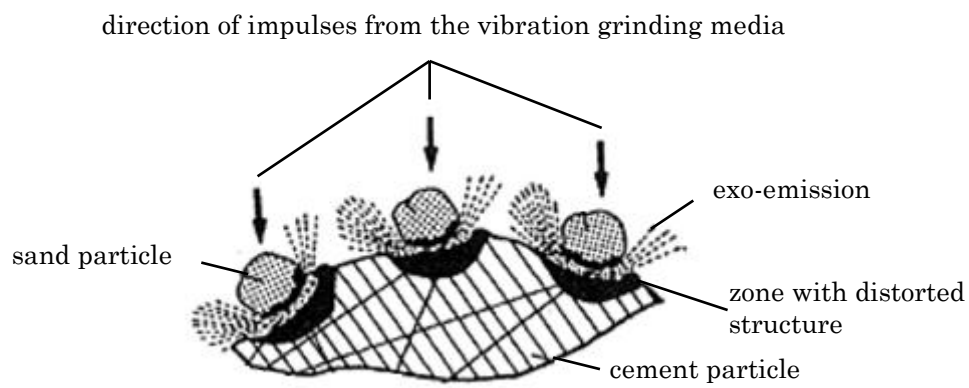


Figure 2.1. Schematic picture of the high intensive interaction of the admixture and Portland cement particles in the vibration grinding mill. (Ronin, Jonasson et al. 1997).

It has been found that EMC-based concrete has several advantages in comparison with OPC. Several projects (Ronin and Elfgren 2009) in Europe and North America have been built by using EMC-based concrete. A bridge with a span of 16m was built in Sweden; a plant to produce EMC with fly ash has been built in the state of Texas, USA; and some pavement projects were carried out by using EMC material in Houston, USA.

2.4 Micronized Sand

The grinding procedure for making EMC cement consumes extra energy, thus increases the cost of the EMC-based concrete. From an economic point of view, it would be desirable to find a solution for producing a more economical, ecological and environment-friendly material. In this research, the grinding procedure is modified by simply blending OPC with quartz sand filler instead of grinding them together. Micronized sand, which is mostly pure quartz, is selected as the filler material. The reason of using micronized sand instead of the original sand is that the particles sizes can be tailor-made by adjusting the grinding process. The production process

is shown in figure 2.2 (www.sibelco.be). The properties of the micronized sand are given in table 2.2 in which 4 types of micronized sand are shown. Micronized sand is normally produced in industrial mills that consist of a cylindrical metallic drum that usually contains steel balls. As the drum rotates the balls inside collide with the particles of the solid, thus crushing them towards smaller diameters.

Table 2.2. Properties of micronized sand.

Type	M6	M10	M300	M600
BET Blaine (m ² /kg)	240	360	400	1300
Density (kg/m ³)	2650			
Hardness (Mohs)	7			
SiO ₂	>99%			

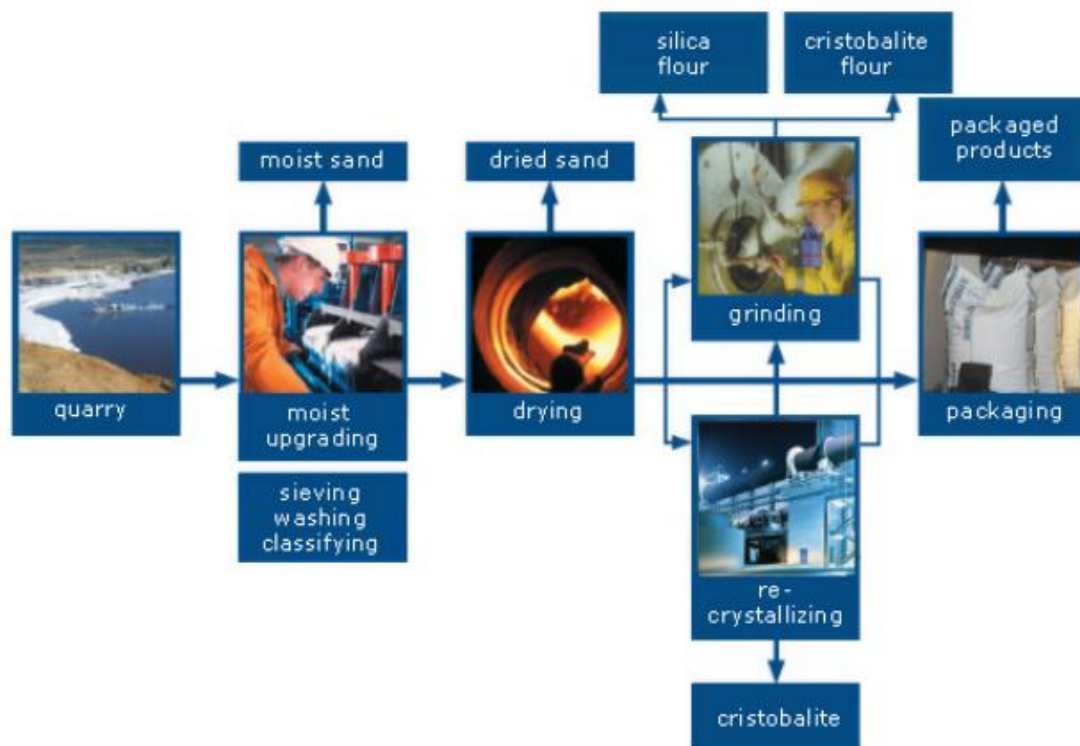


Figure 2.2. Production process of micronized sand (www.sibelco.be).

2.5 Effects of Micronized Sand on Cement Paste

It is to be expected that micronized sand as replacement of cement may influence not only the fresh paste, but also the hardened paste. The hydration kinetics will be modified and the microstructure of the bulk system will be changed. Eventually, the long term properties will be different. Basically, three main effects on the hydration process will be considered when micronized sand is used as a cement replacement

(Lawrence, Cyr et al. 2003; Cyr, Lawrence et al. 2005; Lawrence, Cyr et al. 2005; Cyr, Lawrence et al. 2006).

- a) Dilution effect;
- b) Filler effect;
- c) Nucleation effect.

2.5.1 Dilution effect

The amount of cement in the mixture is reduced when micronized sand is used as a cement replacement. It is defined as the dilution effect of the filler. An increasing replacement percentage of micronized sand results in a decreasing amount of cement and an increasing water/cement ratio, which affects the degree of hydration of cement and the compressive strength of the material. In the research of de Vries (De Vries 2008), the development of compressive strength of cement paste blended with different types of micronized sand has been studied. The results are shown in figure 2.3. The compressive strength is reduced along with an increasing replacement level. The fineness of the sand has a slightly positive effect on the strength: the finer the sand is, the slightly higher the strength is.

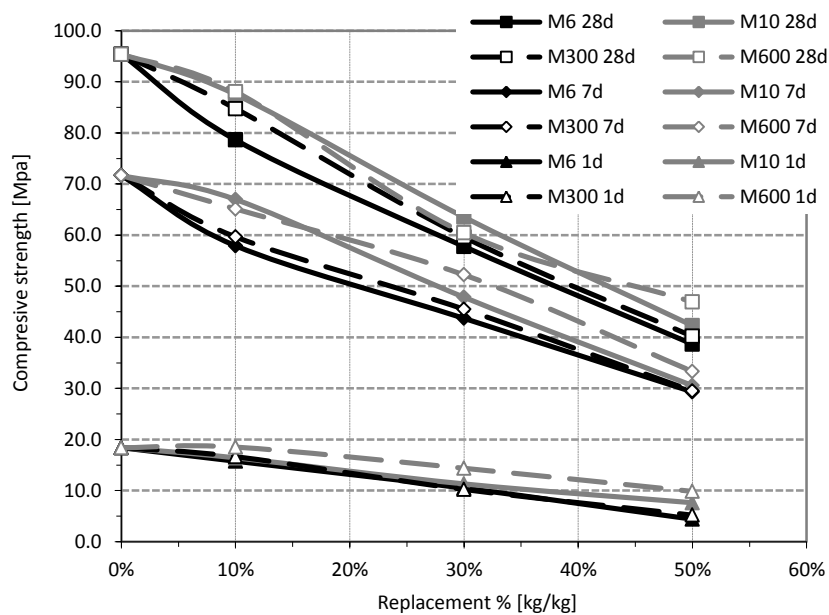


Figure 2.3. Compressive strength of cement paste blended with different micronized sand at 1, 7 and 28 days, with the water/binder ratio of 0.35 (De Vries 2008).

2.5.2 Filler effect

The filler effect of micronized sand is that the added micronized sand particles fill the inter-granular void between cement particles and thus increase the compactness of the concrete (figure 2.4). Fillers which are finer or coarser than the cement material can widen the overall particle size distribution, which will improve the packing density. Cement pastes containing fine particles have a denser structure than the pastes without filler (Moosberg-Bustnes, Lagerblad et al. 2004).

2.5.3 Nucleation effect

According to the theory of *Chemistry of the Solid-Water Interface* (Stumm 1992), nucleation normally occurs at nucleation sites on surfaces contacting the liquid or vapor. Suspended particles can provide nucleation sites. This is called heterogeneous nucleation. Nucleation without preferential nucleation sites is homogeneous nucleation. Homogeneous nucleation occurs spontaneously and randomly and takes place with much more difficulty than heterogeneous nucleation. Heterogeneous nucleation forms at preferential sites and requires less energy than homogeneous nucleation (figure 2.5). At such preferential sites, on which the surface energy is lower, the free energy barrier is diminished and nucleation is facilitated.

In literature (Lawrence, Cyr et al. 2003; Moosberg-Bustnes, Lagerblad et al. 2004), it is concluded that the large specific surface of the small particles can act as a heterogeneous nucleation site that promotes the precipitation of hydration products. Although heterogeneous nucleation is a physical process, it results in the acceleration of the hydration process.

Micronized sand is inert filler, but it can indirectly influence the hydration process and the microstructure of the cement paste in a positive way. If the interfacial energy between micronized sand and calcium hydroxide (one of the hydration product: CH) is smaller than the interfacial energy between the CH and the pore solution, then the nucleation takes place on the surface of micronized sand other than in the pore solution. This process depends on the fineness, the amount of the micronized sand and the affinity of the micronized sand with the hydration products (Stumm 1992; Cyr, Lawrence et al. 2006).

The creation of a nucleus implies the formation of an interface at the boundaries of a new phase (<http://en.wikipedia.org/wiki/Nucleation> ; Stumm 1992). An interfacial zone will be formed when the hydration products precipitate on the surface of micronized sand. The interfacial zone appears to be the region of high porosity and hence it represents the weak link in cement-based system (Diamond and Huang 2001; Scrivener 2004).

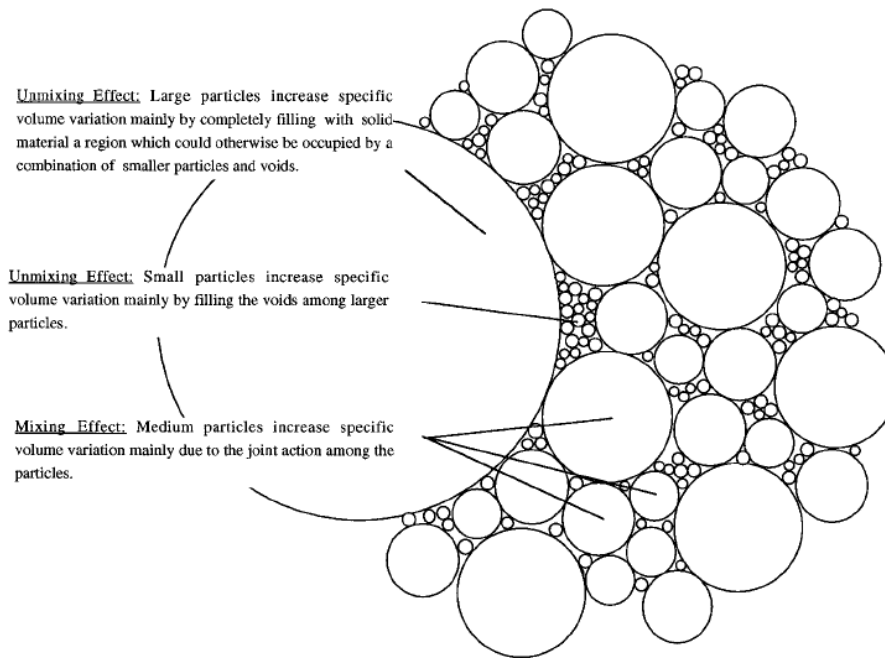


Figure 2.4. Two-dimensional diagram illustrating the random packing structure of particles with their sizes represented by equivalent packing diameters (McNally, Richardson et al. 2005).

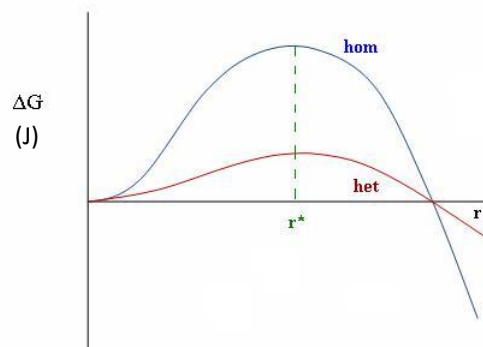


Figure 2.5. Comparison of the free energy barrier for heterogeneous and homogeneous nucleation (r : the radius of nucleus; ΔG : the free energy of the formation of nucleation. *hom*: homogeneous; *het*: heterogeneous.) (<http://en.wikipedia.org/wiki/Nucleation>).

2.6 Pore Structure

Hardened cement paste is a porous medium. The formation of the pore structure largely depends on the degree of hydration and the w/c ratio. Pores in the cement paste matrix include gel pores, capillary pores, and air voids (Aligizaki 2006). A classification of pores in cement paste is presented in table 2.3. The pore structure is particularly important because it relates to several important properties and/or mechanism and it controls the durability of the material. For instance, permeability is a function of the degree of interconnection between the pores, the pore size distribution and its tortuosity (Richardson 2002). The capillary pores,

which form because the hydration products do not fill all the space between hydrating cement particles, are assumed to have a major effect on transport processes. Understanding of the formation of the pore structure is a prerequisite for the design of new materials, and broadens the range of applicability of cement-based materials (Aligizaki 2006).

Table 2.3. Classification of pores in hydrated cement paste, modified from Mindess and Young (Ye 2003).

<i>Designation</i>	<i>Diameter</i>	<i>Description</i>	<i>Affect</i>
Capillary pores	50 nm to 0.5 μ m	Large capillary	Strength, permeability;
	10 to 50 nm	Medium capillary	Strength, permeability, shrinkage.
Gel pores	2.5 to 10 nm	Small capillary	Shrinkage to 50% RH;
	0.5 to 2.5 nm	Micropores	Shrinkage, creep;
	<0.5 nm	Micropores	Shrinkage, creep.

Because of the presence of micronized sand, the microstructure of the blended cement paste will be different from that of the reference cement paste. The replacement percentage and fineness of the micronized sand will influence not only the total porosity and the critical pore diameter, but also the connectivity of capillary pores and thus affect the transport properties.

Before studying the microstructure of cement paste blended with micronized sand, some reference has been reviewed. In the studies of EMC (Justnes, Elfgren et al. 2005; Justnes, Dahl et al. 2007), it has been concluded that the microstructure of OPC blended with quartz is quite porous. In some other blended materials, for instance, cement paste with limestone powder, which is considered as an inert filler and often used in self-compacting concrete (SCC), it has been found that the interface between limestone and hydrates is porous (De Schutter). Less precipitation of hydration products around limestone filler particles makes the interface between the filler particle and hydration products more porous.

In this thesis, the microstructure around the micronized sand particles will be studied. The thickness of the interface zone will be studied for different replacement percentage and different fineness of micronized sand.

2.7 Transport Properties

The durability of concrete structures is defined as the ability to resist weathering action, chemical attack and abrasion, while maintaining its desired engineering properties. The required durability depends on the exposure condition to which the structure will be exposed. The service life will depend on the rate at which water, gases and ions may move into the

concrete (Aligizaki 2006), which are mainly determined by transport properties of materials. Transport properties of concrete are also related to other degradation mechanisms, such as carbonation, sulfate attack, alkali-silica reaction and so on.

Since the microstructure of the blended cement paste will be different because of the presence of micronized sand in the system, the long term properties may be influenced significantly. The durability properties of the material should be evaluated to make sure that with this modified material the engineering requirements can be accomplished.

2.7.1 Permeability

Permeability is defined as the ease with which ions, molecules or fluid may move through the concrete. The permeability of concrete will be predominantly influenced by the permeability of the cement paste. Darcy's law has been used for prediction of the coefficient of permeability of cement paste for decades (Powers, Copeland et al. 1955; Khatri and Sirivivatnanon 1997; Ye 2003):

$$K = \frac{\rho L g Q}{PA} \quad (2.1)$$

where K = coefficient of permeability by flow method, (m/s);

ρ = density of the fluid, (kg/m³);

L = length of the sample, (m);

g = acceleration due to gravity, (m/s²);

Q = net flow rate, (m³/sec);

P = water pressure, (kg·m/sec²)/m²

A = cross-sectional area of the specimen, (m²).

Permeability is a function of the pore structure of the cement paste, which depends on composition, curing and exposure conditions. The most important parameters controlling penetration of external agents (water or gas) are (Ollivier and Massat 1992):

- The size, shape and total volume of the pores of the microcracks and their connectivity;
- The nature of the phases and their reactivity with various chemical species.

In energetically modified cement (EMC) materials, cement paste can contain up to 50% quartz. For those mixtures, the effect of sand filler on the water transport has been evaluated by capillary suction tests. It has been found that the properties of importance for the service life of concrete

structures, i.e. vapor and water permeability, are better for EMC than for the normal concrete (Justnes, Dahl et al. 2007). It also showed that significantly reduced gas and liquid permeability of EMC concrete should have additional positive impact on the resistance against carbonation. The explanation for this must be sought in the inter-grinding procedure of cement and quartz fillers (figure 2.4). The grinding process reduces the size of cement grains. The ground cement particles have very high degree of hydration, which results in a refined pore structure (Justnes, Dahl et al. 2007). Differences in degree of hydration and pore refinement are reflected in the water transport properties.

In cement-based material containing limestone filler, the result of a less permeable microstructure of cement paste blended with limestone filler has been also proved in some studies (De Schutter ; Poppe and de Schutter 2005; Boel, Audenaert et al. 2007). Limestone filler causes a larger particle size distribution and a better packing of mixtures. Furthermore, limestone filler acts as the crystallization nucleus for precipitation of CH. These simultaneous effects produce an acceleration of the hydration of cement grains (Bonavetti, Donza et al. 2003; Poppe and de Schutter 2005) and thus densify the microstructure.

2.7.2 Diffusivity

Diffusivity of concrete, normally represented by the diffusion of chloride ions, is considered as the most important property in view of durability. Chloride diffusivity is normally studied because chloride ions pass through the concrete in the cover and the reinforcement will be damaged (Bertolini, Elsener et al. 2004; McNally, Richardson et al. 2005; Tang 2006). Service life of structures can be reduced eventually.

The rate of ingress of chlorides into concrete is primarily related to the cement paste matrix, which is influenced by the water-cement ratio of the concrete, the degree of hydration of the cement and the pore structure (McGrath and Hooton 1996). Chloride diffusion is controlled by Fick's 2nd law (Neville 2006):

$$\frac{\partial C_x}{\partial t} = -\frac{\partial}{\partial x} \left[-D \frac{\partial C_x}{\partial x} \right] = D \frac{\partial^2 C_x}{\partial x^2} \quad (2.2)$$

where C_x = the concentration of chloride ions at a distance x from the reference point (mol/m³);

t = time (s);

x = the position in the sample (m);

D = the diffusion coefficient (m²/s).

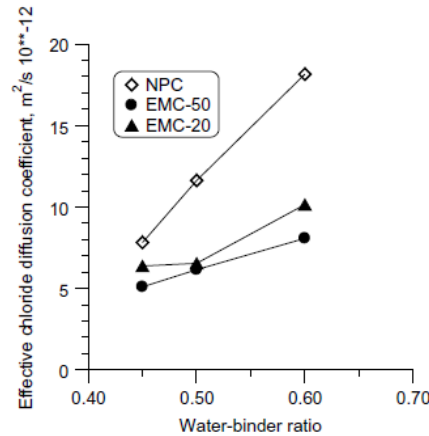


Figure 2.6. Effective chloride diffusion coefficients of NPC, EMC-20 and EMC-50 at 28 days (Justnes, Dahl et al. 2007).

In figure 2.6, the results of chloride diffusion of normal concrete (NPC), EMC blended with 50% quartz (EMC-50) and EMC blended with 20% quartz (EMC-20) show that EMC concrete gives a significantly higher resistance to chloride penetration in comparison with NPC concrete (Justnes, Dahl et al. 2007). This result can be explained by the increased hydration and better distribution of hydration products resulting in a pore size refinement of the hardened binder. The potential pozzolanic activity of quartz filler (very fine one) determined after long time (950 days) also contributes positively to a less permeable microstructure (Justnes, Dahl et al. 2007).

Referring to the material blended with micronized sand in this study, it is important to get knowledge of the diffusion coefficient of cement-based material with the presence of the filler. The results will be also required to predict the service life of structures made of concrete blended with micronized sand.

2.8 Sustainability

Nowadays, sustainability is a big issue in the building industry. Sustainability means, in short, having no net negative impact on the environment (Struble and Godfrey 2004). It is a characteristic of a process or state that can be maintained at a certain level indefinitely (www.concreteSDC.org 2008). Sustainable development focuses on more than environmental issues. Sustainable development has been defined by the World Business Council for Sustainable Development (WBCVSD) as: "Forms of progress that meet the needs of the present without compromising the ability of future generations to meet their needs." Sustainable development policies encompass three general policy areas: economic sustainability, environmental sustainability, and social sustainability. In this thesis, the amount of cement used in concrete will be reduced by adding micronized sand. The environment impact of modified material should be evaluated and compared with normal concrete.

2.8.1 Global warming potential - CO₂ emission

Cement production is an energy-intensive process. Each ton of Portland cement produced releases approximately 1 ton of CO₂ (Rehan and Nehdi 2005). Carbon dioxide (CO₂) is the most significant greenhouse gas from the concrete industry. CO₂ emissions arise from concrete production and its transport to the construction site. Most CO₂ emissions from cement manufacture originate from burning fossil fuels and de-carbonization of limestone. During cement clinker production process about 50% of the CO₂ emissions arise from the chemical reaction which takes place in the kiln. The other 40% come from the combustion of fuels. Since 1990 these emissions increased from 0.5 to 1.4 billion tons of CO₂ per year. Including related combustion emissions, the cement industry accounts globally for about 5-10% of global CO₂ emissions making it one of the most greenhouse gas (GHG) intense industries (Figure 2.7) (Larson 2011).

Intelligent mixture designs of concrete material can significantly reduce the CO₂ emitted throughout the life of a building. A study by the World Business Council on Sustainable Development (WBCSD, 2009) has shown that in recent years the share of blended cement being produced in most countries has considerably increased relative to traditional Portland cement. Consequently average clinker fractions in global cement production have decreased to between 70% and 80% compared to nearly 95% for Portland cement (Olivier, Janssens-Maenhout et al. 2011).

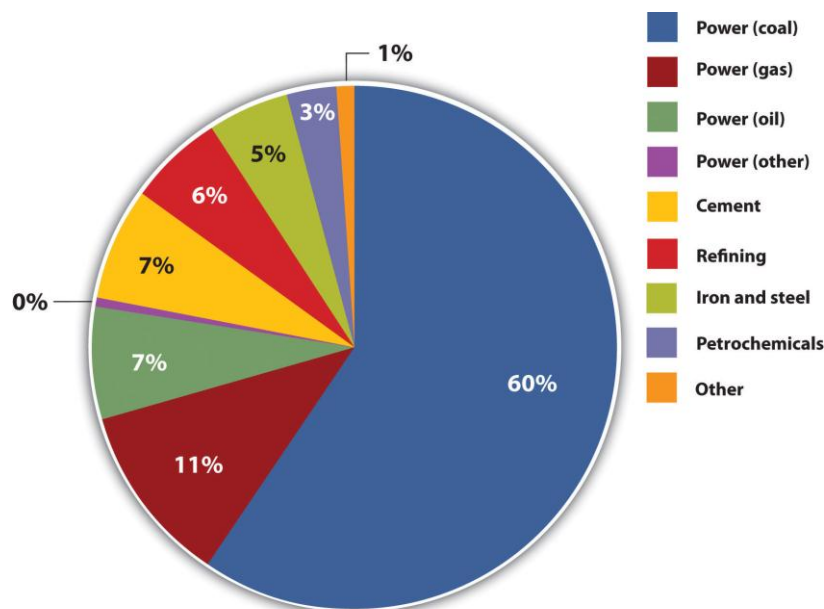


Figure 2.7. Global GHG emissions (CO₂ eq.) (Larson 2011).

In this thesis, micronized sand is selected as an environment-friendly replacement material. The less impact on the environment would be the desired advantage of the modified material. Plus, micronized sand is a

cheaper material than Portland cement. It is also a positive motivation to develop cement-based mixture blended with micronized sand.

2.8.2 Durability and sustainability

The life time of a structure has a direct impact on sustainability (Samir E 2009). The life time of a structure is controlled by the performance of the construction materials. It can be expected that some properties of cement-based material blended with micronized sand will be different from the normal OPC paste. It is possible that the durability and the service life of structures made of blended cement are not the same as for OPC concrete. However, the blended material is environment-friendly and can reduce the cost of the structures. It is possible that the advantages of the blended material in environment and economy can compensate the minor decline on other properties.

Sustainability is one of the properties that cannot be quantified precisely. The influence of a certain material on the environment will be classified by a list of impact categories, including global warming, ozone depletion, acidification, photo-oxidant creation and eutrophication. The impact from concrete blended with micronized sand will be compared with that of the reference concrete.

2.9 Summary

In this chapter, the effects of fillers are discussed and summarized. Micronized sand is selected as the replacement material of cement in this study. Some conclusions of material, energetically modified cement (EMC), are presented here to give the reference to the cement paste blended with micronized sand. Compared with plain cement paste, the cement paste with micronized sand may have lower mechanical properties and a more porous microstructure. However, in bulk applications, the requirement of the strength is less important than the concern of durability. Probably, the mechanical properties are sufficient for the use of the modified cement in a realistic situation. Furthermore, the advantages of the modified material are not only the prospect of reduction in carbon dioxide emission, but also the achievement of a significant reduction in product cost.

Chapter 3

Microstructure of Cement Paste Blended with Micronized Sand

3.1 Introduction

Long-term performance of concrete structures, i.e. service life of concrete structures, is one of the key issues in the building industry. It is known that durability of concrete is essentially influenced by the transport of ions or molecules in the form of liquids and gases moving into/through materials (Richardson 2002; Aligizaki 2006; Neville 2006). The passage of these potentially aggressive agencies is primarily influenced by the permeability of the concrete (Richardson 2002), which is greatly controlled by the details of the porous microstructure (Garboczi 1990). The characteristics of the pore structure, including porosity, critical pore size, pore size distribution and connectivity of capillary pores, determine the microstructure of cement paste. In other words, the total volume, size, shape and connectivity of pores substantially influence the permeability and diffusivity (Aligizaki 2006). Therefore, it is important to get knowledge of microstructure characteristics of material.

3.1.1 Pores in cement paste

In literature, several classifications of pores can be found. In this study, the classification proposed by S. Mindess (Mindess, Young et al. 2002) is referred. In table 3.1, the general classification of pores in cement paste according to the average width is proposed. Capillary pores have a highly irregular shape and their size could range from very small to large, i.e. from 2 nm to 10 μm . They also change with time due to the precipitation of hydration products, mainly C-S-H gel, in the originally water-filled space. Based on the classification described in table 3.1, capillary pores are divided into three groups: small, medium and large capillary pores. Since pores smaller than 10nm in diameter have less influence on permeability, in this study capillary pores are defined as medium and large capillaries, with diameters from 10 nm to 10 μm . Pores in this range will mainly influence the permeability and diffusivity of cement paste. (Aligizaki 2006).

3.1.2 Definition of pore structure parameters

To describe the properties and performance of hardened cement pastes, several parameters are normally used to determine the pore structure.

The information used to characterize the pore structure of the cement-based material is:

- Porosity;
- Critical pore size;
- Pore size distribution;
- Connectivity of capillary pores.

Porosity

Total porosity is the fractional volume of pores with respect to bulk volume of the material, which is expressed by eq. 3.1. It includes both connected and isolated pores.

$$p = \frac{V_p}{V_b} \cdot 100 \quad (3.1)$$

where p is the total porosity (%), V_p is the total pore volume and V_b is the bulk volume of the material.

Table 3.1. Classification of pores in hydrated cement paste, according to Mindess (Mindess, Young et al. 2002).

Name		Diameter	Paste properties affected
Micropores "inter layer"	Gel Pores	Up to 0.5 nm	Shrinkage, creep at all RH
Micropores "inter layer"		0.5 nm to 2.5 nm	Shrinkage, creep at all RH
Small (gel) capillaries		2.5 nm to 10 nm	Shrinkage between 50% and 80% RH
Medium capillaries	Capillary Pores	10 nm to 50 nm	Strength, permeability, shrinkage at high RH, >80%
Large capillaries		50 nm to 10 μ m	Strength, permeability
Entrained air		0.01 mm to 1 mm	Strength

Critical pore size

The critical pore size, d_{cr} , is the diameter of the pore that completes the first interconnected pore pathway in a network developed by a procedure of sequentially adding pores of diminishing size to this network (Katz 1986; Cui 2001; Hu and Stroeven 2003). The critical pore size is determined on the basis of the pore size distribution, and is used to predict the permeability of cement paste with various w/c ratios at different degrees of hydration.

Pore size distribution

The pore size distribution of cement paste is “the manner in which the total volume of pores is mathematically distributed with respect to the diameter of the pores. Thus, a complete pore size distribution contains the same information as a total pore volume and additionally includes further information on the volume on the pores of various diameters which make up the total” (Winslow 1968). It holds:

$$D_v(r) = -\frac{dV}{dr} \quad (3.2)$$

where $D_v(r)$ is the pore size distribution function, dV is a volume increment of the pore volume (mm^3), dr is the change in the pore radii (mm) (Aligizaki 2006).

The pore size distribution can be represented in two ways. A plot of the volume of pores that are smaller than a given size vs. the pore size is the cumulative pores size distribution. The local slope of the distribution curve, plotted against pore size, is the differential pore size distribution. These two characters are used to describe the pore structure of cement-based commonly (Aligizaki 2006).

Connectivity of pores

Connectivity of pores, C , is the fraction of pores with respect to the pore volume constituted only by the open and interconnecting pores. $C = 1$ means all pores are connected; $C = 0$ means that no pore path could go from one side to other side (Bentz and Garboczi 1991; Geoffrey 1999).

$$\text{Connectivity of pores } (C) = \frac{\text{Connected pore volume}}{\text{Total pore volume}} \quad (3.3)$$

Unlike closed pores, interconnected pores provide a continuous channel of communication with the external environment which the material faces to. Therefore, the connectivity of pores is an important indication and determines the permeability (Aligizaki 2006).

3.1.3 Microstructure of cement paste blended with micronized sand

The pore structure of the paste will be different when cement is partially replaced by micronized sand. The total porosity, pore size distribution and connectivity of the capillary pores will be different. It is important to figure out the effects of micronized sand on the microstructure of the cement paste. In this chapter, the results of an experimental study will be presented and discussed, considering the effects of the replacement percentage and the fineness of the micronized sand on the microstructure and transport properties of blended pastes.

3.2 Materials and Methods

3.2.1 Materials

Material information

In this study, cement paste specimens were prepared by using Portland cement, CEM I 42.5N, produced by ENCI, in the Netherlands. The basic chemical composition of the cement is given in table 3.2. The four main constituents of cement are listed in table 3.3.

Three different types of micronized sand, named M6, M300 and M600, are used in the experiments. The chemical composition and specification of micronized sand are given in tables 3.4 and 3.5, respectively (www.sibelco.be). Table 3.4 shows that, basically, micronized sand is quartz with a very high SiO₂ content.

Table 3.2. Chemical composition of ordinary Portland cement.

<i>Composition</i>	<i>%</i>
CaO	63.96
SiO ₂	20.00
Al ₂ O ₃	4.88
Fe ₂ O ₃	3.36
SO ₃	2.40

Table 3.3. Constituents of CEM 1 42.5N cement.

<i>Phase</i>	<i>%</i>
C ₃ S	62.0
C ₂ S	10.5
C ₃ A	7.3
C ₄ AF	10.2

Table 3.4. Chemical composition of micronized sand.

<i>Proportion (%)</i>	<i>SiO₂</i>	<i>Fe₂O₃</i>	<i>Al₂O₃</i>	<i>TiO₂</i>	<i>K₂O</i>	<i>CaO</i>
M6	99.5	0.03	0.2	0.03	0.04	0.02
M300	99.5	0.03	0.2	0.03	0.05	0.02
M600	99.2	0.05	0.4	0.03	0.05	0.02

Table 3.5. Physical specification of micronized sand.

	Fineness (Blaine) (cm^2/g)	D_{10} (μm)	D_{50} (μm)	D_{90} (μm)	Density (g/cm^3)
M6 (coarse)	2400	5	30	90	2.65
M300 (medium)	4000	3	17	40	2.65
M600 (fine)	13000	2	4	9	2.65

The particle size distribution (PSD) of the three micronized sands are compared with OPC and shown in figure 3.1 (De Vries 2008). M6 is coarser and M600 is much finer than cement. In other words, a mixture of cement blended with M6 or M600 will have a wider particle size distribution.

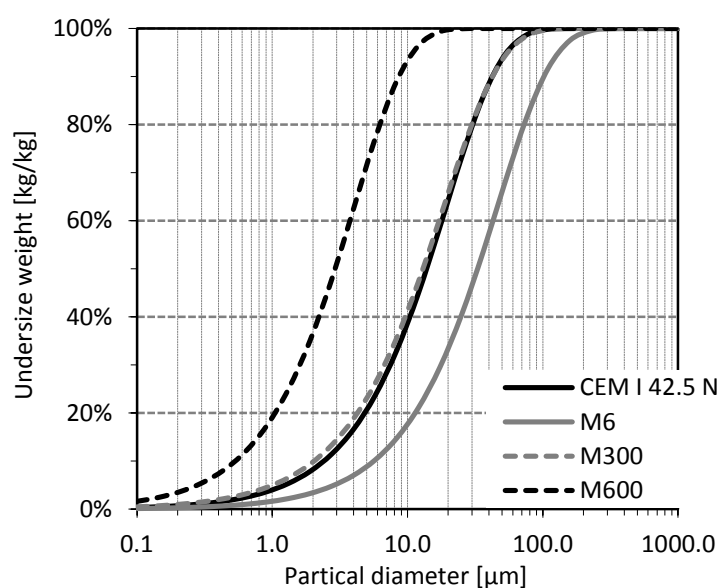


Figure 3.1. Particle size distribution of OPC and micronized sand (De Vries 2008).

Mixture design

The effect of fineness of micronized sand on the microstructure of the cement paste will be studied based on the mixtures blended with M6, M300 and M600. Different replacement percentages, i.e. 10%, 20% and 30%, are selected to explore the effect of the replacement percentage of micronized sand on the microstructure and transport properties of the blended material. The mixture compositions are listed in table 3.6.

Table 3.6. Mixture composition of OPC and the blended cement paste.

Name	OPC (%)	Micronized sand (%)	Sand/Binder* (s/b)	Water/Cement (w/c)	Water/Binder* (w/b)
OPC 0.40	100	0	0	0.40	0.40
M6_10%	90	10	0.1	0.44	0.40
M6_20%	80	20	0.2	0.50	0.40
M6_30%	70	30	0.3	0.57	0.40
M300_20%	80	20	0.2	0.50	0.40
M600_20%	80	20	0.2	0.50	0.40

*: Binder= OPC+ micronized sand

3.2.2 Methodology for characterizing the microstructure

Mercury Intrusion Porosimetry (MIP)

A wide variety of techniques has been used for determining the characteristics of the pore structure of the materials. Mercury intrusion porosimetry (MIP) has proven to be a useful technique for characterizing the pore structure of cement-based material over several decades (Cook and Hover 1999; Moro and Böhni 2002; Aligizaki 2006). Although there is debate about the validity of this method (Moro and Böhni 2002), mainly because of the ink-bottle effect, data from MIP measurements on cement paste have been used to represent the pore structure of cement paste. Parameters that can be analyzed are the total pore volume, pore size distribution and critical pore size. Thus, MIP has become a convenient, fast and the only available technique for pore structure characterization, which is supposed to cover nearly the whole range of pore sizes from 7nm to 500 μ m. A schematic drawing of the most frequently used plots from the MIP experiment is shown in figure 3.2. The total porosity obtained from the cumulative porosity curve corresponds to the point of highest pressure and the smallest equivalent pore size (Fig 3.2c). The peak in figure 3.2d corresponds to the critical pore size (Aligizaki 2006).

The pores are assumed to be cylindrical. The relation between applied pressure and the pore diameter is described by the Washburn equation (Washburn 1921):

$$P = -\frac{4\gamma\cos\theta}{d} \quad (3.4)$$

where P is the mercury injection pressure (MPa), γ is the surface tension of mercury (N/m), θ is the contact angle between solid and mercury ($^{\circ}$), and d is the pore access diameter (m).

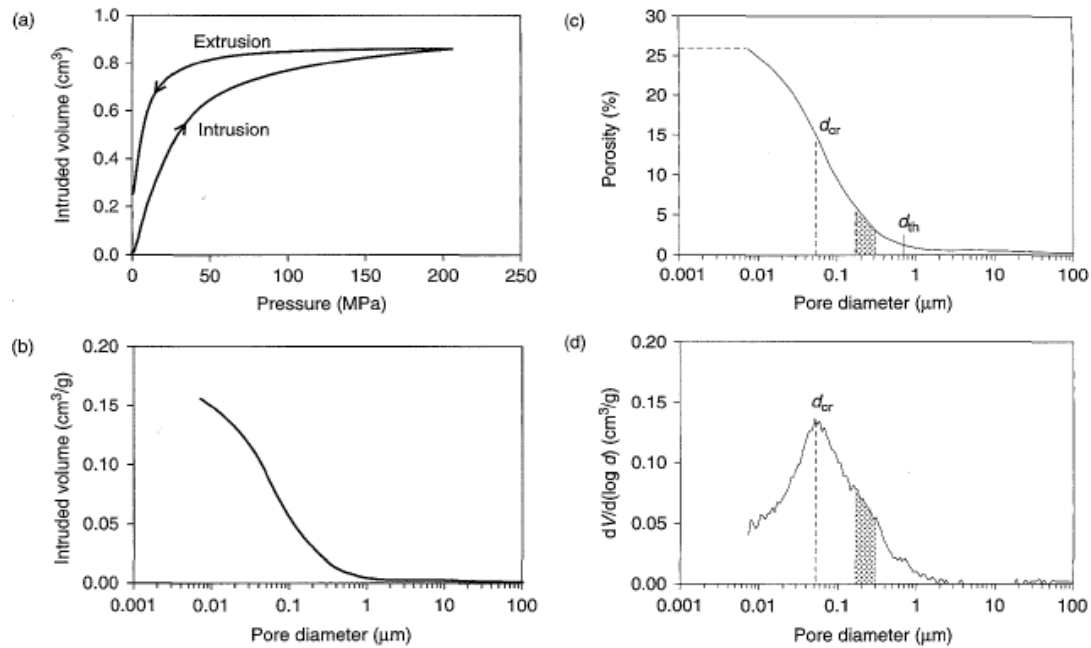


Figure 3.2. Plots used most frequently in MIP to report experimental results (Aligizaki 2006). (a) Pressurization curve; (b) cumulative intruded volume curve; (c) cumulative pore size distribution; (d) differential pore size distribution.

In this study, MIP tests were performed with a Micromeritics PoreSizer 9320. The PoreSizer 9320 is a 207-MPa mercury intrusion porosimeter, which determines pore sizes in the range from 7 nm to 500 µm. The measurement is conducted in two stages: a low pressure from 0 to 0.170 MPa and a high pressure from 0.170 to 205 MPa. For cement-based material, a surface tension value of 480 (N/m) and a contact angle of 139° have been suggested (Cook and Hover 1991) for the intrusion process

Environmental Scanning Electron Microscope (ESEM)

Because of some drawbacks in the measurement of MIP, for instance, the “ink-bottle” effect, the results from this technique can be easily misinterpreted (Diamond 2000; Moro and Böhni 2002; Zhou, Ye et al. 2010). Therefore, direct observation of the microstructure through optical and electron microscopy can provide additional insight into the spatial character of the pore structure (Lange, Jennings et al. 1994). Scanning electron microscope (SEM) technique has been developed, improved and successfully used in studying the pore structure in cement-based material for many years (Diamond 2001; Scrivener 2004; Wong, Head et al. 2006). A large amount of information can be obtained from images, including pore structure and phase distribution characteristics of hydration products (Wang, Ye et al. 2008).

With the backscattered electron (BSE) detector, information about the distribution and composition of hydration products can be obtained in the images (Wong, Head et al. 2006). The main objective of image analysis is

to aid quantifying the parameters of interest using contrast differences in two dimensional images (Scrivener 2004). Image analysis consists of several steps including proper sample preparation, area selection, image acquisition and digitization, image processing, feather recognition and data analysis and output. Sample preparation and image acquisition have been discussed by several researchers (Bentz and Stutzman 1994; Lange, Jennings et al. 1994; Stutzman and Clifton 1999; Diamond 2001). Pixels, corresponding to each of the components in every image, are separated by binary segmentation (threshold) based on the grey level (Diamond and Huang 2001; Ye 2003). The unhydrated phases of cement particles appear brightest; the calcium hydroxide (CH) appears light grey and the other hydration products (C-S-H) look as various shades of darker grey. The pores, usually filled with epoxy resin in specimen preparation, appear uniformly black and can be segmented accurately. A picture of cement paste with 20% replacement of M6 (coarse) at the age of 7 days is shown in figure 3.3.

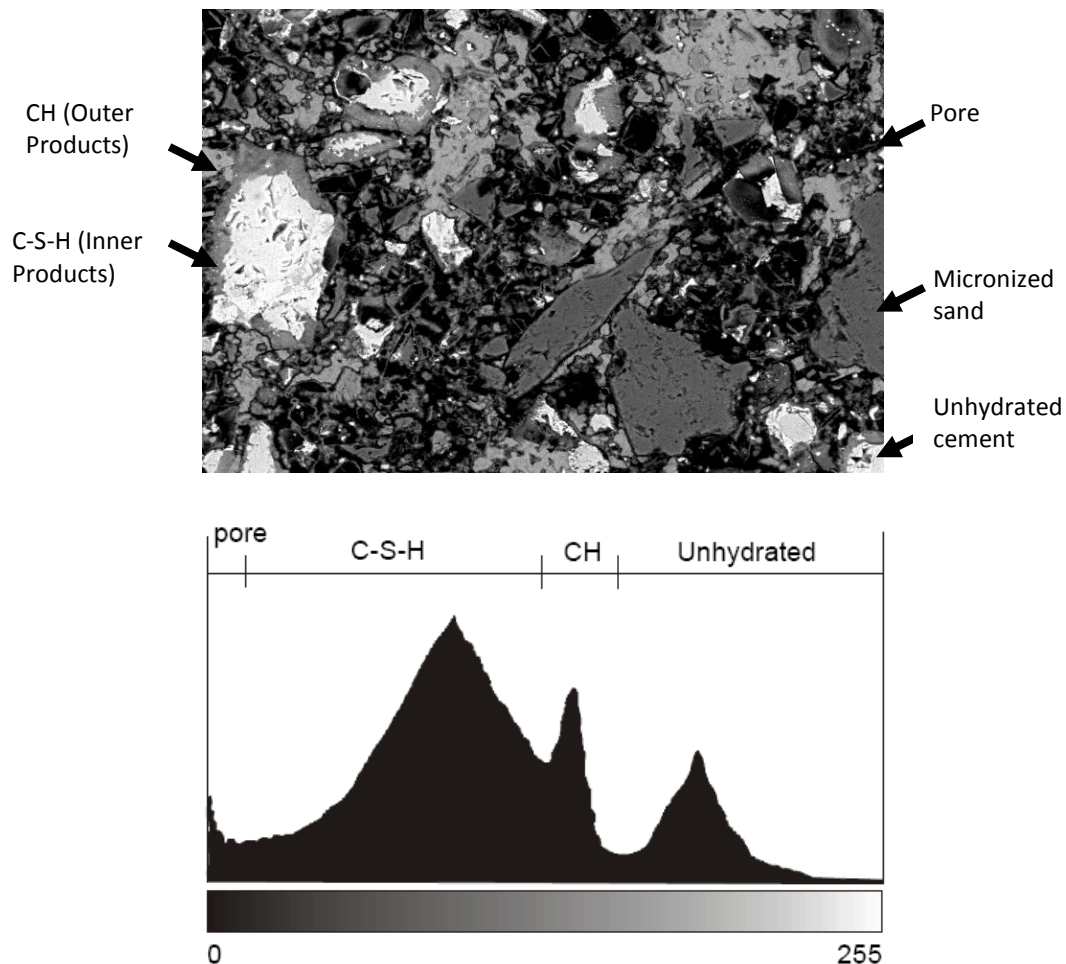


Figure 3.3. SEM image of cement paste with 20% replacement of M6 (coarse) at the age of 7 days and the typical grey level schematic histogram (Ye 2003).

The area fraction of individual phases can be calculated by applying image analysis software. Certain phase area fractions calculated from a 2-D image analysis are assumed equal to the volume to the volume fraction in a simple way, viz:

$$\text{phase volume fraction } (\mu\text{m}^3) = \text{phase area fraction } (\mu\text{m}^2) \quad (3.5)$$

In order to get reliable results, a total number of 12 images with magnification of 500 was required at least (Ye 2003). In this study, 15 images were captured for every sample to guarantee the degree of confidence ($\geq 95\%$).

Non-Evaporable Water Test

The degree of hydration of the cement in the paste sample was obtained by determining the non-evaporable water content, W_n/c . W_n/c is defined as the mass loss per gram of original cement, measured after heating the sample from 105°C up to 1000°C (Copeland and Hayes 1953). The degree of hydration was then determined as the ratio of the measured non-evaporable water content per gram of cement to the amount at full hydration. The W_n/c content of hydrated pastes on the ignited sample was calculated by eq. (3.6):

$$\frac{W_n}{c}(\%) = 100 \cdot \frac{\text{dried weight of paste} - \text{ignited weight of paste}}{\text{ignited weight of paste}} \quad (3.6)$$

For the degree of hydration, $\alpha(t)$, at time t , it holds (Molina 1992):

$$\alpha(t) = \left[\frac{W_n(t)}{c} \right] / \left[\left(\frac{W_n}{c} \right)_{\text{complete}} \right] \quad (3.7)$$

3.2.3 Sample preparation

All the cement paste samples were mixed with distilled water. A HOBART® mixer for paste preparation was used for mixing. After mixing properly, the pastes were poured into a plastic bottle (Figure 3.4), of which the volume is approximately 70ml. The bottles were shaken for 3 minutes in order to remove air bubbles and then sealed with plastic tape. The specimens are stored in a climate room of 20°C until the age of testing. Measurements were carried out after the ages of 1, 3, 7, 28 or 90 days. After achieving the required age, the plastic bottle was broken and the sample was removed and split into small pieces, about 1 cm³ each (Figure 3.4). These pieces of samples are separated into two groups. One is prepared for MIP and SEM tests; the other is prepared for non-evaporable water test.

Samples for MIP

The freeze-drying method was applied to stop the hydration reaction (Gallé 2001). Several pieces of cement paste were first immersed into liquid nitrogen (-195°C) for 5 minutes (figure 3.4). After freezing, the samples were placed in a freeze-dryer (figure 3.4) with a temperature of -24°C and vacuum of 10^{-1} Pa. Water loss was recorded each 24 hours until a stable mass loss of 0.01%/day was reached (Gallé 2001; Ye 2003). Around 5~6 g sample is used for each MIP measurement.

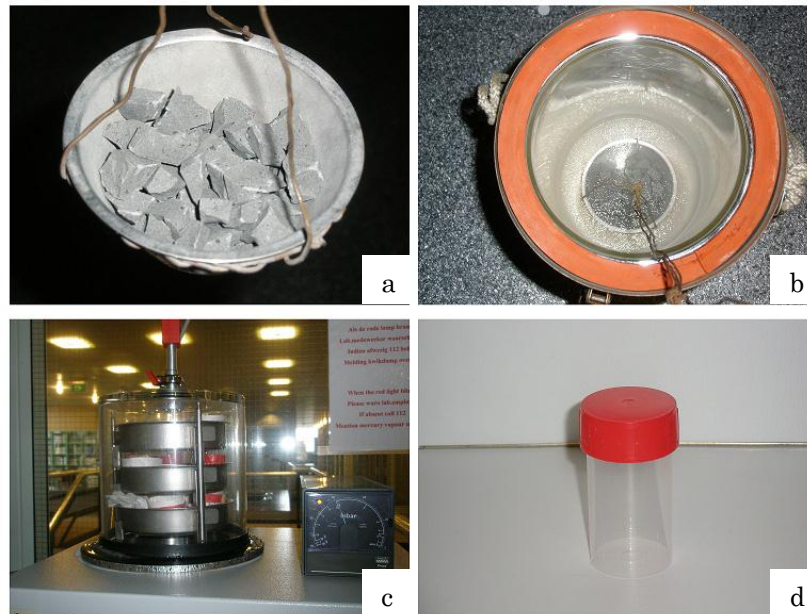


Figure 3.4. a. Small pieces of sample. b. Emerge samples into liquid nitrogen. c. Freeze-dryer. d. Plastic bottle.

Samples for SEM tests

Around 30 g of paste samples were selected after stable weight was reached by the freeze-dry method. After the samples were placed in the chamber for evacuation at 0 torr for 3 hours, the procedure of epoxy impregnation was applied. The impregnated samples were stored at atmospheric pressure at 35°C for 24 hours. Then the samples were ready for cutting, grinding and polishing (Bentz and Stutzman 1994; Ye 2003). The rough surface was removed by a diamond saw, followed by a delicate grinding procedure. The sample was ground on a rotating plate with p320, p500, p1200, p2000 and p4000 sand papers. Final polishing was done on a lap wheel with 6, 3, 1 and $0.25\ \mu\text{m}$ diamond paste for 2-3 minutes each (Bentz and Stutzman 1994; Ye 2003). Then the samples were ready to be observed in SEM. The relevant apparatuses are shown in figure 3.5.

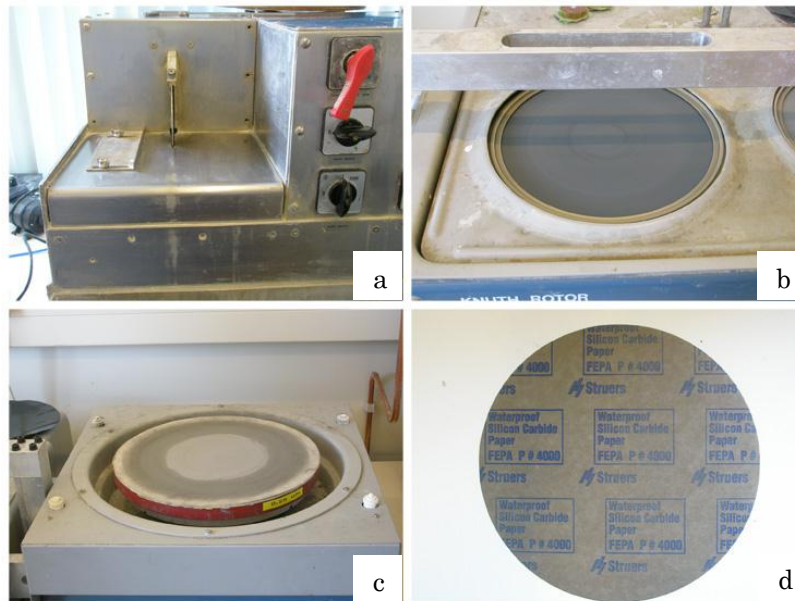


Figure 3.5. a. Sawing machine. b. Grinding machine. c. Polishing machine. d. Sand paper.

Samples for non-evaporable water tests

Samples, in the group for the non-evaporable water content (W_n/c) determination, were ground to powder by using a mortar and pestle. Around 4g powder was prepared and then placed in 3 crucibles separately. To determine the W_n/c content, 3 crucibles with around 1.1g hydrated paste were dried in an oven at 105°C for at least 12 hours, and were then heated at 1000°C in a furnace for 3 hours. The mass loss was recorded by measuring the crucibles and samples before and after placing them in the furnace.

3.3 Results and Discussions

3.3.1 Effect of micronized sand on the hydration process

The degree of hydration of cement determined by the non-evaporable water tests is presented in figure 3.6. With the w/b of 0.40, the degree of hydration of cement in the blended samples is higher in comparison with the reference OPC paste sample. At the age of 28 days, around one third of cement material is still unhydrated in the reference cement paste. To some extent, at that moment the unhydrated cement particles acts as expensive filler material. In the modified cement pastes, a higher effective w/c ratio, because of the replacement of micronized sand, results in a higher rate of hydration reaction. In these blended mixtures the cement is used more effective.

The results also show that the degree of hydration of cement in the blended cement pastes increases with increasing fineness of the micronized sand. With the same replacement percentage, i.e. 20%, samples with M300 or M600 have higher degree of hydration in comparison with the sample with M6.

M300 and M600 have higher fineness than that of M6, which can be seen in table 3.5 and figure 3.1. This indicates that mixtures with M300 and M600 have a lot small sand particles that can to be nucleation sites during the hydration reaction. Therefore, heterogeneous nucleation takes place more easily in the samples with M300 and M600. This effect will influence the speed and degree of hydration. Although micronized sand is considered as inert filler, because of its potential to act as nucleation sites it indirectly modifies the hydration kinetics.

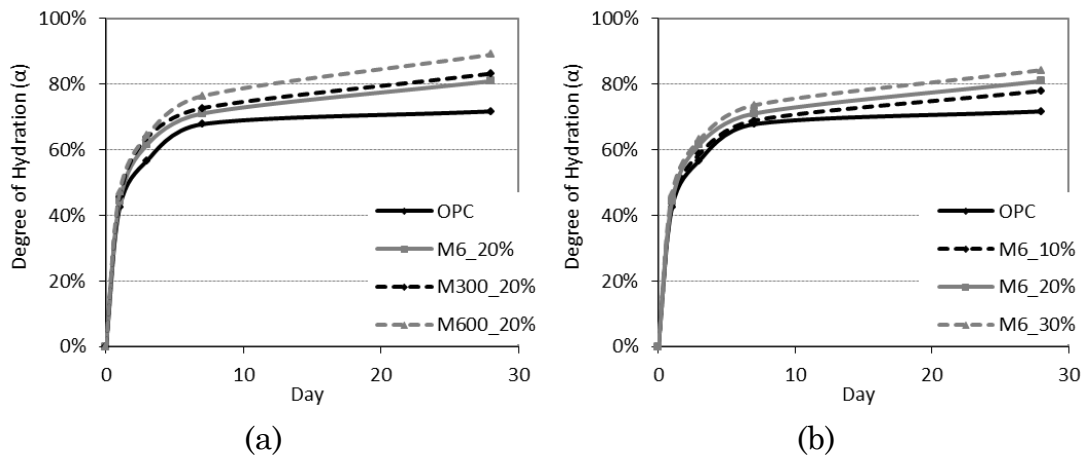


Figure 3.6. Degree of hydration of cement in pastes blended with micronized sand with (a) 20% of M6, M300 and M600; (b) 10, 20 and 30% of M6.

3.3.2 Effects of micronized sand on the pore structure of cement paste

3.3.2.1 Effect of micronized sand fineness

The total porosity of paste samples blended with 20% micronized sand with different fineness is presented in figure 3.7. Compared to the reference sample, i.e. OPC paste, the total porosity is higher in the pastes blended with micronized sand. That is because the effective w/c is increased because of the use of micronized sand. The total porosity of the blended pastes decreases with the fineness of the micronized sand in the corresponding samples before the age of 28 days. It is noticed that after 90 days the effect of the fineness of the micronized sand does not result in much difference in the porosity of the pastes. Obviously, the effect of micronized sand fineness on cement hydration is more obvious at early stage.

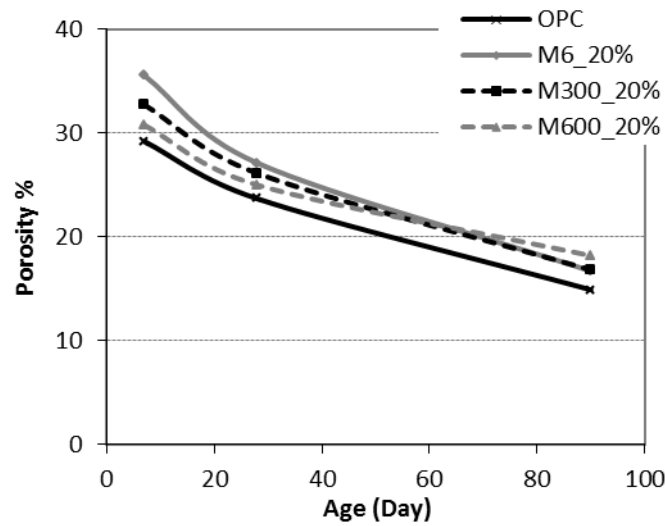


Figure 3.7. Total porosity of paste samples with $w/b=0.40$ as a function of age (20% replacement).

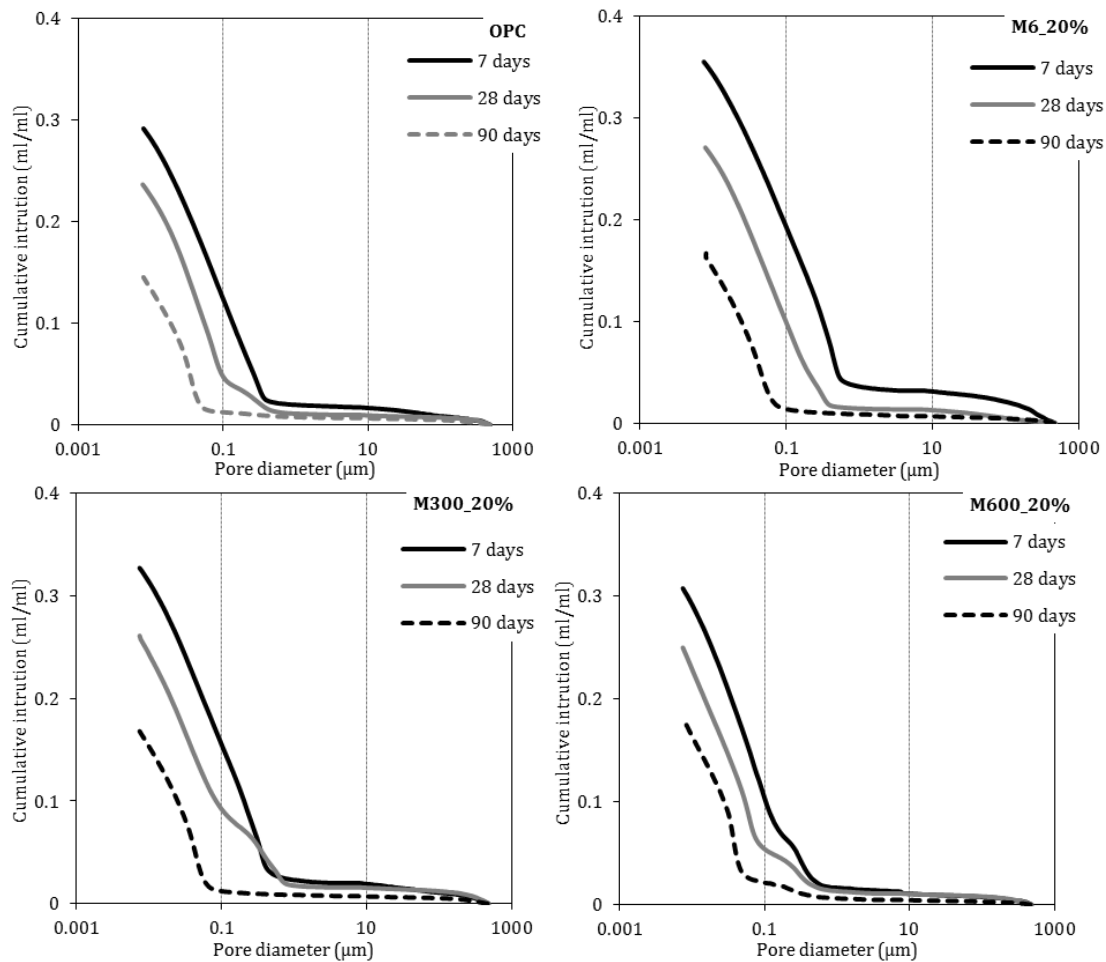


Figure 3.8. The cumulative pore size distribution curves of cement blended with 20% M6, M300 and M600 at the ages of 7, 28 and 90 days.

The cumulative and differential pore size distribution curves of cement paste blended with 20% micronized sand are shown in figures 3.8 and 3.9.

The peak in figure 3.9, which is called “critical pore size”, shifts to the smaller pores size at the age of 90 days, which means that the pore structure of the paste is refined with progress of the hydration process. At the age of 90 days, the pores larger than 0.1 μm are vanished in all the samples. The differential intrusion curves of the blended pastes show a similar trend, but with higher differential pore volume in the range of the pore diameters from 0.01 to 0.05 μm compared with the reference sample.

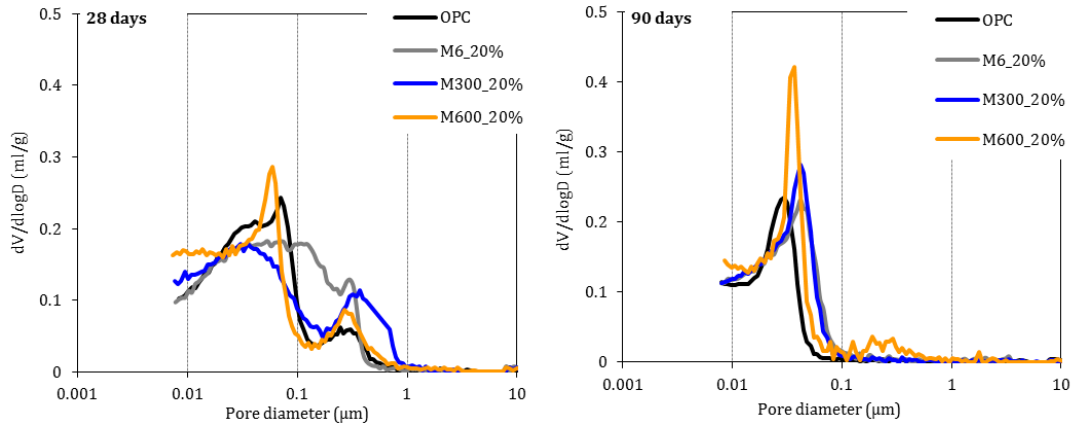


Figure 3.9. The differential intrusion curves of cement blended with 20% M6, M300 and M600 at the ages of 28 days (left) and 90 days (right).

3.3.2.2 Effect of micronized sand content

The total porosity of paste samples blended with M6 (the coarse sand) with different replacement percentages is presented as a function of time in figure 3.10. The total porosity decreases along with the progress of the hydration process. The porosity in the blended samples is higher with increasing sand content. The “dilution effect” is becoming stronger with increasing sand content. M6_10% shows lower porosity than the reference (OPC) paste. The addition of a mineral admixture will fill the intergranular void which is known as packing effect mentioned in chapter 2. The microstructure can be refined by the presence of the micronized sand. In addition, the higher degree of hydration in M6_10%, discussed in section 3.3.1, contributes to the refinement of the microstructure of the paste. The dilution effect of micronized sand is more important and the packing effect of micronized sand is limited when the content of micronized sand is higher than 20%.

The cumulative and differential pore size distribution curves of cement paste blended with 20% micronized sand are shown in figures 3.11 and 3.12. It can be seen that at the age of 28 days, 20% and 30% coarse micronized sand (M6) results in a higher differential pore volume in the range of pore diameters between 0.1 to 0.5 μm compared with the reference and M6_10% samples. After 90 days the pores larger than 0.1 μm are almost vanished in all the samples. The curve of differential

intruded pore volume of sample M6_10% has the same trend as the one of the reference OPC.

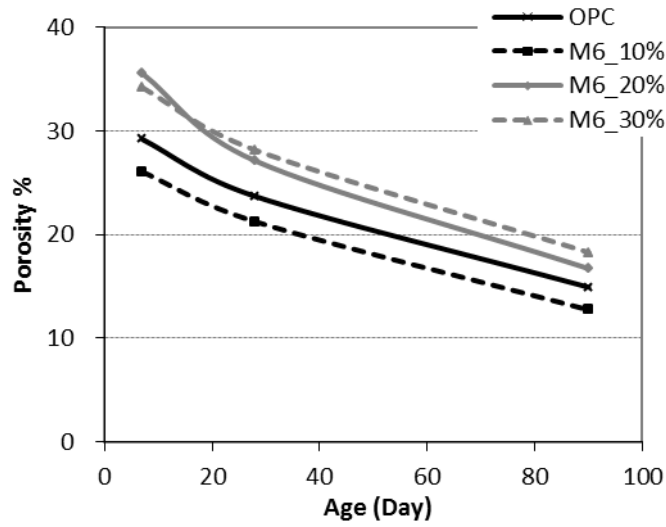


Figure 3.10. Total porosity of paste samples with $w/b=0.40$ as a function of age (different replacement of M6).

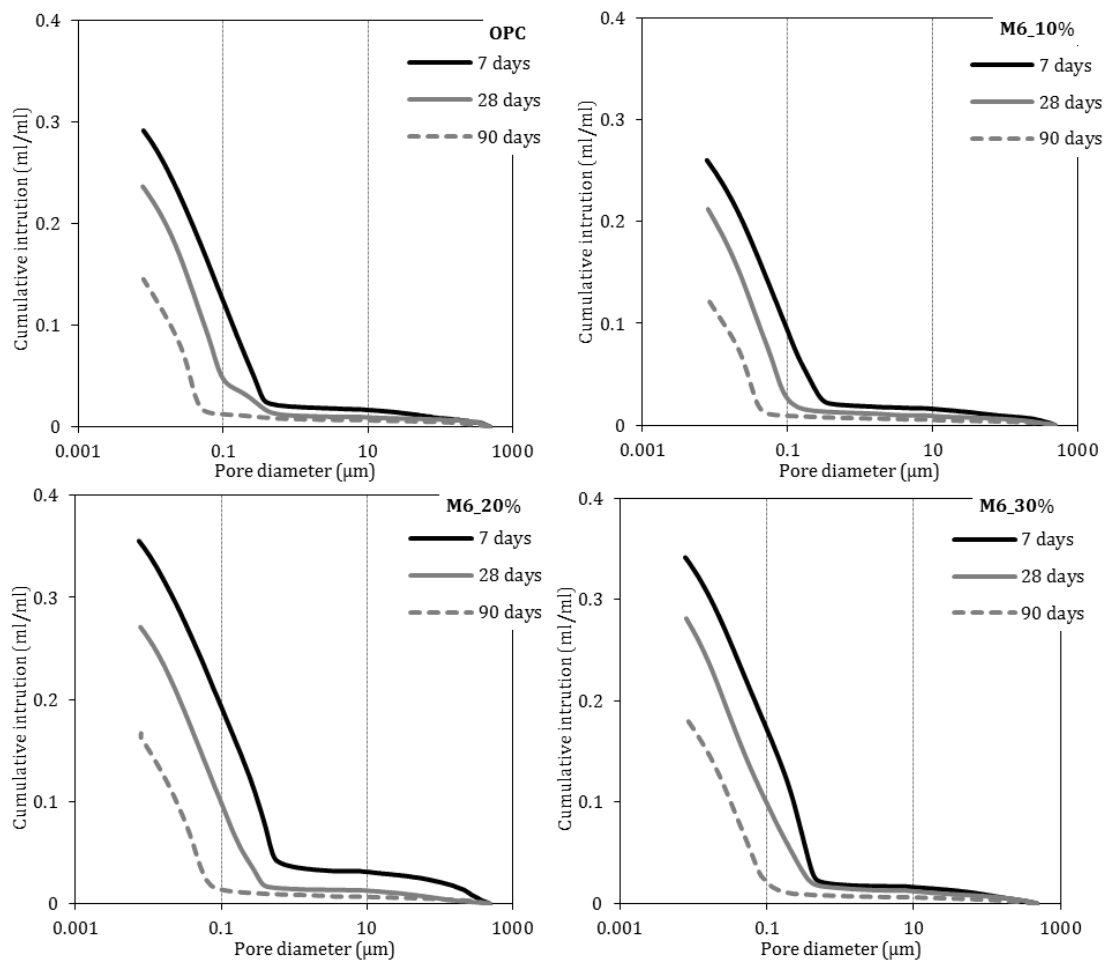


Figure 3.11. The cumulative pore size distribution curves of cement blended with 10, 20 and 30% M6 at the ages of 28 days (left) and 90 days (right).

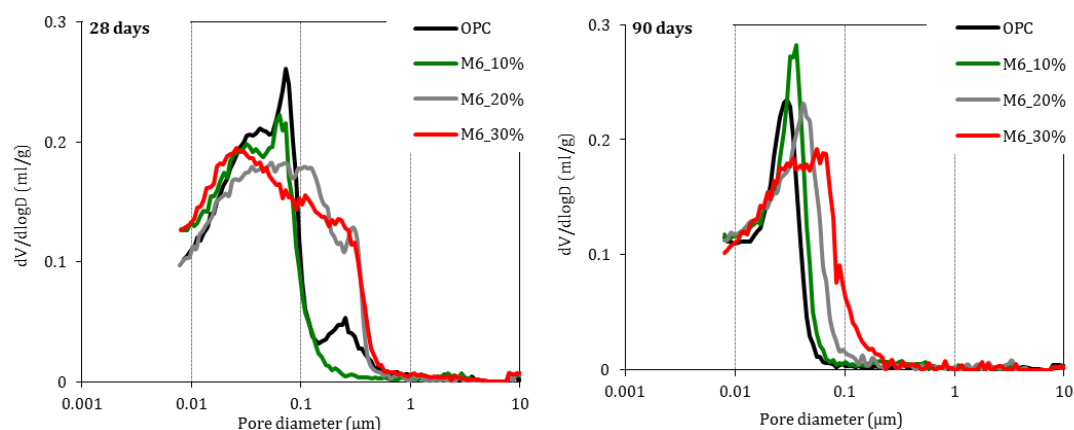


Figure 3.12. The differential intrusion curves of cement blended with 10, 20 and 30% M6 at the ages of 28 (left) and 90 days (right).

3.3.3 Observation of microstructure

A clear picture of the microstructure of cement paste, including the distribution of hydration products and the shape of pores, can be obtained from SEM observations. In figure 3.13, the BSE image of the sample M6_20% is shown and compared with the reference paste at the age of 28 days (S and C indicate sand and unhydrated cement). It can be seen that in the blended pastes the fraction of unhydrated cement grains is lower and the unhydrated cement cores are smaller (figure 3.13a) than in the OPC paste (figure 3.13b).

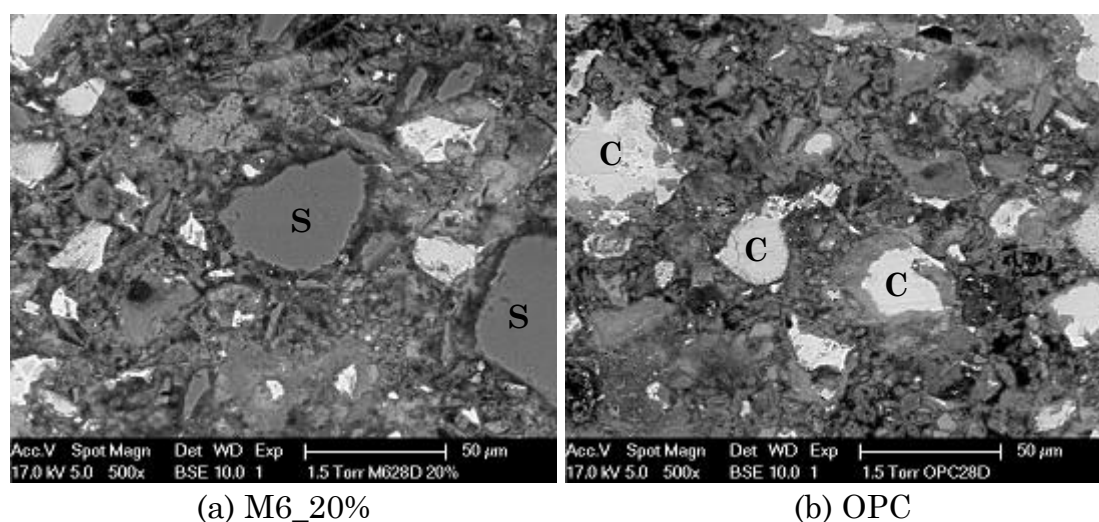


Figure 3.13. BSE images of M6_20% (a) and OPC (b) at the age of 28 days. (C: unhydrated cement particle; S: micronized sand particle)

The porosity of the paste samples was calculated based on 15 images. The thus obtained porosity is compared with the results from MIP measurements, presented in table 3.7.

Table 3.7. Comparison of porosities determined from BSE image analysis and MIP measurement of paste samples at the age of 28 days.

Sample	MIP (%)	SEM (%)
OPC	23.68	9.90
M6_20%	27.11	15.60
M300_20%	26.12	13.90
M600_20%	25.00	11.70

The data in table 3.7 show that the porosity measured by MIP is much larger than that obtained from image analysis. The difference between these two measurements is in good agreement with the results found by Lange et al. (Lange, Jennings et al. 1994) and Diamond et al. (Diamond and Leeman 1994). They have explained the reason for the difference: MIP technique measures the larger pores only by intruding mercury through smaller bottlenecks and thus the technique systematically misinterprets their size. Pore maybe considered as smaller than it should be by this so-called “ink-bottle” effect. On the other hand, the images resolution from BSE is about 0.18 μm , a size that corresponds to the size of large capillary pores in the paste (table 3.1). Particles smaller than this size usually have a too low contrast with the background to be counted efficiently, indicating that only pores larger than 0.18 μm can be detected. The limitation of the SEM image analysis technique is that only 2D information is available and the accuracy of the results is limited by the resolution of the images.

The combination of MIP measurement data and SEM image analysis allows to determine the development of microstructure and to get a better insight, not only in the pore size distribution, but also in the pore geometry and connectivity. MIP measurement can give accurate total porosity, whereas SEM images can visualize the pores. Furthermore, the combination of the microstructural information generated by SEM and MIP is also fundamental for validating the microstructure of cement paste generated from the numerical simulation.

3.3.4 The thickness of the interfacial zone between micronized sand and hydration products

In figure 3.13, it can be seen that the morphology of the reaction products around a micronized sand particles is different from that around cement particles. Figure 3.14 shows more details of the microstructure under the magnification of 2000. Less hydration products precipitate on the surface of the micronized sand particles forming a clear interfacial zone between sand surface and hydration products. This new interfacial zone is distinguishing from the one between aggregate and paste, since it is in a lower level. The microstructure in this interfacial zone is more porous in comparison with the bulk matrix. It can be expected that this porous interfacial zone caused by the presence of micronized sand will influence

the transport properties of the material. In this section, the interfacial zone around micronized sand will be studied by quantitative analysis of the SEM images.

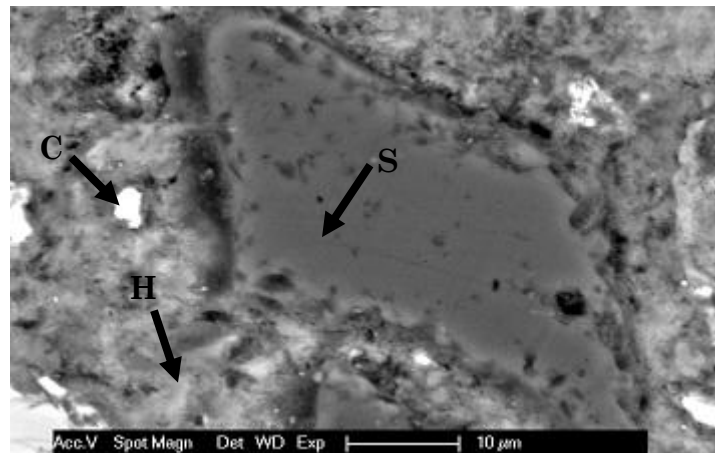


Figure 3.14. Microstructure of M6_20% after 28 days hydration. (C: unhydrated cement, H: hydration products, S: sand).

Around 100 sand particles were captured from the images with a magnification of 1000. The micronized sand particles were selected randomly and varied in size from 8 to 70 μm, for instance the one in figure 3.15. Each particle was subdivided into 10 frames (figure 3.16) and the left side of each frame was put along the surface of the micronized sand particles. The grey level of each frame was obtained by using image read software. The grey level is plotted over the distance from the sand particle (figure 3.17). The thickness of the interfacial zone between the sand particle and the hydration products can be obtained from the average value of the grey level of the frames.

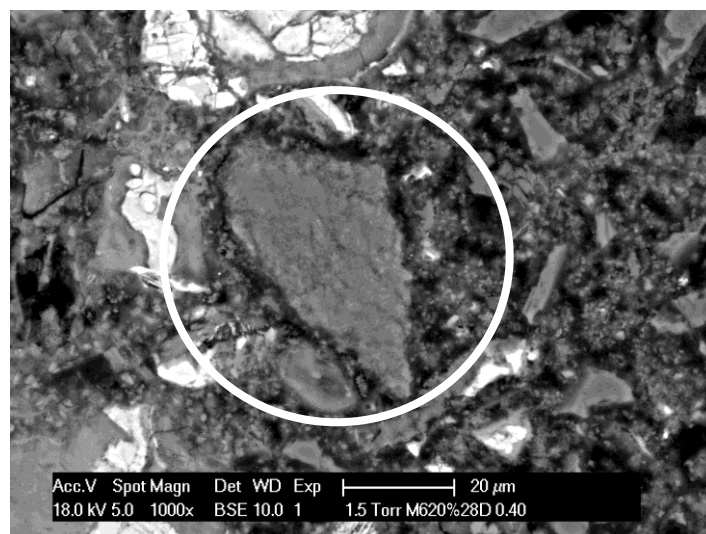


Figure 3.15. ESEM image with selected micronized sand particle.

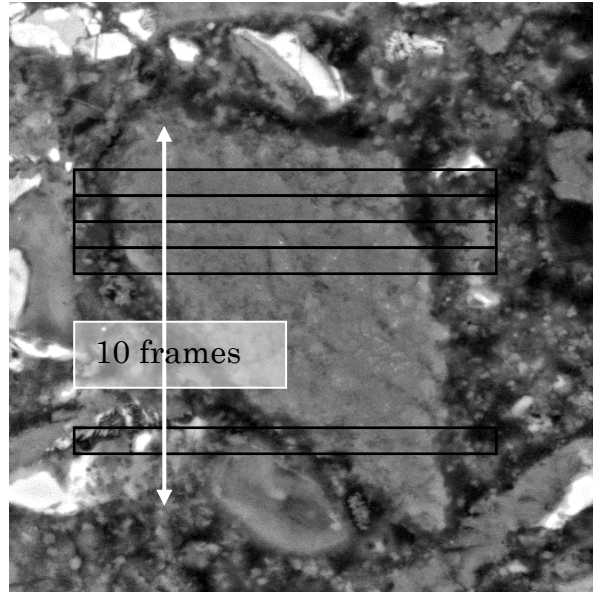


Figure 3.16. Selected micronized sand particle with frames.

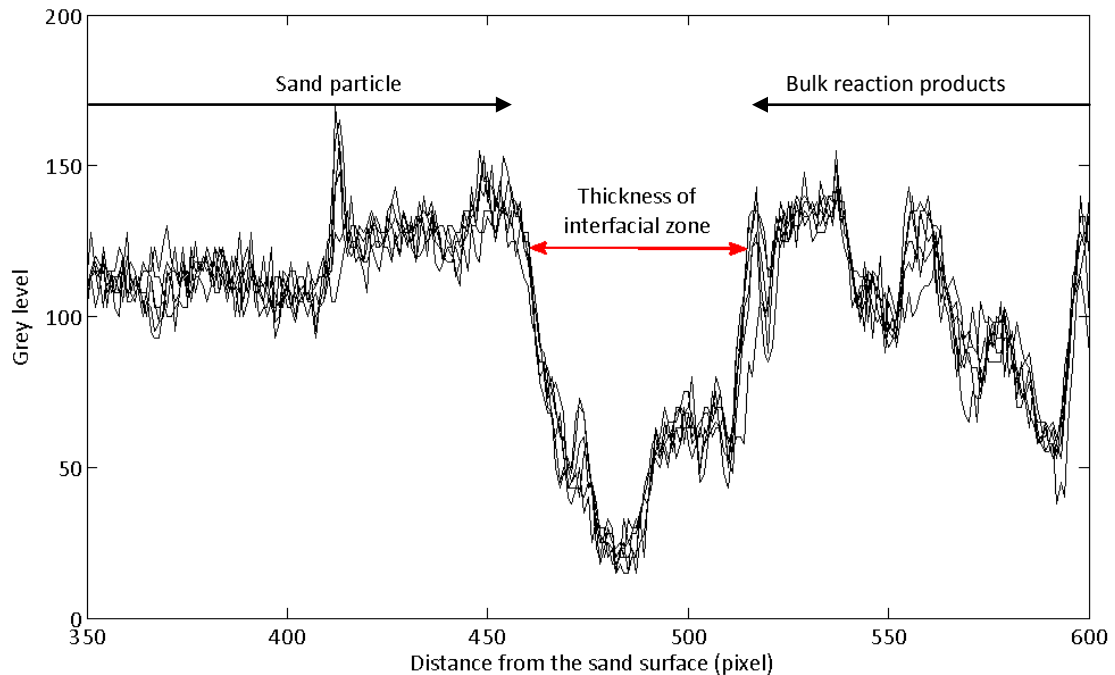


Figure 3.17. Grey levels of selected frames.

Parameters, including replacement percentage and fineness of micronized sand and ages of the samples were considered. The thickness of the interfacial zone plotted against the particle size is presented in figures 3.18 and 3.19. The thickness of interfacial zone varies from 1 to 3 μm and mainly fluctuates around 2 μm at the age of 28 days. The thickness of the ITZ is reduced to 1 to 1.5 μm at the age of 90 days. During the development of the hydration reaction, the amount of hydration products increased; more and more hydration products filled the pores and the microstructure becomes denser. There is no clear relation between the particle size of micronized sand and thickness of interfacial zone. It seems

that the thickness is independent of the fineness or the percentage of micronized sand in the mixtures considered in this study. This value is determined by the interfacial energy of the individual elements, as explained by Stumm (Stumm 1992). The creation of a nucleus is accompanied by the formation of an interface at the boundaries of a new phase. An interfacial zone appears when the hydration products precipitate on the surface of micronized sand. That is the important zone that influences the transport properties.

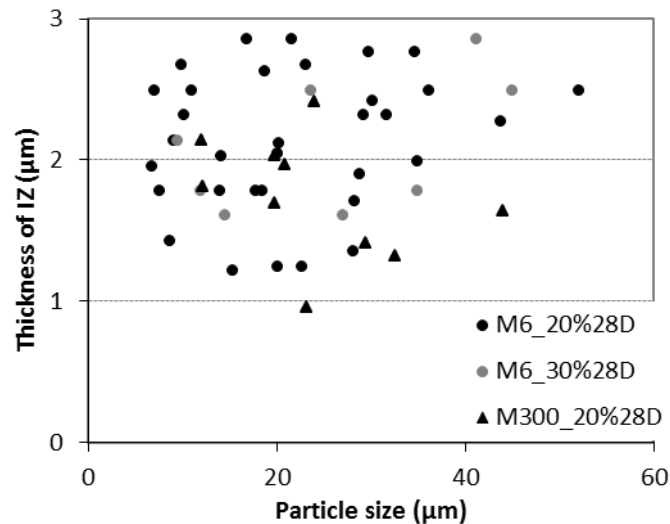


Figure 3.18. Thickness of interfacial zone of micronized sand particles in different mixtures (28 days).

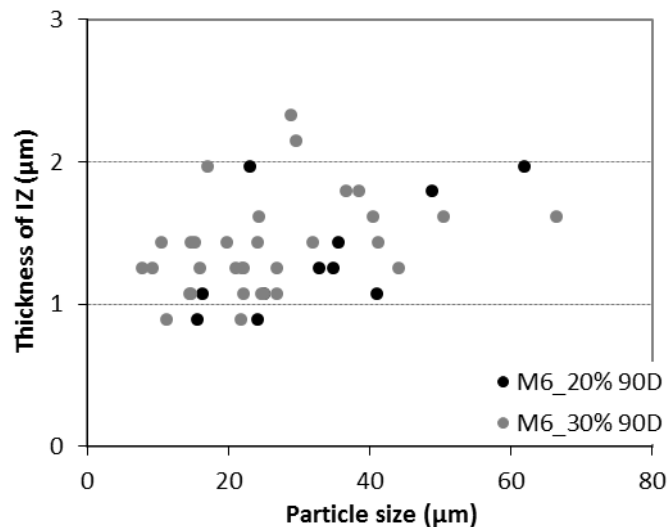


Figure 3.19. Thickness of interfacial zone of micronized sand particles in different mixtures (90 days).

It can be noticed that there are rarely sand particles detected under the size of 8 μm in figures 3.18 and 3.19. Heterogeneous nucleation takes place when the interfacial energy between the micronized sand particle and CH/C-S-H is smaller than the interfacial energy between CH/C-S-H

and the pore solution. The interfacial energy of the element is mainly depending on the chemical composition of the material and inversely proportional to the surface area (Stumm 1992). Small particles can easily become the nucleation sites and embedded in the hydration products. The sand particles under the size of 8 μm are considered as the nucleation sites in this thesis.

3.4 Summary

In this chapter, the degree of hydration of cement, porosity and pore size distribution of cement paste incorporating micronized sand were studied and compared with the reference OPC paste. The following conclusion can be drawn:

- Almost one third of the cement grains remains unhydrated at the age of 28 days (CEM I 42.5 w/c=0.40), acting as an expensive filler material. The degree of hydration of cement in the blended samples is higher in comparison with the reference one. From this point of view, the use of micronized sand is a potential solution to partially replace cement in concrete.
- Although micronized sand is considered as inert filler, it can indirectly modify the hydration kinetics and influence the microstructure of the paste. The effect of fineness of micronized sand plays an important role in the hydration reaction up to 28 days.
- The effects of micronized sand on the microstructure of the blended cement paste are the dilution effect and the heterogeneous nucleation effect. These effects are determined by the replacement percentage and fineness of micronized sand.
- The pore structure of cement paste is influenced by the presence of micronized sand. A different pore size distribution in the range from 0.1 μm -0.5 μm appears in the blended samples in comparison with the reference paste. Pores in this range are defined as large capillary pores, which influences the permeability.
- The relation between MIP results and the actual pore size distribution and connectivity can be better understood with the use of image analysis.
- There is a clear interfacial zone between micronized sand and hydration products. Its thickness is independent of the fineness or replacement level (up to 30%) of micronized sand. This interfacial zone caused by the micronized sand is considered as the decisive factor which will influence the transport properties of the material.

Chapter 4

Water Permeability and Chloride Diffusivity of Cement-based Material Blended with Micronized Sand

4.1 Introduction

Porosity and transport properties are widely recognized as being important for durability, since they determine the resistance of the material against penetrating agents. In the previous chapter, the microstructure of cement paste blended with micronized sand was studied. The pore structure of the blended paste samples is affected by the presence of micronized sand. The pore structure determines the transport properties and plays an important role in the durability of concrete as well (Garboczi 1990; Ollivier and Massat 1992; Halamickova, Detwiler et al. 1995; Basheer, Kropp et al. 2001; Aligizaki 2006; Neville 2006). In this chapter the transport properties, including permeability and diffusivity, will be studied on samples blended with micronized sand. Effects of the fineness and the replacement percentage of micronized sand on the water permeability and chloride diffusivity will be investigated experimentally.

4.2 Water Permeability

4.2.1 Darcy's law

Permeability of a porous material determined the flow under a pressure differential (Neville 2006). It governs the rate at which an agent penetrates into the material (Khatri and Sirivivatnanon 1997) Meyer 2009. The permeability is determined experimentally by measuring the rate of fluid flow through a specimen in saturated condition. The measured flow rate is used to calculate the coefficient of permeability by using Darcy's equation (Muskat 1937; Powers, Copeland et al. 1955; Banthia and Mindess 1989), viz.:

$$\frac{dq}{dt} \frac{l}{A} = \frac{\kappa \rho g}{\eta} \frac{\Delta h}{L} \quad (4.1)$$

where dq/dt = rate of flow of water, (m³/s);

A = cross-sectional area of the sample, (m²);

Δh = drop in hydraulic head through the sample, (m);

- L = thickness of the sample, (m);
 η = dynamic viscosity of the fluid, (Ns/m²);
 ρ = density of the fluid, (kg/m³);
 g = acceleration due to gravity, (m/s²).
 κ = coefficient representing the intrinsic permeability of the material, (m/s).

The coefficient of permeability for water, k_w , can be expressed as function of the intrinsic permeability, κ :

$$k_w = \frac{\kappa \rho_w g}{\eta} \quad (4.2)$$

The flow equation can thus be written as:

$$\frac{dq}{dt} \frac{l}{A} = k_w \frac{\Delta h}{L} \quad (4.3)$$

In this study, permeability will always refer to the water permeability.

4.2.2 Material and method used to determine k_w

The materials and the mixture composition used for preparing the paste samples for water permeability measurements are the same as described in chapter 3. Except the size of the samples, the mixing and curing process are the same as the samples for the MIP and SEM tests in chapter 3. The specimens used in this chapter were cast in a plastic disk-shape mould with a diameter of 95 mm. The thickness of the specimens varies from 15 mm to 25 mm. The mixture design for paste samples is presented in table 4.1. The samples were stored in a climate box at 20°C until the moment of testing.

Table 4.1. Mix design for paste specimens.

Name	OPC (%)	Micronized sand (%)	Sand/Binder (s/b)	Water/Cement (w/c)	Water/Binder (w/b)
OPC 0.40	100	0	0	0.40	0.40
M6_10%	90	10	0.1	0.44	0.40
M6_20%	80	20	0.2	0.50	0.40
M6_30%	70	30	0.3	0.57	0.40
M300_20%	80	20	0.2	0.50	0.40
M600_20%	80	20	0.2	0.50	0.40

After demoulding, the paste samples were immersed in the water and kept under vacuum. The saturation condition can be reached by keeping specimens under vacuum for 6 hours. Then the specimens were ready to test.

The experimental setup is shown in figure 4.1. The permeability apparatus is shown schematically in figure 4.2 (Ye 2003). The system includes a regulated gas pressure source, a gas/water reservoir, three parallel permeability cells, a computer controlling system and appropriate valves and tubes. The chosen pressure, 0.7 MPa, is applied at the top of the specimens. After reaching the steady flow, the water passing the samples was recorded to calculate the water permeability coefficient: k_w .



Figure 4.1. Setup of the experiment. (a). Vacuum machine. (b). Specimens in the Vacuum machine. (c). Set-up cell for the test. (d). Three parallel samples.

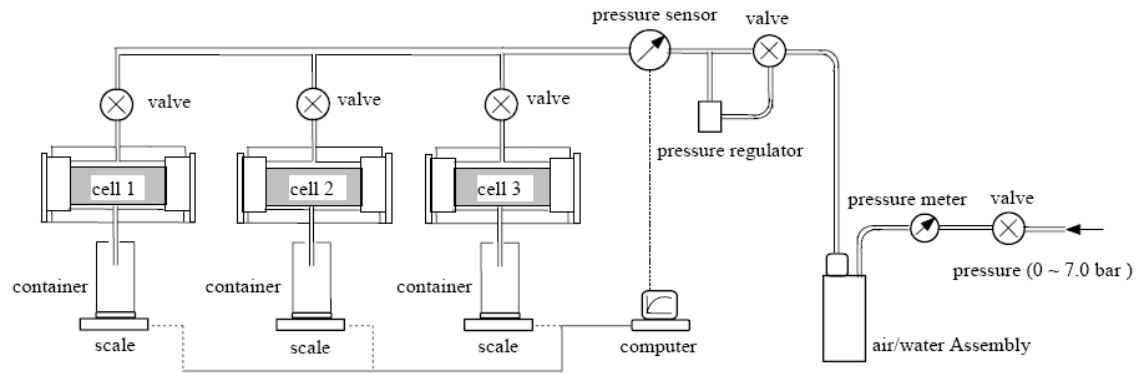


Figure 4.2. Permeability test system (Ye 2003).

The steady flow can be determined by plotting the cumulative volume of water coming from the specimens versus elapsed time (figure 4.3). When the cumulative flow curve is linear over the last 10 or more records, the steady-state flow is obtained. The flow rate Q during the steady state can be calculated from eq.4.4. The linearity of the curve is determined by the least-squares linear regression procedure. A regression coefficient of $R \geq 0.99$ is recommended and applied here as adequate for linearity (Ye 2003).

$$Q = \frac{\Delta V}{\Delta t} \quad (m^3 / s) \quad (4.4)$$

where ΔV = the incremental volume, (m^3);

Δt = the interval time of the incremental volume collected, (s).

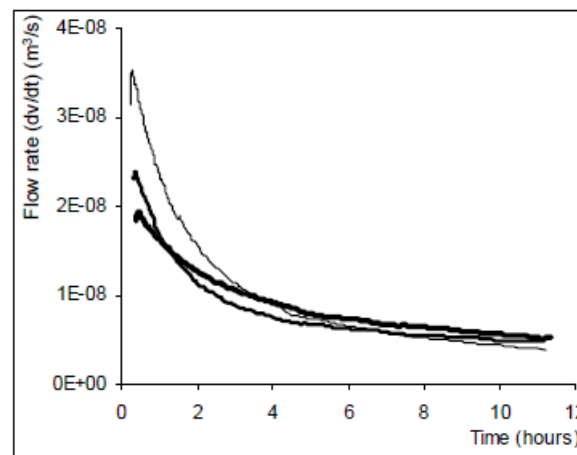


Figure 4.3. Flow rate with elapse of time.

4.2.3 Results and discussions

4.2.3.1 Effect of fineness of micronized sand and age

Figure 4.4 shows that in the period from 7 days to 90 days the value of the water permeability coefficients drops 3 orders of magnitude. Since more and more hydration products are formed and the system becomes denser with the age, capillary pores become blocked and the connectivity of pores is reduced. Then the permeability of the samples decreases. Blended samples have relatively higher values of permeability coefficients than the reference paste sample. At the age of 90 days, the permeability coefficients of all the specimens are in the same order of magnitude. There is no big difference between reference and blended samples. This indicates that the effect of the fineness of micronized sand on the permeability is limited at later ages. Obviously, the permeability of cement paste at later age does not change very much with 20% replacement percentages of micronized sand.

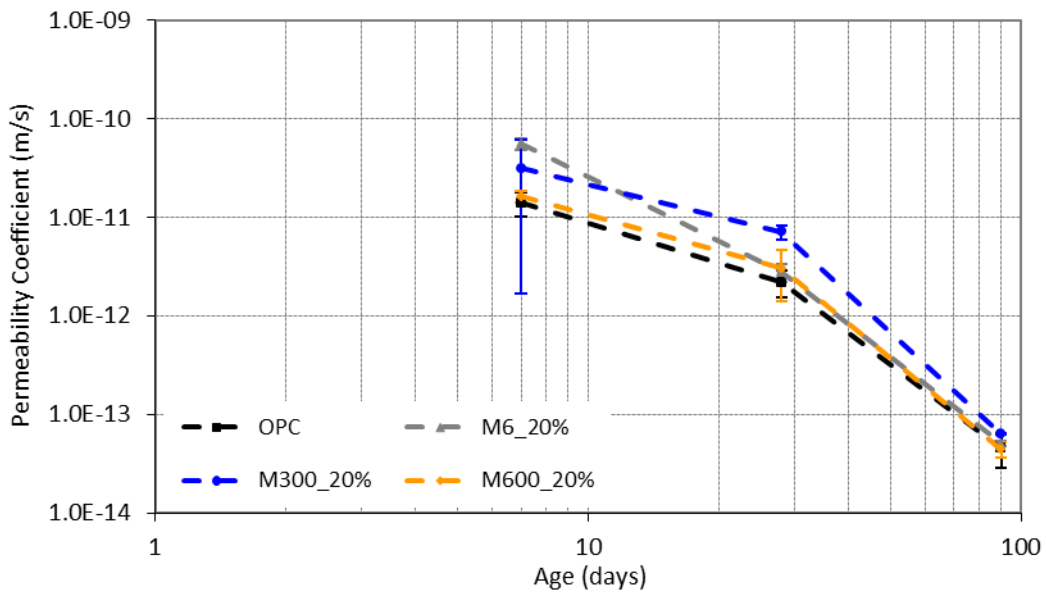


Figure 4.4. Water permeability coefficients of cement paste with different fineness of micronized sand as a function of the age.

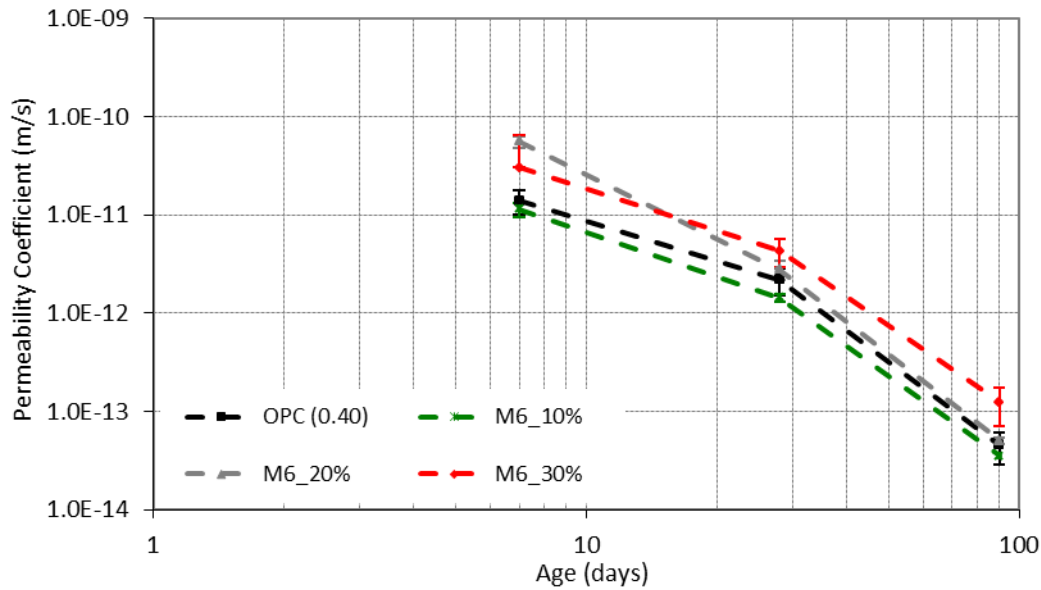


Figure 4.5. Water permeability coefficients of cement paste with different replacement percentage of coarse micronized sand M6 as a function of the age.

4.2.3.2 Effect of replacement percentage of micronized sand and age

Figure 4.5 shows that in the period from 7 to 90 days the permeability coefficients of the reference and blended samples decrease by about 3 orders of magnitude. The coefficient k_w increases with increasing replacement percentage in the period from 7 to 90 days. Specimen with 10% of coarse micronized sand (M6) has the lowest permeability coefficient at all ages. These results are in good agreement with the results of porosity mentioned in the previous chapter. The pore structure is refined by adding 10% coarse micronized sand, M6. The better packed system and higher degree of hydration of cement in the M6_10% sample results in a denser microstructure and a less permeable material.

4.2.3.3 Pore structure and water permeability

To get more information about the relationship between the microstructure and the permeability of the material, the water permeability coefficients k_w and the total porosity of different mixtures at the age of 28 and 90 days were plotted in figures 4.6 and 4.7.

Figure 4.6a shows that the figures of total porosity have the same trend as those of the permeability coefficients. With increasing replacement percentages, the water permeability coefficients, k_w , are in a good agreement with total porosity at the ages of 28 and 90 days. Samples with higher porosity are supposed to be more permeable. However, in figure 4.7, the sample M6_20% with higher porosity is yet less permeable in

comparison with the sample M300_20%. Thus the total porosity is not the only factor that indicates the permeability.

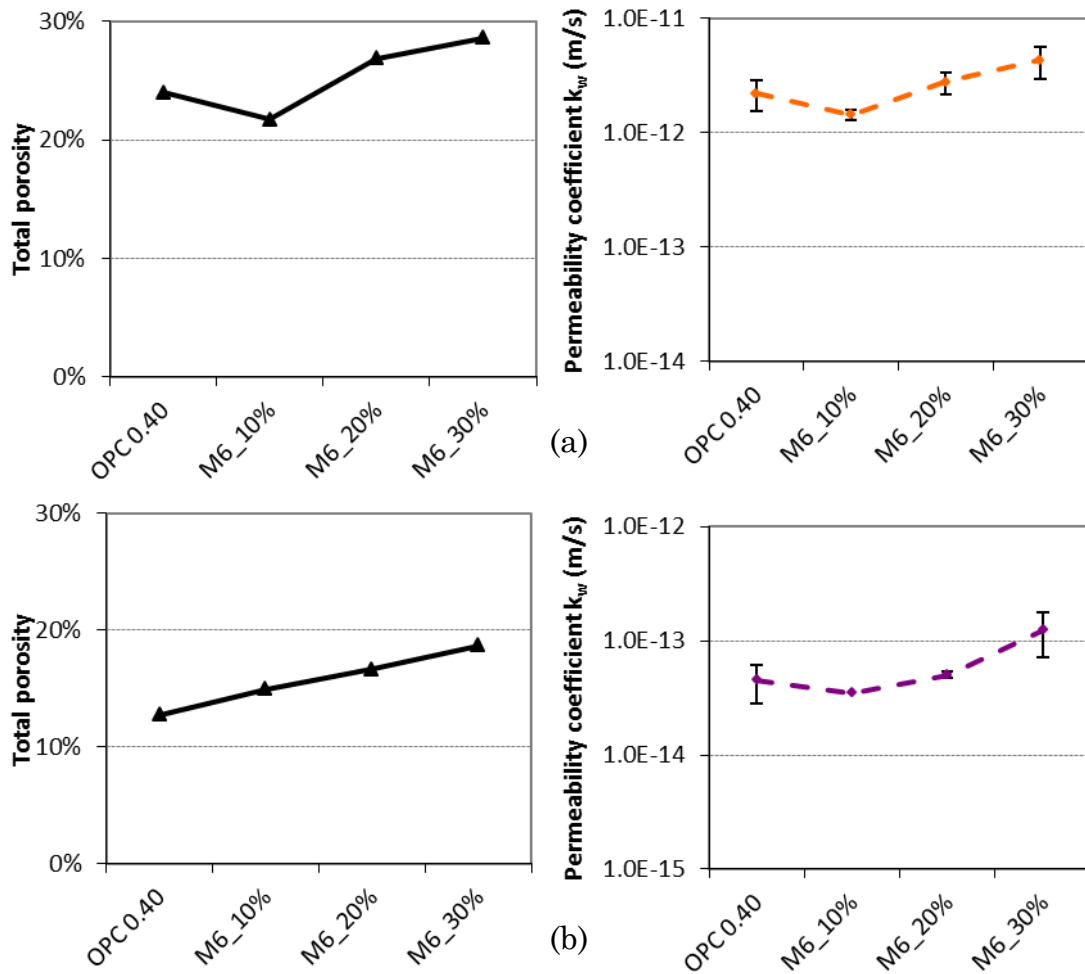


Figure 4.6. Total porosity and permeability coefficient of mixtures with different replacement percentages of coarse micronized sand, M6 (a) at the age of 28 days; (b) at the age of 90 days.

In chapter 3 it has been found and discussed that there is an interfacial zone, with higher porosity, between micronized sand and hydration products in the blended samples. This porous region affects the connectivity of the pores, which is the most important factor determining the permeability of the materials. Figure 4.8 schematically shows the interfacial zone in the blended samples, with the same replacement percentage by weight of micronized sand. The mixture systems blended with coarse sand and fine sand are presented in figure 4.8a and figure 4.8b, respectively. The number of micronized sand particle is larger in the mixture with the finer sand (higher specific surface) and vice versa. As shown in figure 4.8b, the interfacial zone can be connected more easily in the mixture with larger number of micronized sand. It gives higher opportunity to form a connected pore network. The fraction of interfacial

zone in the microstructure is thus quantitatively related to the micronized sand particles in the mixture.

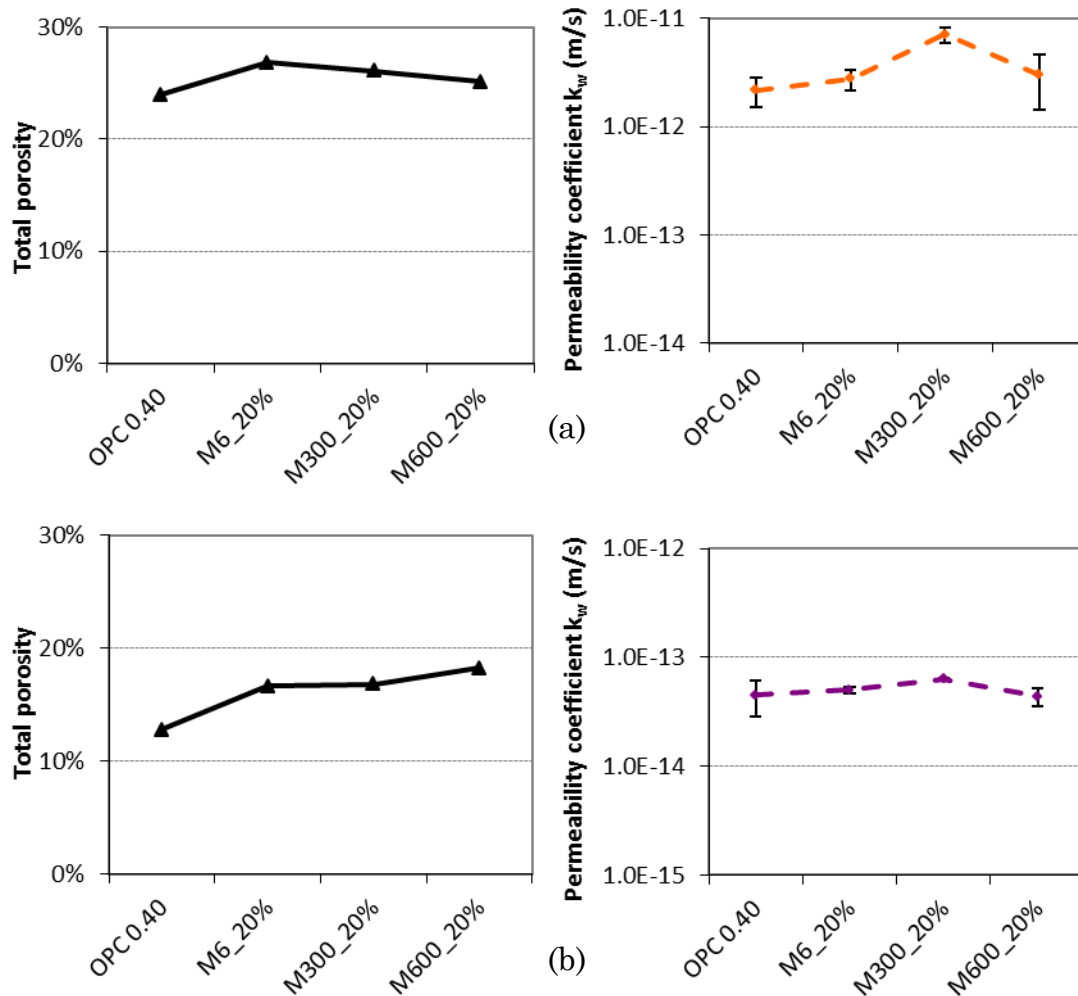


Figure 4.7. Total porosity and permeability coefficient of mixtures with 20% of micronized sand. (a) at the age of 28 days; (b) at the age of 90 days.

The experimental results in chapter 3 showed that the thickness of the interfacial zone is hardly depending on the fineness or replacement percentage of micronized sand. The width of the interfacial zone between micronized sand and bulk paste varies from 1 to 3 μm and mainly fluctuates around 2 μm at the age of 28 days. Small micronized sand particles can easily act as nucleation sites. Based on the observation from SEM images, the interfacial zone can be found exclusively around the micronized sand particles which are larger than 8 μm . In table 4.2, the numbers of M6, M300 and M600 particles in the mixtures are listed, which are calculated based on a unit mixture volume ($100 \times 100 \times 100 \mu\text{m}^3$). The fraction of particles larger than 8 μm in M6, M300 and M600 materials can be found from the particle size distribution of micronized sand as shown in figure 3.1. The volume of interfacial zone was estimated

with the hypothesis that the particles are spherical and the thickness of interfacial zone is 2 μm at the age of 28 days, 1.5 μm at the age of 90 days.

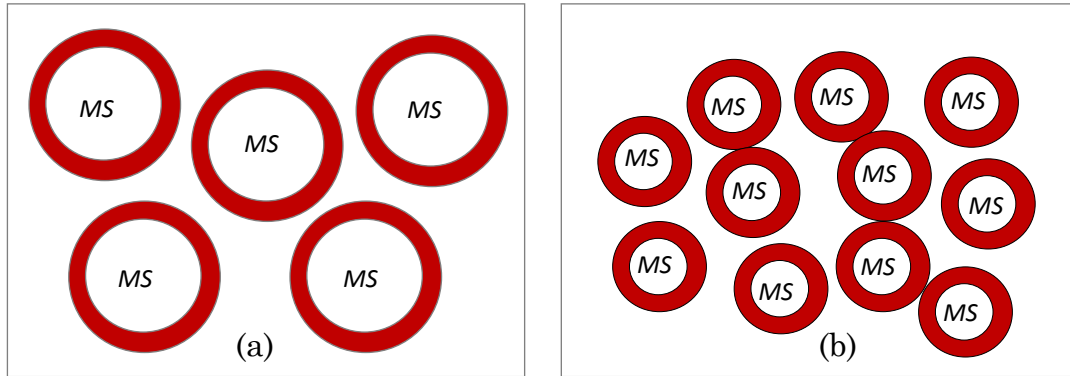


Figure 4.8. Schematic demonstration of the proportion of interfacial zone in the microstructure. a: cement paste blended with coarse micronized sand (MS); b: cement paste blended with fine micronized sand; ■ : the interfacial zone.

Table 4.2. Number of micronized sand (MS) particles and volume of interfacial zone ($100 \times 100 \times 100 \mu\text{m}^3$).

Sample	number of MS	number of MS ($\geq 8 \mu\text{m}$)	Volume of interfacial zone (μm^3)
M6_10%	1228	49	159400
M6_20%	2098	102	336868
M6_30%	2628	136	479358
M300_20%	2913	284	517558
M600_20%	8181	87	188153

The relation between the water permeability coefficient of the sample and the corresponding volume of interfacial zone can be found in figure 4.9 and figure 4.10. The values of permeability coefficients are in good agreement with the volume of interfacial zone in the corresponding samples. The number of filler particles is important to quantify the interfacial zone, which affects the connectivity of the pores in a significant way. If a sample blended with micronized sand has a higher fraction of the interfacial zone, indicating a higher connectivity of pores, the microstructure of the material is more permeable.

However, it is not easy to determine the connectivity from direct measurements or to reconstruct it from a two-dimensional representation of the microstructure (Navi and Pignat 1996). By means of numerical simulation, it is possible to model and visualize the cement hydration and microstructure development. Thus, the pore structure and the connectivity of the pores can be obtained depending on the simulated microstructure. Detailed information of simulated pore structures, the connectivity and transport properties will be analyzed and discussed in chapter 5.

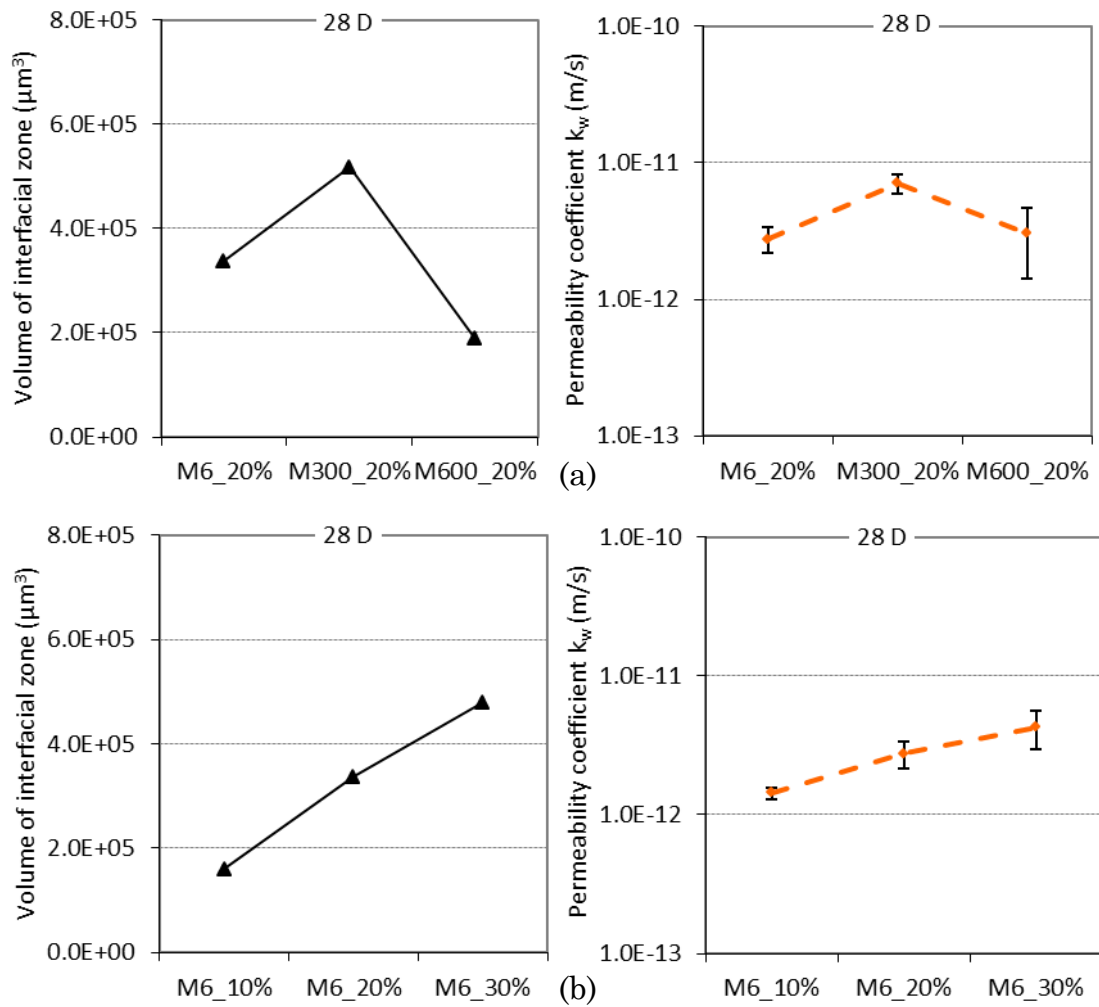


Figure 4.9. Water permeability coefficients in a relation with the volume of interfacial zone (28 days). (a) increasing replacement levels of coarse sand, M6; (b) 20% of micronized sand with different fineness.

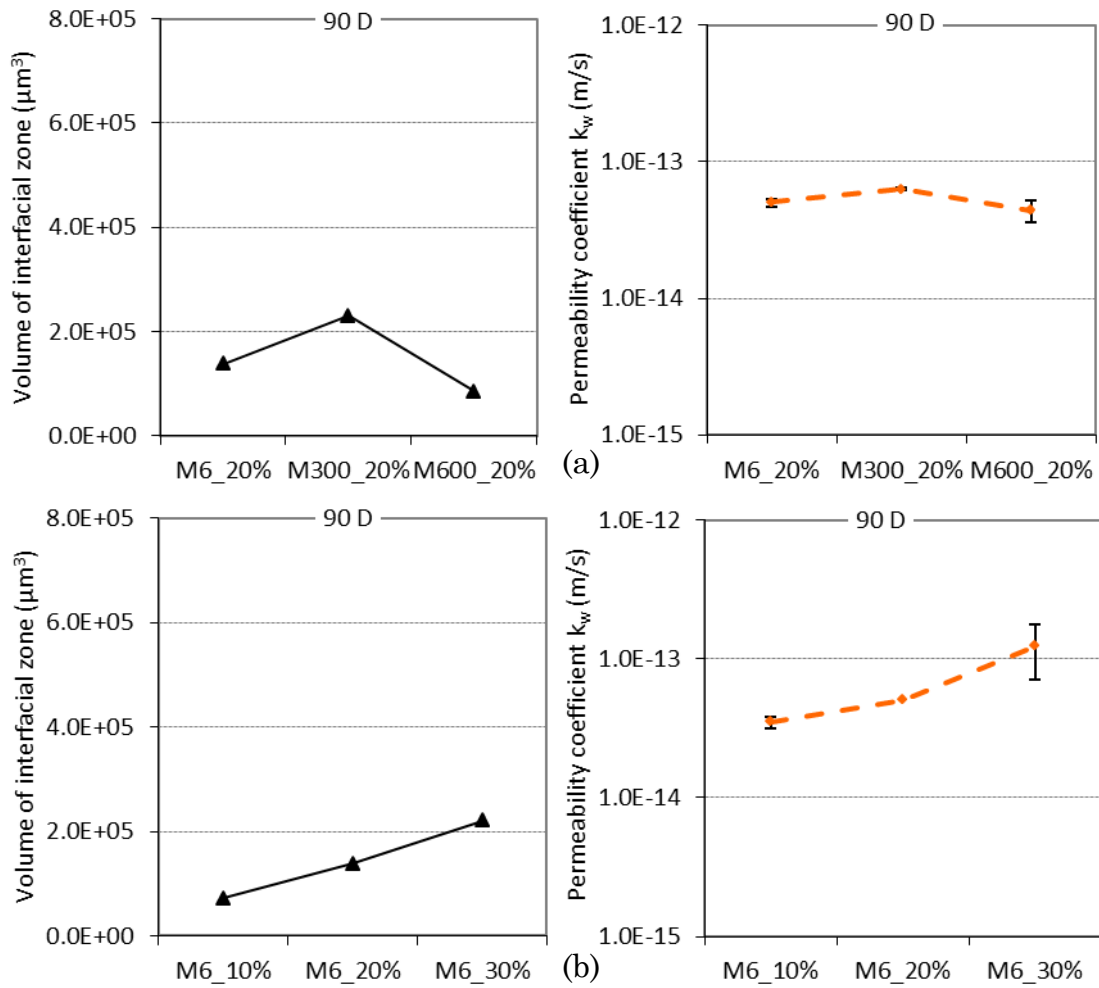


Figure 4.10. Water permeability coefficients in a relation with the volume of interfacial zone (90 days). (a) increasing replacement levels of coarse sand, M6; (b) 20% of micronized sand with different fineness.

4.3 Diffusivity

4.3.1 Mechanism

Chloride diffusivity is one of the most important properties of concrete affecting the durability of a structure (McNally, Richardson et al. 2005). Chloride ingress can initiate corrosion of reinforcement and hence reduce the service life of reinforced concrete structures (Richardson 2002; Neville 2006). The first step towards a better prediction of service life is a quantitative study of chloride transport (Francy and François 1998). Chloride diffusion is controlled by Fick's 2nd law (Neville 2006):

$$\frac{\partial C_x}{\partial t} = -\frac{\partial}{\partial x} \left[-D \frac{\partial C_x}{\partial x} \right] = D \frac{\partial^2 C_x}{\partial x^2} \quad (4.5)$$

where C_x = the concentration of chloride ions at a distance x from the reference point (mol/m^3);

t = time (s);

x = the position in the sample (m);

D = the diffusion coefficient for chloride ions (m^2/s).

4.3.2 Material and method

Samples prepared for studying chloride diffusivity are concrete blended with micronized sand. The results, i.e. diffusion coefficients, will show the influence of micronized sand as a substitute of cement on concrete and, more important, the values can be used as resistance of chloride in service life predictions in chapter 7.

The rapid chloride migration (RCM) test (NT BUILD 492 1999) is used for evaluating the resistance of concrete to chloride ingress. This procedure is to determine the chloride migration coefficient in cement-based materials from non-steady-state migration experiments.

The materials used for preparing concrete samples for RCM measurements are CEM I 42.5N, micronized sand and aggregates. The specimens used in this test were cast in a plastic cylindrical mould with a diameter of 100 mm. The mixture design for the concrete samples is presented in table 4.3. After casting, the samples were stored in a climate room at a temperature of 20°C and a relative humidity of 90% until the age for testing.

Table 4.3. Mix design for concrete specimens.

Sample	OPC (kg/m^3)	micronized sand (kg/m^3)	Water (kg/m^3)	Sand (0-4) (kg/m^3)	Gravel (4-16) (kg/m^3)	w/c	w/b
Ref	390	0	156	498	1103	0.40	0.40
M6_10%	351	39 (M6)	156	498	1103	0.44	0.40
M6_20%	312	78 (M6)	156	498	1103	0.50	0.40
M6_30%	273	117 (M6)	156	498	1103	0.57	0.40
M300_20%	312	78 (M300)	156	498	1103	0.50	0.40
M600_20%	312	78 (M600)	156	498	1103	0.50	0.40

After 28 days, 3 concrete samples with a thickness of 50 ± 2 mm were cut from the concrete cylinders. The samples were placed in vacuum container for vacuum treatment. The absolute pressure in the vacuum container was reduced to a pressure in the range of 10–50 mbar (1–5 kPa) within a few minutes. Then the vacuum was maintained for three hours and then, with the vacuum pump still running, the container was filled with the saturated $\text{Ca}(\text{OH})_2$ solution. The container was kept vacuum for another hour before allowing air to re-enter the container. The specimens were

kept in this solution for 18±2 hours (NT BUILD 492 1999). Then the specimens were considered saturated and ready for testing.

The experimental set-up of the RCM test is shown in figure 4.11 and 4.12. Under an external electrical potential, the chloride ions in the catholyte are forced to migrate into the specimen.

After a certain test duration (typically 24 hours), the specimen was axially split into two pieces and a 0.1 M silver nitrate solution is sprayed on the freshly split sections (figure 4.13a). The chloride penetration depth can then be measured from the white silver chloride precipitation (figure 4.13b), after which the chloride migration coefficient can be calculated from this penetration depth (Tang 2006). The procedure strictly follows the standard method NT BUILD 492.

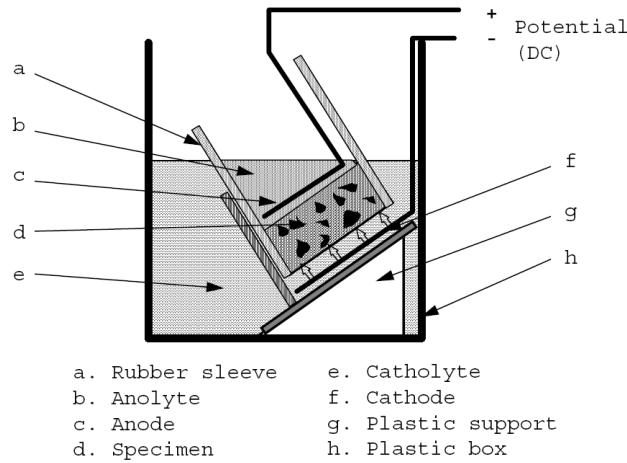


Figure 4.11. Rapid chloride migration test set-up (NT BUILD 492 1999).

The diffusion coefficient can be calculated according to:

$$D_{nssm} = \frac{0.0239(273+T)L}{(U-2)t} (x_d - 0.0238 \sqrt{\frac{(273+T)Lx_d}{U-2}}) \quad (4.6)$$

- where D_{nssm} = non-steady-state migration coefficient, $\times 10^{-12}$ (m²/s);
 U = absolute value of the applied voltage, (V);
 T = average value of the initial and final temperatures in the anolyte solution, (°C);
 L = thickness of the specimen, (mm);
 x_d = average value of the penetration depths, (mm);
 t = test duration, (hour).

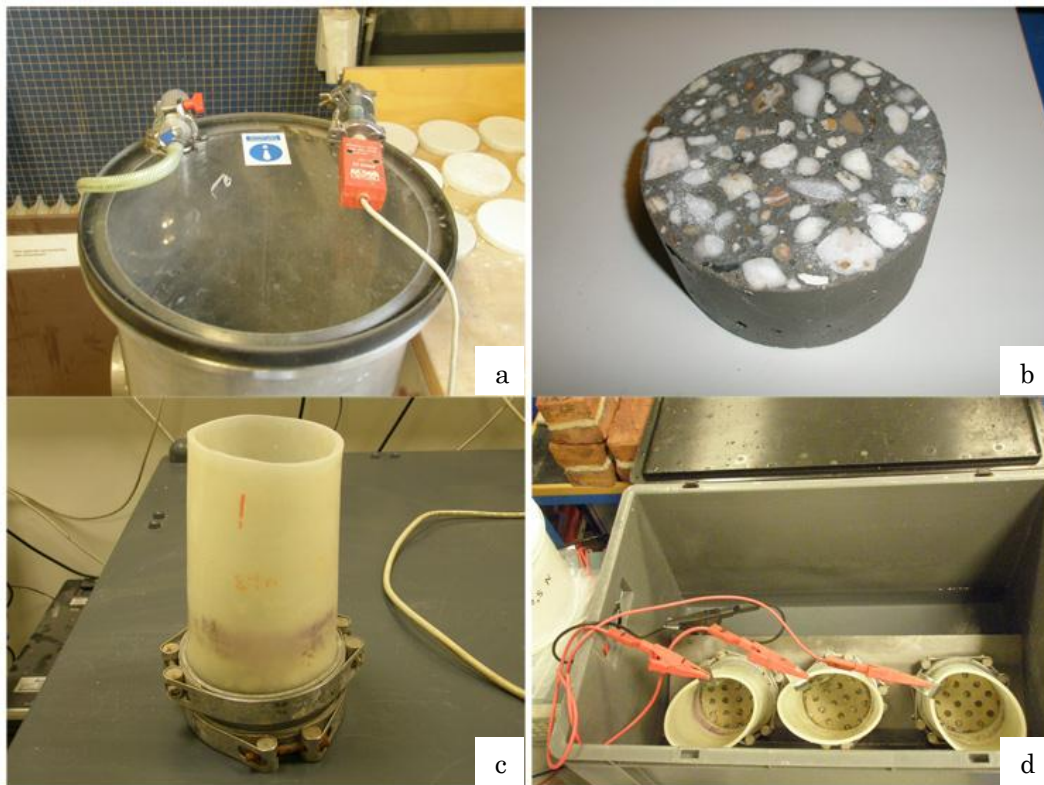


Figure 4.12. Setup and sample the experiments. (a) Vacuum container; (b) one sample; (c) sample with rubber sleeve set-up; (d) 3 parallel samples.

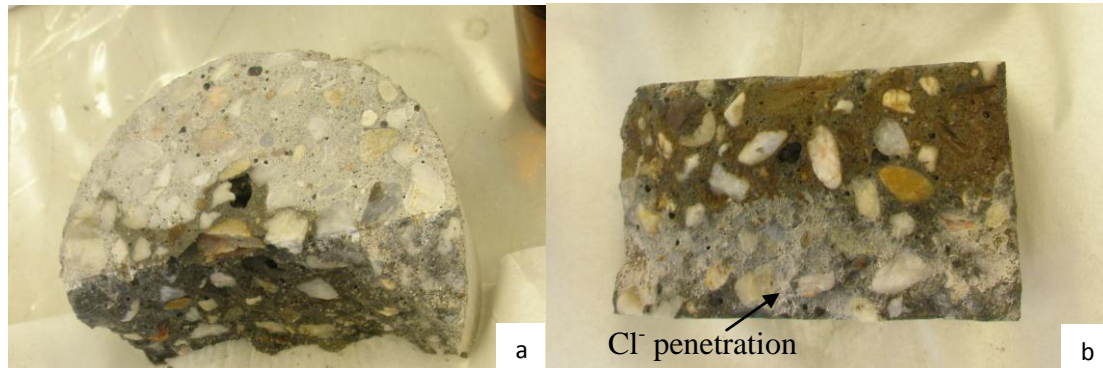


Figure 4.13. Samples after measurements. (a) split sample; (b) after spraying silver nitrate on the surface of section.

4.3.3 Results and discussions

Chloride diffusion coefficients of concrete were determined by eq. 4.6. The results of blended and reference samples are shown in figures 4.14 and 4.15.

In figure 4.14, the chloride diffusion coefficients of concrete blended with coarse micronized sand (M6) are shown as function of the replacement percentage. The diffusion coefficients are in the same order of magnitude,

between 1 and 3×10^{-11} m²/s, and increase with increasing amount of coarse micronized sand (M6) in the blended samples.

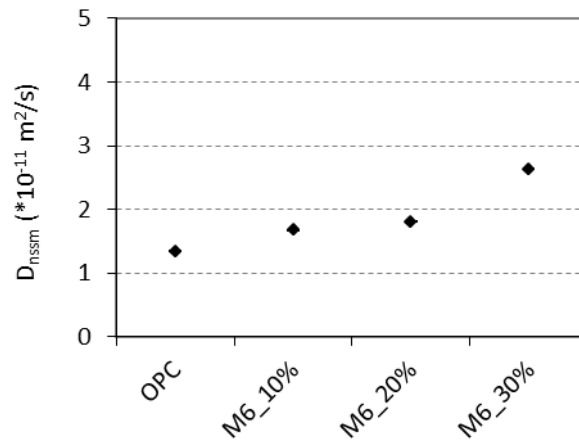


Figure 4.14. The chloride diffusion coefficients (D_{nssm} , $\times 10^{-11}$ m²/s) as a function of the replacement percentage of M6 (coarse) at 28 days.

The chloride diffusion coefficients of concrete blended with the same amount of micronized sand, but with different fineness, are shown in figure 4.15. The values from the measurements are in the same order of magnitude, i.e. 10^{-11} m²/s. There is no big difference between the blended samples with different fineness of the micronized sand. The effect of the fineness of micronized sand on the chloride diffusivity is not significant.

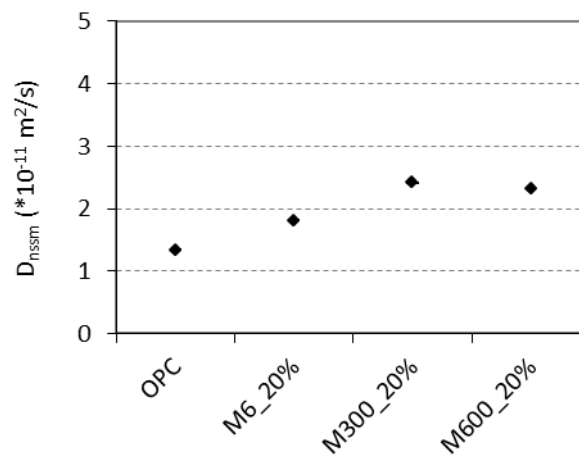


Figure 4.15. The chloride diffusion coefficients (D_{nssm} , $\times 10^{-11}$ m²/s) of concrete samples blended with micronized sand at 28 days.

In summary, the replacement percentage of micronized sand in the cement paste is up to 30%. In the concrete samples, the proportions of micronized sand in the mixtures are around 1.8%-5.4%. This small amount of micronized sand does not affect the diffusivity of the concrete significantly.

4.4 Summary

In this chapter, the transport properties of cement paste blended with micronized sand were studied. Water permeability coefficients of cement paste with micronized sand are compared with those of plain OPC paste. Chloride diffusion coefficients of concrete made with micronized sand were measured. Several conclusions can be drawn:

- After 90 days, with $w/b=0.4$, the permeability coefficients of the blended cement pastes were in the same order of magnitude as those of plain OPC paste. The permeability was hardly affected by the presence of micronized sand after long term.
- The connectivity of pores, represented by the volume of the interfacial zone in blended paste samples, strongly influences the material properties, particularly the permeability, which affects the resistance to harmful penetrants.
- The values of the chloride diffusion coefficients of OPC-based concrete and concrete blended with micronized sand, with replacement percentages from 10% to 30%, were in the same order of magnitude. These results will be used in the chapter 7 for service life prediction.
- The results of water permeability tests and chloride diffusivity tests show that the presence of micronized sand in the mixture, up to replacement percentages of 30%, does not change the long-term transport properties very much. The application of materials blended with the micronized sand is, therefore, very promising.

Chapter 5

Simulation of Microstructure of Cement Paste Blended with Micronized Sand

5.1 Introduction

In the previous chapters, the microstructure and the water permeability of cement paste blended with micronized sand were studied. It is not only difficult but also time and energy consuming to test long-term properties of materials by means of experiments. In addition, some characteristics of the pore structure cannot be determined by experiments easily. For instance, accurate information about the connectivity of the pores cannot easily be detected by MIP or by other direct means. Therefore, it is important to develop a numerical model to get knowledge of the properties which are not easy to get from experiments. Furthermore, it can provide information about the material at the micro-level. The understanding of the cement hydrations process and the formation of the pore structure in the blended samples may lead to the development of new materials with optimization, and broaden the range of applicability of cement-based materials.

In the past decade, some computer-based cement hydration models have been developed (Jennings and Johnson 1986; Bentz and Garboczi 1991; van Breugel 1991; Navi and Pignat 1996). These models are basically developed from two concepts. One is the spherical growth model (Jennings and Johnson 1986; van Breugel 1991; Navi and Pignat 1996). The other is the pixel-based model (Bentz and Garboczi 1991). In this chapter, HYMOSTRUC3D (van Breugel 1991; Koenders 1997; Ye 2003) is used and extended to simulate the development of hydration and microstructure of the material blended with micronized sand. Parameters, including the fineness and the replacement percentages of micronized sand, will be taken into account. Characteristics, including porosity, pore structure and pore connectivity etc., will be discussed. The obtained information about the microstructure will be validated by the results from experiments. The simulated microstructure can be used to study the connectivity of the pores and to predict water permeability.

5.2 HYMOSTRUC3D Simulation—incorporating micronized sand

5.2.1 HYMOSTRUC

HYMOSTRUC is the model first proposed by van Breugel (van Breugel 1991) in 1991 and further developed by Koenders (Koenders 1997) and Ye (Ye and van Breugel 2009). In this model the evolution of the degree of hydration (DOH) is simulated as a function of the particle size distribution and of the chemical composition of the cement, the water-cement ratio and the reaction temperature. The cement particles are modeled as spheres randomly distributed in a three-dimensional body and the hydrating cement grains are simulated as growing spheres. As cement hydrates, the cement grains gradually dissolve and a porous shell of hydration products is formed around the grain. This results in an outward growth, or "expansion", of the particles. The hydration products around the cement grains firstly cause the formation of small isolated clusters. Big clusters are formed when small cement particles become embedded in the outer shell of other particles, which promotes the outward growth of these particles (figure 5.1). As hydration progresses, the growing particles become more and more connected and the material changes from the state of a suspension to the state of a porous solid.

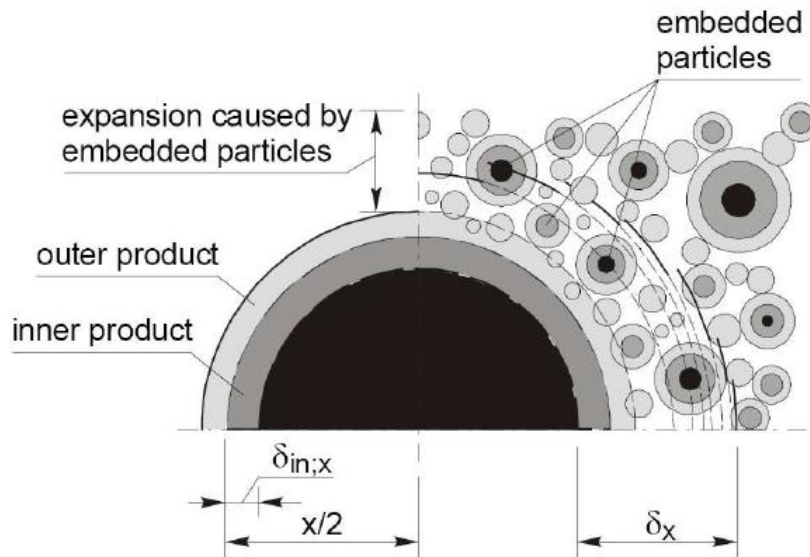


Figure 5.1. Principle of the basic HYMOSTRUC model. Interaction mechanism for expanding particles: free expansion and formation of inner and outer product (left); embedding of small particles (right) (van Breugel 1991; Ye and van Breugel 2009).

The hydration kinetics of a single particle, x , is described with a so called basic rate formula, giving the rate of penetration of the reaction front in an individual cement particle at time t_j :

$$\frac{\Delta\delta_{in,x,j+1}}{\Delta t_{j+1}} = K_0(\cdot) \cdot \Omega_1(\cdot) \cdot \Omega_2(\cdot) \cdot \Omega_3(\cdot) \cdot F_1(\cdot) \left[F_2(\cdot) \cdot \left(\frac{\delta_{tr}(\cdot)}{\delta_{x,j}} \right)^{\beta_1} \right]^\lambda \quad (5.1)$$

where $\Delta\delta_{in,x,j+1}$ = the increase of the penetration depth in time step Δt_{j+1} ;

Δt_{j+1} = the time step;

K_0 = the basic rate factor of the boundary reaction;

δ_{tr} = the transition thickness (μm);

$\delta_{x,j}$ = the thickness of the product layer at time t ;

Ω_i = the various effects of water withdrawal of particles in the shell of a central cement particle;

F_i = the influence of temperature of the hydration process;

λ = the factor depending on the rate-controlling mechanism, a boundary reaction ($\lambda=0$), or a diffusion controlled reaction ($\lambda=1$);

β_1 = an empirical constant.

The HYMOSTRUC model takes into account the effect of various parameters, such as chemical and mineralogical compositions of cement, size distribution of cement particles, water-cement ratio and temperature. In the HYMOSTRUC model the effect of physical interactions between hydrating cement particles on the rate of hydration of individual cement particles is taken into account explicitly. For the resulting, kinetic formula the term “integrated kinetic” was proposed. This integrated particle kinetics model will be applied to investigate the microstructure development, the effect of small inert grains on cement hydration, and the inter-particles contact surfaces (van Breugel 1991; Navi and Pignat 1996). For a complete description of the original HYMOSTRUC model, details can be found in (van Breugel 1991).

5.2.2 Extensions and modifications of HYMOSTRUC3D

The simulation of the hydration reaction and microstructure development of cement paste blended with micronized sand is based on the HYMOSTRUC3D. In the original HYMOSTRUC model, only plain cement paste is considered. In order to simulate the hydration reaction of blended cement paste, i.e. cement blended with micronized sand, some extensions and modifications are needed.

From previous chapters, the effects of micronized sand on the hydration development and the microstructure (Eff_{total}) can be summarized as: 1) the dilution effect ($Eff_{dilution}$) and 2) the heterogeneous nucleation effect ($Eff_{nucleation}$). Therefore, an extra amount of cement is hydrated at a certain time.

$$Eff_{total} = Eff_{dilution} + Eff_{nucleation} \quad (5.2)$$

The extensions and modifications of the simulation are carried while considering the following three aspects:

- *Stereological aspect.* The cumulative particle size distribution of micronized sand in the mixture is represented using Rosin-Rammler function.
- *Dilution effect of micronized sand.* If concrete is made with micronized sand-blended cement with a w/s similar to a w/c of plain concrete with no micronized sand, the effective w/c of the micronized sand-blended concrete is higher compared to that of a plain mixture. This will modify the hydration characteristics of the cement.
- *Heterogeneous nucleation effect of micronized sand.* As has been mentioned in chapter 2 and 3, heterogeneous nucleation effect of micronized sand has a significant effect on the development of microstructure.

The hydration kinetics of cement is generally divided into three stages: (1) an initial dormant period, (2) a phase boundary controlled stage, and (3) a diffusion-controlled stage. HYMOSTRUC cannot yet simulate the dormant period. Therefore, the model for the reaction of cement is assumed to consist of two processes – a phase boundary reaction process and a diffusion process (van Breugel 1991). Figure 5.2 shows the two phases in the hydration process.

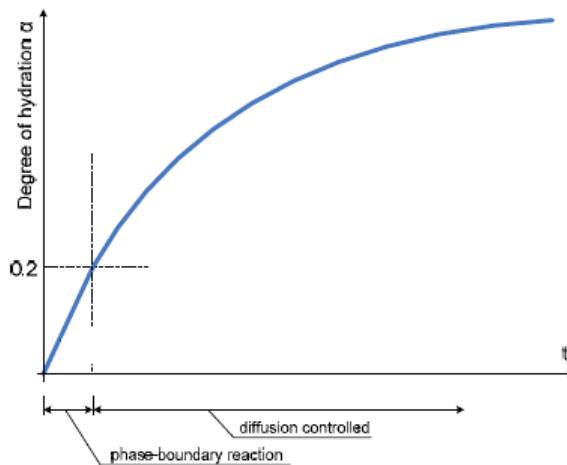


Figure 5.2. Two phases in the hydration process (NGUYỄN 2011).

Figure 5.3 shows the conditions of the hydration development of cement particle in the initial phase, the cement particle in the plain paste and the one in the blended paste with the presence of micronized sand. Apparently, the thickness of the hydrated layer formed around cement grains is reduced when micronized sand is used in the mixtures ($e > e'$). The cement

particles can be still in the boundary phase, rather than the diffusion-controlled phase. This leads to an enhancement of cement hydration.

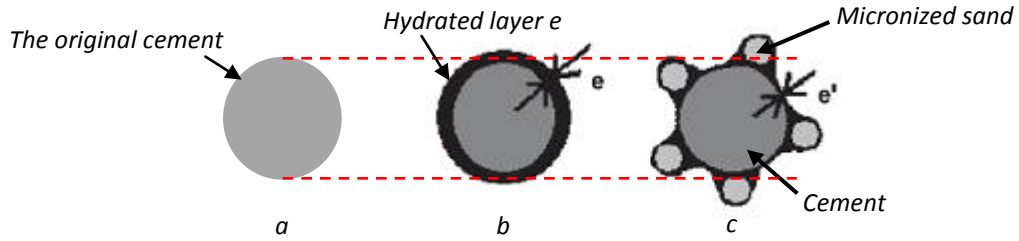


Figure 5.3. Schematic figure explaining the effect of micronized sand. a: cement particle at the initial stage; b: cement particle in the plain paste; c: the cement particle in the blended paste.

In the original HYMOSTRUC model, only cement particles were considered. In order to simulate the hydration of cement blended with micronized sand, the characteristics of the paste have to be modified.

Particle size distribution

The cumulative particle size distribution of micronized sand is described as that of cement particles which uses the Rosin-Rammler function:

$$G_{MS}(x) = 1 - \exp(-b_{MS} \cdot x^{n_{MS}}) \quad (5.3)$$

where $G_{MS}(x)$ = the under-size of micronized sand particles $<x$ μm ;
 b_{MS}, n_{MS} = Rosin-Rammler constants.

The micronized sand mass $W_{MS(x)}$ of the fraction $F_{MS(x)}$ is obtained with eq. 5.4:

$$W_{MS}(x) = \gamma \cdot b_{MS} \cdot n_{MS} \cdot x^{n_{MS}-1} \cdot e^{-b_{MS} \cdot x^{n_{MS}}} \quad (5.4)$$

where γ = a correction factor in order to establish the physical consistency of the Rosin-Rammler function disregarding particles $x < x_{\min}$ as well as particles $x > x_{\max}$ (van Breugel 1991).

For the volume $V_{MS, x}$ of micronized sand particles in fraction $F_{MS, x}$, it holds:

$$V_{MS, x} = \frac{W_{MS}(x)}{\rho_{MS}} \quad (5.5)$$

where ρ_{MS} = the specific mass of the micronized sand.

The number of particles $N_{MS,x}$ in fraction $F_{MS,x}$ is found by dividing the volume $V_{MS,x}$ of fraction $F_{MS,x}$ by the volume of a single spherical particles $v_{MS,x}$, with the diameter of x .

$$N_{MS,x} = \frac{V_{MS,x}}{v_{MS,x}} = \frac{\gamma \cdot b_{MS} \cdot n_{MS} \cdot x^{n_{MS}-1} \cdot e^{-b_{MS}x^{n_{MS}}}}{\frac{\pi \cdot x^3}{6} \cdot \rho_{MS} \cdot 10^{-12}} \quad (5.6)$$

Paste characteristics

The paste is considered to contain cement and micronized sand particles. Micronized sand ratio, p , is defined as the mass of micronized sand relative to the mass of the cement.

$$p = \frac{\text{mass of MS}}{\text{mass of cement}} \quad (5.7)$$

The w/b ratio, ω_b , is defined as:

$$\omega_b = \frac{\text{mass of water}}{\text{mass of binder}} = \frac{\text{mass of water}}{\text{mass of cement} + \text{mass of MS}} = \frac{m_w}{m_{cem} + m_{MS}} \quad (5.8)$$

The w/c ratio, ω_0 , can be expressed as a function of the w/b ratio, ω_b , and the micronized sand ratio, p (eq. 5.9):

$$\omega_0 = \omega_b \cdot (1 + p) \quad (5.9)$$

The specific mass ρ_{pa} of a paste blended with micronized sand with a w/c ratio, ω_0 , can be determined by dividing the mass of the water and binder, i.e. water, cement and micronized sand, by the volume of the paste.

$$\rho_{pa} = \frac{\rho_{cem} \cdot (1 + p + \omega_0)}{1 + \frac{\rho_{cem}}{\rho_{MS}} \cdot p + \frac{\rho_{cem}}{\rho_w} \cdot \omega_0} \quad (5.10)$$

ρ_{cem} , ρ_{MS} , ρ_w , are the specific mass of cement, micronized sand and water, respectively.

The (volumetric) density of the paste blended with micronized sand, ζ_{pa} , is defined as the volume of binder, V_b , relative to the volume of fresh paste, V_{pa} :

$$\zeta_{pa} = \frac{\text{volume of binder}}{\text{volume of fresh paste}} = \frac{1 + \frac{\rho_{cem}}{\rho_{MS}} \times p}{1 + \frac{\rho_{cem}}{\rho_{MS}} \times p + \frac{\rho_{cem}}{\rho_w} \times \omega_0} \quad (5.11)$$

Cell volume and cell density

In the original HYMOSTRUC model, a cell I_x^c is defined as a cubic space in which the largest cement particles has a diameter x , and the further consists of $1/N_{x;cem}$ times the original water volume and of $1/N_{x;cem}$ times the volume of all particles with diameter smaller than that of particle x . When the model incorporates micronized sand, the cell definition is determined as:

$$I_x^c = \frac{(V_w + V_{cem \leq x} + V_{MS \leq x})}{N_{cem,x}} \quad (5.12)$$

where V_w = the initial water volume;

$V_{cem \leq x}$ = cement volume of particles $\leq x$;

$V_{MS \leq x}$ = micronized sand volume of particles $\leq x$;

$N_{cem,x}$ = the number of cement particles in fraction $F_{cem,x}$.

The volumetric cell density is:

$$\zeta_x = \frac{\text{volume of binder in cell } I_x^c}{\text{volume of cell } I_x^c} = \frac{(V_{cem \leq x} + V_{MS \leq x}) \cdot N_{cem,x}^{-1}}{(V_w + V_{cem \leq x} + V_{MS \leq x}) \cdot N_{cem,x}^{-1}} \quad (5.13)$$

Shell density

The shell density of the binder, $\zeta_{sh;x,d_u}$, is defined as the binder volume in a spherical shell with thickness d_u relative to the total shell volume.

$$\zeta_{sh;x,d_u} = \frac{\text{binder volume in spherical shell with thickness } d_u}{\text{total shell volume}} = \frac{\zeta_x \cdot I_x^c - v_x}{I_x^c - v_x} \quad (5.14)$$

Interaction mechanisms

The sample structure is defined as a closed medium with finite volume ($100 \times 100 \times 100 \mu\text{m}^3$), which is filled with cement and micronized sand particles. If the water-binder ratio (w/b), the micronized sand content and the particle size distribution are known, the particle structure can be determined. In the blended sample, the micronized sand percentage is interpreted as a percentage relative to the amount of binder. If particles

overlap, the current position is erased and a new random position is determined until the particle is placed correctly. If particles cross the boundary surface of the cube, an additional particle will be placed at the opposite of the position of the current particle, with respect to the center of the cube (periodic boundary conditions). In this way, boundary effects at the surface of the cube are negligible.

Unlike cement particles, the micronized sand will not expand during hydration. When the hydrating expanding cement grains meets the micronized sand particles, the overlapping volume is smeared out around the outer shells of the expanding cement particle.

Particle expansion during hydration

At a particular time, i.e. $t=t_j$, the DOH of the central cement particle is $\alpha_{x,j}$. The corresponding penetration depth $\delta_{in;x,j}^{cem}$ of cement is:

$$\delta_{in;x,j}^{cem} = \left(\frac{x}{2}\right) \cdot \left[1 - (1 - \alpha_{x,j})^{\frac{1}{3}}\right] \quad (5.15)$$

The volume of the outer product $V_{ou;x,j}^{cem}$ for the cement particle x , that corresponds to the DOH $\alpha_{x,j}$ of particle x is:

$$V_{ou;x,j}^{cem} = (v^{cem} - 1) \cdot \alpha_{x,j} \cdot V_x^{cem} \quad (5.16)$$

with v the ratio between the volume of reaction products and the reactant.

The outer radius of the expanding central cement particle is:

$$R_{ou;x,j}^{cem} = \left[\frac{V_{ou;x,j}^{cem}}{\frac{4\pi}{3}} + \left(\frac{x}{2}\right)^3 \right]^{\frac{1}{3}} \quad (5.17)$$

For the thickness $\delta_{ou;x,j}^{cem}$ of the outer shell, it follows:

$$\delta_{ou;x,j}^{cem} = R_{ou;x,j}^{cem} - \frac{x}{2} \quad (5.18)$$

The volume of expanded outer shell follows from:

$$V_{ou,ex;x,j}^{cem} = \frac{V_{ou;x,j}^{cem}}{1 - \zeta \left(\chi \delta_{ou;x,j}^{cem} \right) \left[(1 - v_{MS}) \cdot (1 + (v_{cem} - 1) \cdot \alpha_{<x,j}) + v_{MS} \right]} \quad (5.19)$$

where v_{MS} = the volume percentage of micronized sand ($v_{MS} = V_{MS} / (V_{cem} + V_{MS})$).

v_{cem} = the volume percentage of cement ($v_{cem} = V_{cem} / (V_{cem} + V_{MS})$).

The outer radius of the expanded outer shell can be written as:

$$R_{ou,ex;x,j}^{cem} = \left[\frac{V_{ou,ex;x,j}^{cem}}{\frac{4\pi}{3}} + \left(\frac{x}{2} \right)^3 \right]^{\frac{1}{3}} \quad (5.20)$$

The total volume of all the embedded particles is:

$$V_{em;x,j}^{cem,t} = V_{ou,ex;x,j}^{cem} - V_{ou;x,j}^{cem} \quad (5.21)$$

The original volume of embedded cement particles follows from:

$$V_{em;x,j}^{cem,0} = \frac{(1 - v_{MS}) \cdot V_{em;x,j}^{cem,t}}{\left[(1 - v_{MS}) \cdot (1 + (v_{cem} - 1) \cdot \alpha_{<x,j}) + v_{MS} \right]} \quad (5.22)$$

The original volume of embedded micronized sand is:

$$V_{em;x,j}^{MS,0} = \frac{v_{MS} \cdot V_{em;x,j}^{cem,t}}{\left[(1 - v_{MS}) \cdot (1 + (v_{cem} - 1) \cdot \alpha_{<x,j}) + v_{MS} \right]} \quad (5.23)$$

Embedded and Free Particles

The ratio, $\lambda_{z,j}^{cem}$, between the embedded cement volume and the cement volume of all particles smaller than z (μm) at time t_j follows from:

$$\lambda_{z,j}^{cem} = \frac{V_{em;z,j}^{cem,0}}{\frac{(1 - m_{MS}) \cdot G_{cem}(z - 1)}{\rho_{cem}}} \quad (5.24)$$

The number of cement particles $n_{em;z,j}^{cem}$ with particle diameter x embedded in the outer shell of particle $z \geq x$ at time t_j is:

$$n_{em,x;z,j}^{cem} = \lambda_{z,j}^{cem} N_x^{cem} = \frac{V_{em;z,j}^{cem,0}}{(1 - m_{MS}) \cdot G_{cem}(z - I)} \cdot N_x^{cem} \quad (5.25)$$

ρ_{cem}

The number of cement particles $\Delta N_{em,x;z,j}^{cem}$ belonging to fraction F_x and embedded in the outer shells of the free particles of the fraction F_z is:

$$\Delta N_{em,x;z,j}^{cem} = n_{em,x;z,j}^{cem} \cdot N_{z,fr}^{cem} \quad (5.26)$$

For the number of cement particles with diameter x embedded in the outer shells of all free cement particles $z \geq x$, it follows:

$$N_{em,x;j}^{cem} = \sum_{z=x+1}^{x_{max}} \Delta N_{em,x;z,j}^{cem} \quad (5.27)$$

The number of free cement particles, or free clusters, $N_{x,fr,j}^{cem}$, in fraction F_x with central particle x at time t_j is

$$N_{x,fr,j}^{cem} = N_x^{cem} - N_{em,x;j}^{cem} \quad (5.28)$$

Degree of Hydration (DOH)

The increase of the DOH $\Delta \alpha_{x,j}$ of particle x that corresponds to an increase of the penetration depth $\Delta \delta_{x,j}$ in particle x during Δt_j follows from:

$$\Delta \alpha_{x,j} = \left[1 - \frac{2\delta_{x,j-1}^{cem}}{x} \right]^3 - \left[1 - \frac{2(\delta_{x,j-1}^{cem} + \Delta \delta_{x,j})}{x} \right]^3 \quad (5.29)$$

For the DOH of particles x , i.e. fraction F_x , at time t_j is:

$$\alpha_{x,j} = \sum_{i=1}^j \Delta \alpha_{x,i} \quad (5.30)$$

The DOH of the cement in a cell I_x follows from adding up the hydrated cement volume in fractions $F_z < F_x$ and dividing the sum by the original amount of cement in the cell:

$$\alpha_{\leq x,j} = \frac{1}{(1 - m_{MS}) \cdot G_{cem}(x - I)} \sum_{z=x_{min}}^{x-1} \alpha_{z,j} \cdot (1 - m_{MS}) \cdot W_{cem}(z) \quad (5.31)$$

The overall DOH of a cement paste blended with micronized sand is:

$$\alpha_j = \frac{1}{(1 - m_{MS}) \cdot G_{cem}(x_{max} - 1)} \sum_{z=x_{min}}^{x_{max}-1} \alpha_{z,j} \cdot (1 - m_{MS}) \cdot W_{cem}(z) \quad (5.32)$$

5.2.3 Short summary

In section 5.2.2 modifications of the HYMOSTRUC3D model have been developed in order to simulate the hydration process and the microstructural development of cement pastes blended with micronized sand. As the micronized sand is considered as inert, it is represented by a non-reacting particle in the model. Simulations have been executed in which a certain percentage by weight of the cement is replaced by inert micronized sand. In the next paragraph, the simulated microstructure of the blended pastes is compared with the reference OPC paste.

5.3 Simulation Results and Validation

In this section, the simulation results for cement blended with micronized sand are discussed and compared with experimental results.

5.3.1 Input parameters

In tables 5.1, 5.2 and 5.3, properties of materials and the parameters needed in the HYMOSTRUC3D are listed. The mixture composition is shown in table 3.6. The size of the simulated cubic cement paste volume is $100 \times 100 \times 100 \mu\text{m}^3$. The total number of distributed cement particles and micronized sand particles in the cube are listed in table 5.4.

5.3.2 Simulation results

5.3.2.1 Degree of hydration (DOH)

The DOH of cement in the paste system simulated with HYMOSTRUC is presented in figure 5.4. The simulated results are compared with the values derived from measured by non-evaporable water content (discussed in chapter 3). The simulated results were in good agreement with the experiments.

5.3.2.2 Porosity

The simulated porosity of the paste at the age of 28 days is compared with the results from SEM image analysis in table 5.5. The values from these two methods show the same tendency. The porosity of the samples decreases with increasing fineness of micronized sand in the blended

samples. Compared with the reference OPC paste sample, the samples blended with micronized sand have higher porosity.

Table 5.1. The properties of cement CEM I 42.5N.

<i>Chemical composition</i>	<i>Percentage by weight</i>
CaO	63.96
SiO ₂	20
Al ₂ O ₃	4.88
Fe ₂ O ₃	3.36
SO ₃	2.4

<i>Mineral composition</i>	<i>Percentage by weight</i>
C ₃ S	62
C ₂ S	10.5
C ₃ A	7.3
C ₄ AF	10.2

<i>Particle size distribution</i>	<i>Value</i>
n	1.076
b	0.041
fineness, [cm ² /g]	4200
D _{max} , [μm]	50
D _{min} , [μm]	1

Table 5.2. The properties of micronized sand.

<i>Particle size distribution</i>	<i>M6</i>	<i>M300</i>	<i>M600</i>
n	1.065	1.016	1.108
b	0.017	0.051	0.212
fineness, [cm ² /g]	2400	4000	13000
D _{max} , [μm]	50	50	20
D _{min} , [μm]	1	1	1

Table 5.3. Other values.

<i>Other parameters</i>	<i>Value</i>
Specific gravity of cement (ρ_{cem}), [kg/m ³]	3150
Specific gravity of micronized sand (ρ_{MS}), [kg/m ³]	2650
w/p	0.40

Table 5.4. The number of cement and micronized sand particles distributed in the cube of $100 \times 100 \times 100 \mu\text{m}^3$.

Sample	Cement	Micronized sand
OPC	137190	0
M6_20%	110749	25768
M300_20%	110749	42526
M600_20%	109833	131482
M6_10%	122939	16471
M6_30%	97054	28981

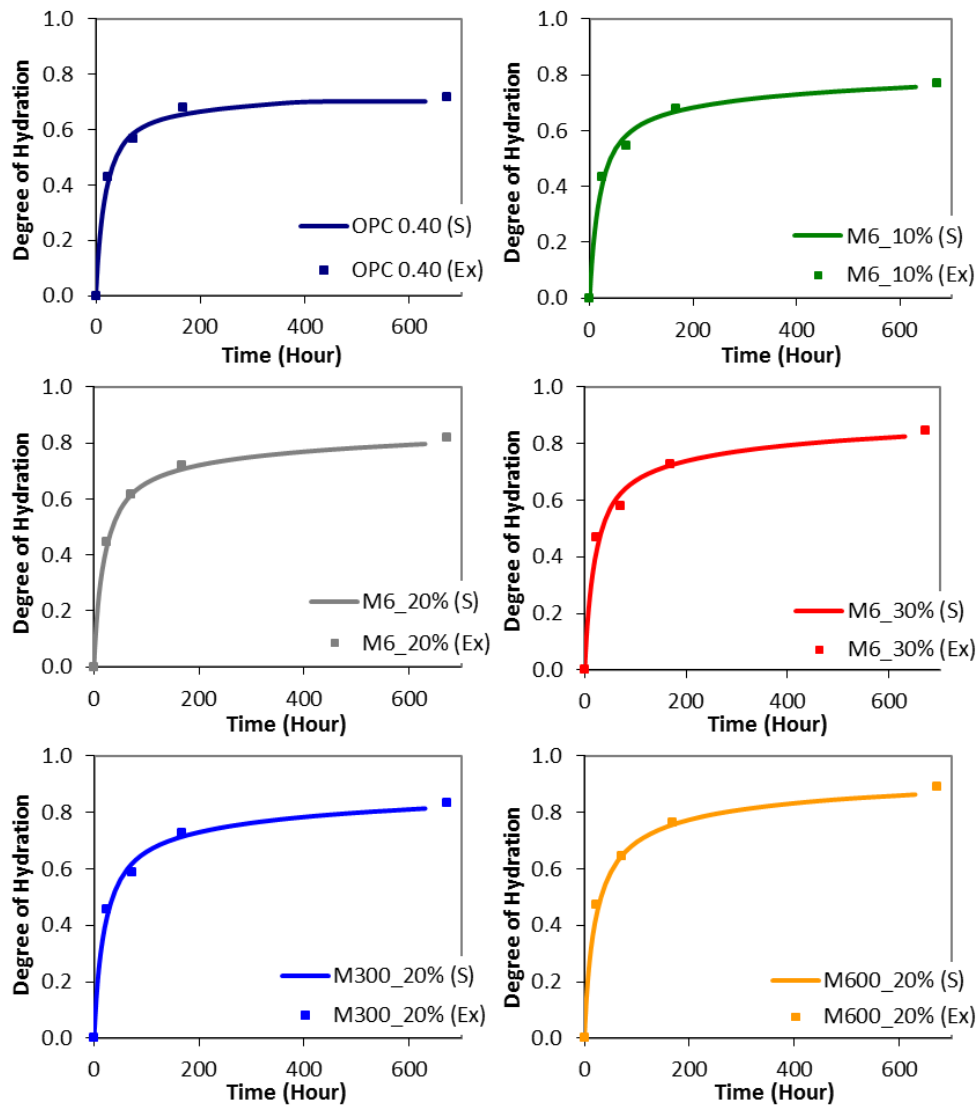


Figure 5.4. Degree of hydration of cement as a function of time with the mixture design shown in table 3.6 (S: simulation; Ex: experiment.).

Table 5.5. Comparison of porosity obtained from numerical simulation with the HYMOSTRUC3D model and the experimental values from SEM image analysis.

Porosity	28 days	
	Image analysis (SEM)	Simulation
OPC	9.90%	10.62%
M6_20%	15.60%	12.9%
M300_20%	13.90%	11.2%
M600_20%	11.70%	10.8%

The results from the simulation are slightly lower than those obtained from image analysis. The experimental results were obtained from 2D images, whereas the simulated results were derived from the 3D structure. The resolutions used in the SEM images and the simulated structures were 5.6 pixel/ μm and 1 pixel/ μm , respectively. Some pores are neglected because of the lower resolution in the simulation.

The simulated capillary porosities are plotted in figure 5.5 for the samples with different micronized sand contents. The capillary porosity decreases with the increase of degree of hydration. For a given degree of hydration, the porosity is larger for the paste with higher micronized sand content, which can be attributed to the higher effective w/c in the paste.

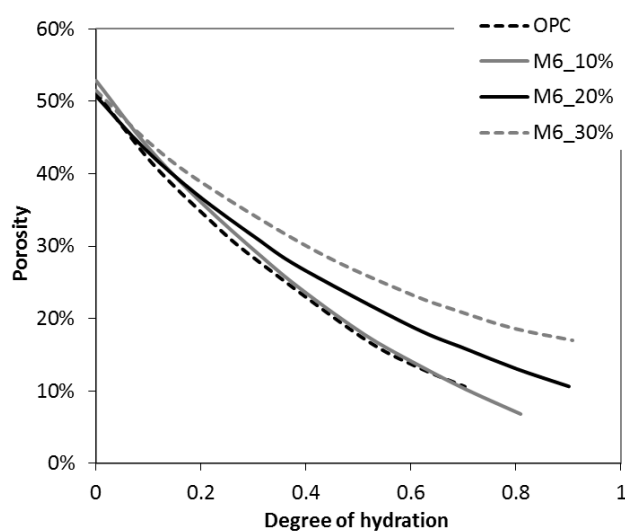


Figure 5.5. Simulated capillary porosity as a function of degree of hydration ($w/b=0.40$).

5.3.2.3 Visualization of microstructure

From the simulated microstructures, information can be inferred about details of the pore structure. The blended samples with 10% to 30% micronized sand in the system were compared with the reference OPC paste.

a. Microstructure of the samples at the age of 28 days

The simulated microstructures of samples at the age of 28 days are shown in figure 5.6. The samples made with blended material are compared with reference OPC paste samples. Micronized sand particles are represented by the grey spherical particles with no shell of inner or outer product.

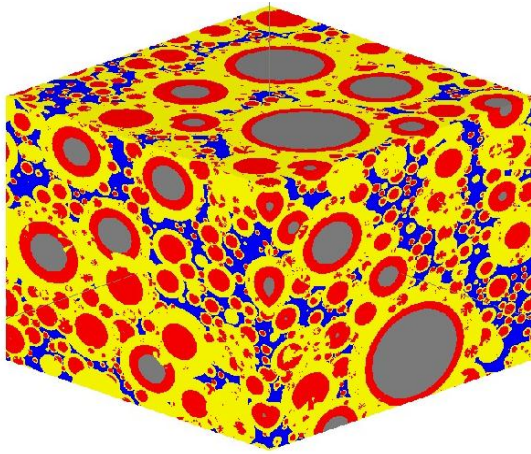
It can be seen that at the same age, the outer shell of expanding central cement particles (represented by the yellow part) in the blended samples is larger (cement particles in figure 5.6 b, c, d, e and f) than the one in the reference sample (cement particles in figure 5.6 a). This shows that the cement particles in the blended paste have a higher degree of hydration.

The microstructure is more porous when the amount of M6, coarse sand, applied in the system is higher (in figure 5.6 e, b and f). In the blended sample blended with 30% of M6 (f) the amount of hydration products is lower compared to the reference paste. The amount of cement is decreased because of the replacement of micronized sand. That substantially increases the effective w/c ratio, resulting in the more porous microstructure.

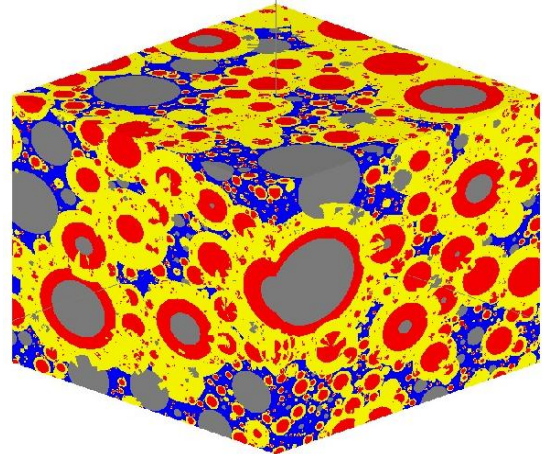
b. Experimental results from SEM images

A comparison of the 2D images obtained from the numerical simulation and SEM images is given in figure 5.7. The left one presents the simulated microstructure at a DOH of 0.72, achieved at the age of 28 days. The one on the right shows the SEM image of M6_20% paste at the age of 28 days. Different grey levels represent different phases in the paste bulk (referred to figure 3.3). From figure 5.7a it can be seen that the porosity around the micronized sand particles is much higher than the porosity around hydrated cement particles. This is consistent with the SEM image of figure 5.7b showing a quite porous interface area between micronized sand and hydration products. From this point of view, the simulation represents the real microstructure quite reliably.

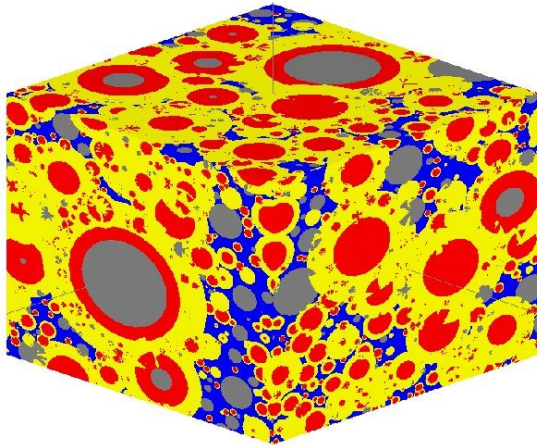
a: OPC



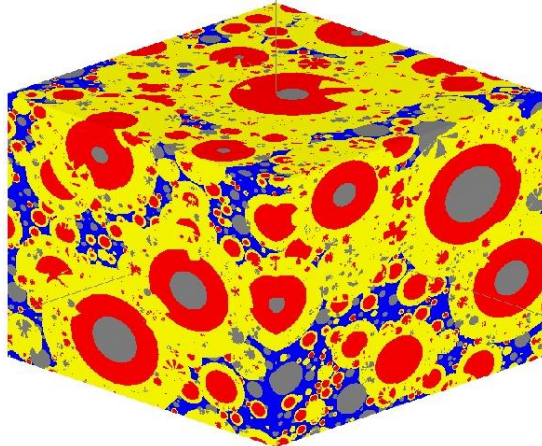
b: M6_20%



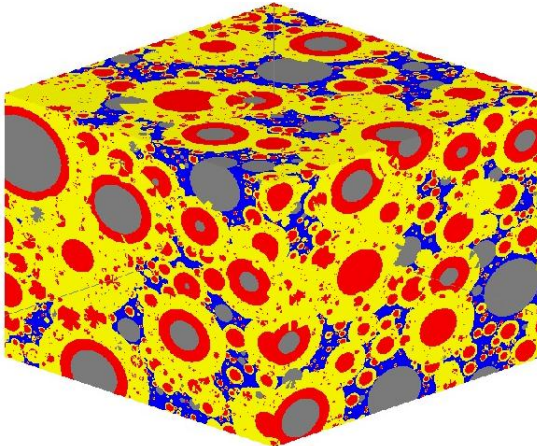
c: M300_20%



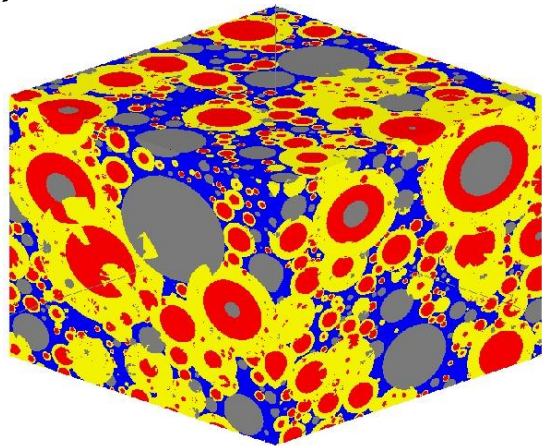
d: M600_20%



e: M6_10%



f: M6_30%



<div style="display: inline-block; width: 15px; height: 15px; background-color: grey; border: 1px solid black; margin-right: 5px;"></div> Unhydrated cement/micronized pores	<div style="display: inline-block; width: 15px; height: 15px; background-color: yellow; border: 1px solid black; margin-right: 5px;"></div> Outer product
<div style="display: inline-block; width: 15px; height: 15px; background-color: red; border: 1px solid black; margin-right: 5px;"></div> Inner product	<div style="display: inline-block; width: 15px; height: 15px; background-color: blue; border: 1px solid black; margin-right: 5px;"></div> Capillary

Figure 5.6. Simulated microstructures at the hydration age of 28 days ($w/b=0.4$).

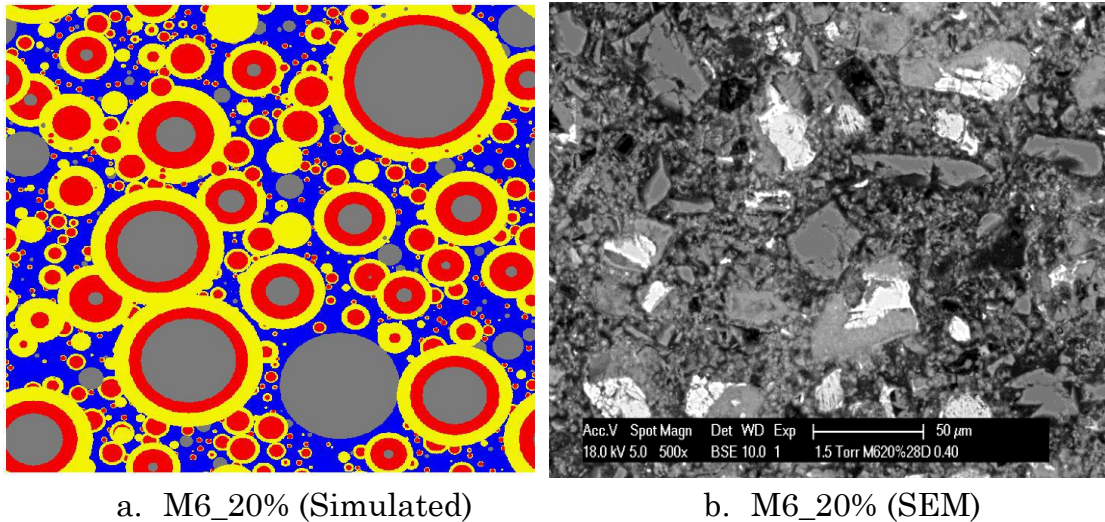


Figure 5.7. 2D picture of microstructure at the DOH of 0.72 (a). BSE image at 28 days (b). ($w/b=0.40$)

5.3.3 Summary

In this section, the HYMOSTRUC3D model has been modified and extended in order to simulate the microstructure of cement paste blended with micronized sand. The development of microstructure and the hydration process of cement blended with micronized sand were compared with the one of plain cement paste. Furthermore, the results from the simulation were compared with the experimental data. From the comparison it could be concluded that the simulated microstructure exhibited similar characteristics as obtained in SEM pictures. Based on the generated microstructures, some properties of the pore structure can be studied: the connectivity of pores can be analyzed and the water permeability of material can be predicted.

One thing needed to point out is that the minimum of particles was assumed as 1 μm for all the materials. Particles smaller than 1 μm were not considered. For M600 filler, 20% of the particles are smaller than 1 μm . The assumption would affect the simulated results of M600_20%. The real microstructure could be denser than the simulated one because the small particles can fill up the void and act as nucleation sites. This is the limitation of HYMOSTRUC which should be improved later.

5.4 Studies Based on the Simulated Microstructure of Cement Paste Incorporating Micronized Sand

5.4.1 Connectivity of pores calculated based on the simulated microstructure

Aside from porosity, the connectivity of pores is important pore structure characteristics of cement-based materials to understand better the effect

of microstructure on transport processes (Bentz 2008). However, the connectivity of pores is not easy to measure experimentally. From a simulated microstructure, however, it is possibility to get at least some information about this feature. The microstructures of cement paste and pastes blended with micronized sand were generated with HYMOSTRUC3D. The information of the pore structure will be input in a program, named Perc_3D (Zhang, He et al. 2011), to calculate the amount of connected pores in the system. The connectivity of pores can be obtained (eq. 5.33)

$$\text{Connectivity of pores } (C) = \frac{\text{Connected pore volume}}{\text{Total pore volume}} \quad (5.33)$$

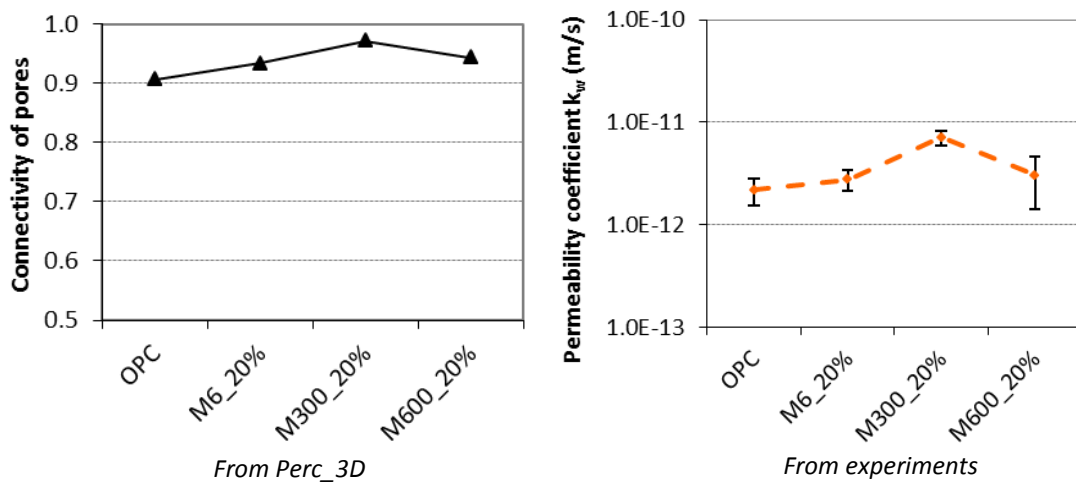


Figure 5.8a. Connectivity of pores and water permeability coefficients of mixtures with 20% replacement of micronized sand (M6, M300 and M600) at age of 28 days.

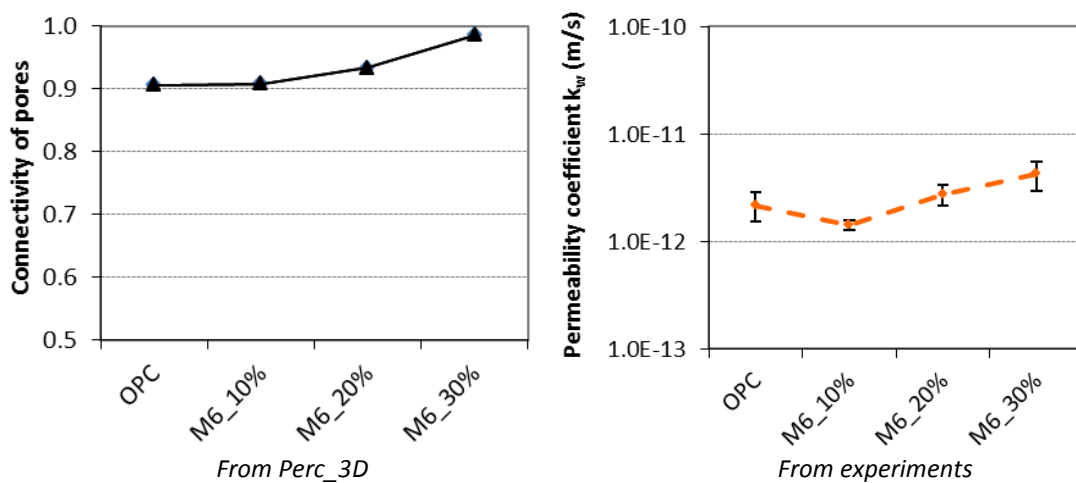


Figure 5.8b. Connectivity of pores and water permeability coefficients of mixtures with different replacement percentages of M6 (10%, 20% and 30%) at age of 28 days.

Water permeability coefficients, k_w , of different mixtures determined from experiments (chapter 3) and the connectivity of pores from simulated microstructures of the samples are shown in figure 5.8. The curve of the connectivity of pores is similar to the curve of the water permeability coefficients. From this observation it can be concluded that the proposed connectivity parameter C appears to be a good parameter for indicating the permeability.

5.4.2 Water permeability coefficients calculated from the simulated microstructure

The simulated 3D microstructure of the reference and the blended cement pastes, consisting of capillary pores, hydration products and unhydrated cement particles, serves as the base for the calculation of the permeability coefficients. For that purpose a program developed by Zhang and Ye (Zhang, Ye et al. 2011) will be used. This program is based on the Lattice Boltzmann method (Kutay, Aydilek et al. 2006). Except capillary pores, all other components of the microstructure are considered as impermeable solid.

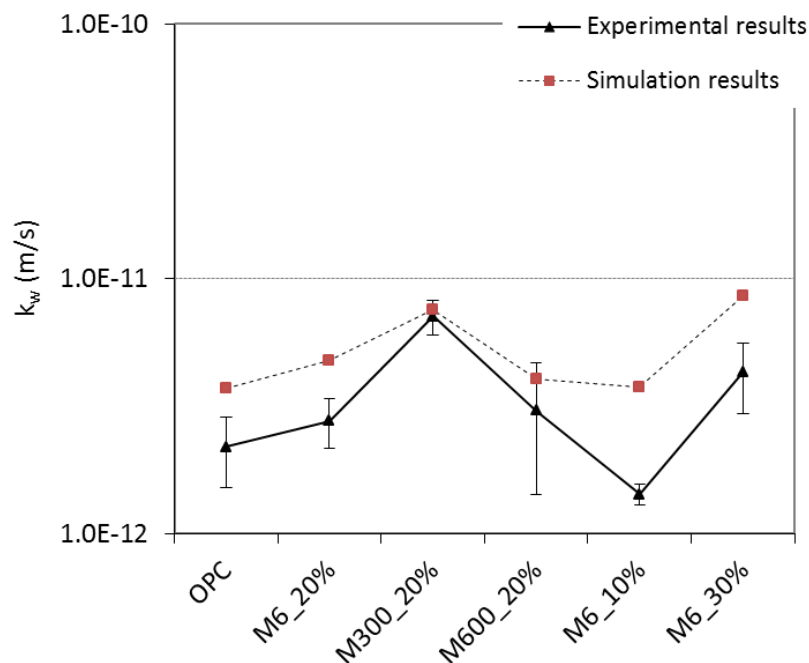


Figure 5.9. Simulated water permeability coefficients compared with the experimental results (samples are at the age of 28 days with w/b of 0.40).

The values obtained from simulations are compared with the experimental results and are shown in figure 5.9. The simulated results have the same order of magnitude as the experimental values and exhibit the same tendency. The simulated results show a bit higher values in comparison with the experimental data. For the experiments, it usually takes several days to get stable and reliable results. During this period, the hydration

process is still continuing and the microstructure is getting denser. After reaching the stable stage, the results are actually the ones of the cement pastes with older age and denser microstructure than those they represent. The simulated results of the samples, however, exactly represent the certain test age. Therefore, the results from experiment are lower than the simulated ones.

5.4.3 Short summary

The microstructure of cement paste blended with micronized sand can be simulated by the modified HYMOSTRUC3D model. The simulated microstructure was used for a quantitative evaluation of the connectivity of the capillary pores and the permeability. The predicted water permeability coefficients were in good agreement with the experimental results.

5.5 Summary

In this chapter, the HYMOSTRUC3D model has been modified and extended in order to simulate the microstructure of cement paste incorporating micronized sand. The most relevant conclusions of this chapter are:

- The effect of micronized sand on the hydration process is divided into 2 parts, viz.: the dilution effect and the heterogeneous nucleation effects. They are related to the replacement level and fineness of micronized sand, respectively.
- The simulated degree of hydration and porosity were compared with experimental results. The simulated results were in good agreement with these experimental results.
- The connectivity of pores and the water permeability coefficients were calculated. The connectivity of pores inferred from the simulated microstructure exhibited a strong correlation with the transport property. The simulated results of the water permeability coefficients were in good agreement with the experimental results. From these studies, the microstructures of cement paste blended with micronized sand can be simulated by the modified and extended HYMOSTRUC3D model. The simulated microstructures are important to predict material properties.

Chapter 6

Optimization of Cement-based Material Blended with Micronized Sand

6.1 Introduction

Based on the results from the previous chapters, micronized sand as a replacement material has two effects on the hydration of cement-based material. One is “dilution effect” which mainly depends on the replacement percentage of micronized sand and results in more porous microstructure. The other is “heterogeneous nucleation effect” which largely depends on the fineness of the micronized sand and accelerates the cement hydration reaction.

In the previous chapters it was shown that the porosity of cement paste blended with micronized sand was a bit higher than that of the reference OPC paste. The water permeability coefficients of the blended materials were slightly higher, but in the same order of magnitude as that of the reference OPC paste. In chapter 5 with the numerical simulation approach, microstructures of blended samples were generated. The water permeability was estimated based on the generated microstructures. On the basis of experimental work and numerical simulations, the mixture designs of cement paste incorporating micronized sand will be studied in this chapter. Cement will be replaced by one or/and two types of micronized sand, i.e. fillers with different fineness, in order to achieve to the optimal packing system. Properties, including the microstructure and permeability of the blended materials will be evaluated.

6.2 Optimum Packing Systems

In chapter 2 it has been mentioned that the inter-granular voids in the mixture can be reduced by adding smaller size particles (figure 6.1). Fillers finer or coarser than cement particles can widen the overall particle size distribution (PSD) and improve the packing density. The improved packing density can have positive effects on several material properties, such as workability, strength and durability (de Larrard 1989; Lange, Mörtel et al. 1997; Bentz, Garboczi et al. 1999; Zhang, Yu et al. 2011; He 2012). The optimum packing in cement-based material is referred to the densest possible packing of the dry mix.

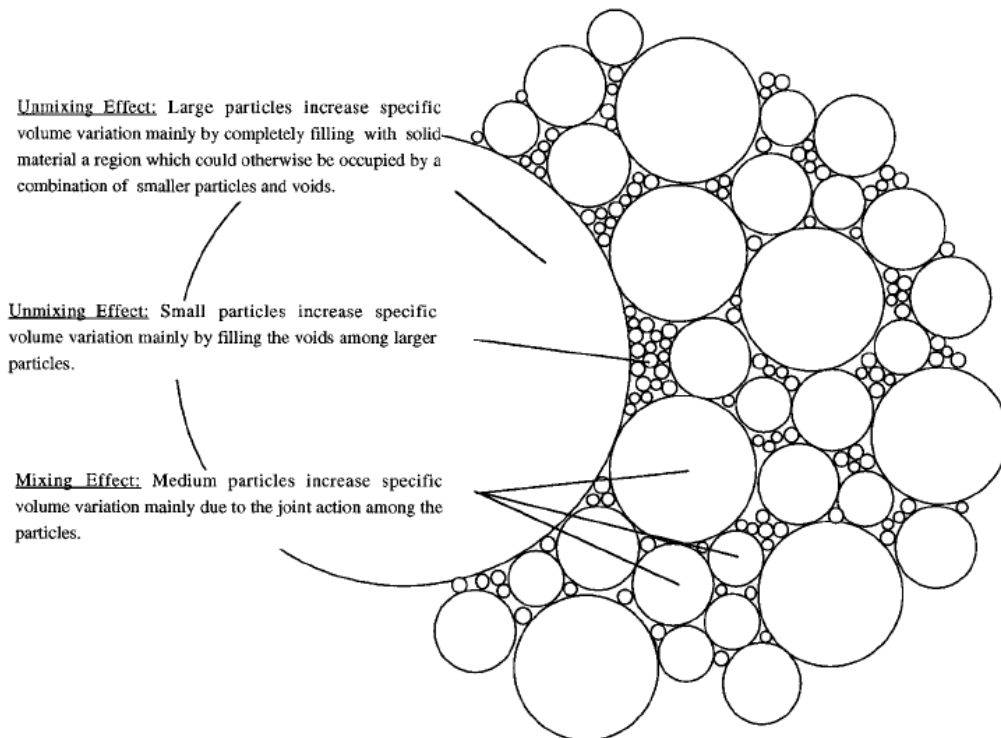


Figure 6.1. Two-dimensional diagram illustrating the random packing structure of spherical particles with their sizes represented by equivalent packing diameters (Jones, Zheng et al. 2002).

6.2.1 Packing model

Packing density is defined as the volume fraction of the system occupied by solids (Stovall, de Larrard et al. 1986). The basis of packing begins with a mono-size virtual packing. The virtual packing density of this mix is 0.74 (figure 6.2a). When using a multi-size particle mixture, the packing can be improved. In theory, a packing approaching 1 can be reached by infinitely adding increasingly smaller particles in the voids left by coarser particles (figure 6.2b). In practice the PSD can be tailored to certain extent (by combining fractions), but an infinite size range is impossible. A model, called the Linear Packing Model (LPM), was developed by de Larrard in 1986 (de Larrard 1989; de Larrard and Sedran 1994) to calculate the packing of a given PSD and estimate the packing density/void ratio of the particle mix system accurately.

The LPM from De Larrard describes the packing of mixtures made with discrete grain classes (Stovall, de Larrard et al. 1986; de Larrard and Sedran 1994). This model requires the PSD to be measured for all constituent materials. A class of large grains is dominant when it fills all the spaces available in such a way that adding a few smaller grains would merely fill the voids between large grains without pushing these large particles apart. Additionally, a class of small grains is dominant when it consumes more space than the voids available between the large particles.

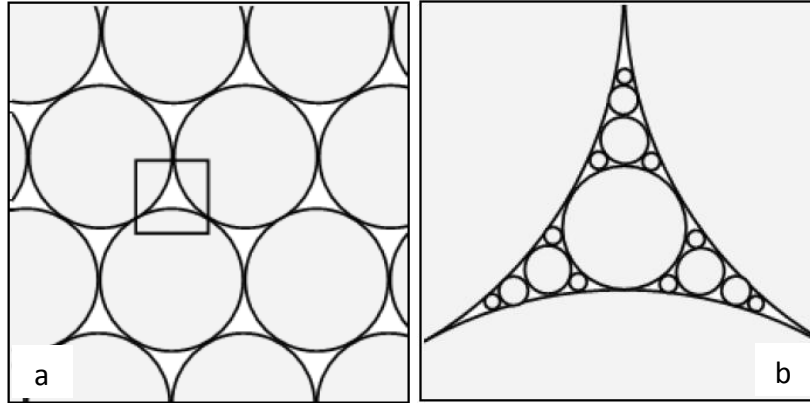


Figure 6.2. (a) Mono-size packing and (b) multi-size packing (De Vries 2008).

$$\gamma_i = \frac{\beta_i}{1 - \sum_{j=1}^{i-1} \left[1 - \beta_i + b_{ij} \beta_i \left(1 - \frac{1}{\beta_j} \right) \right] y_j - \sum_{j=i+1}^n \left[1 - a_{ij} \frac{\beta_i}{\beta_j} \right] y_j} \quad (6.1)$$

where γ_i = packing density of mixture with one particle size class i ;

y_i = volume fraction retained in each size class i ;

β_i = mono-sized packing density of grain i ;

a_{ij} = represented the loosening effect;

b_{ij} = represented the wall effect.

The PSD of the cement material and filler material is better described by a continuous distribution. The LPM is adjusted and transformed to a continuous description to calculate the packing of a mixture with a number of grain classes (Stovall, de Larrard et al. 1986; de Larrard and Sedran 1994; De Vries 2008), described as:

$$\left. \begin{aligned} \phi(t) &= \frac{\phi_0}{1 - (\phi_0) \int_t^{\infty} g \cdot \Phi \cdot dx - \int_0^t f \cdot \Phi \cdot dx} \\ \gamma &= \text{Min}(\phi(t)) \end{aligned} \right\} \quad (6.2)$$

where ϕ_0 = the mono-sized packing density;

Φ = the particle volume fraction function;

t = the particle size of the grain class;

g, f = the functions for the loosening and wall effect, which are described in eq. 6.3.

γ = the packing density of the mixture.

$$g = \left(1 - \frac{t}{x}\right)^{1.6};$$
$$f = \left(1 - \frac{x}{t}\right)^{3.1} + 3.1 \cdot \frac{x}{t} \cdot \left(1 - \frac{x}{t}\right)^{2.9}$$
(6.3)

For detailed information, it can be found in references (Stovall, de Larrard et al. 1986; de Larrard and Sedran 1994; Jones, Zheng et al. 2002; De Vries 2008).

In the continuous model, the particle volume fraction function, Φ , is described by the PSD, represented by the Rosin-Rammler function:

$$G(x) = (1 - e^{-bx^n}) \cdot 100\%$$
(6.4)

If the mixture has several constituents with known fractions, the PSD of the combination can be represented as:

$$G_{sum}(x) = a_1 \cdot G_1 + a_2 \cdot G_2 + a_3 \cdot G_3 + \dots + a_n \cdot G_n$$
$$a_1 + a_2 + a_3 + \dots + a_n = 1$$
(6.5)

where a_1, a_2, a_3 and a_n are the fractions of every constituent and G_1, G_2, G_3 and G_n are the corresponding PSD represented by Rosin-Rammler functions.

6.2.2 Optimum packing

In this section, the packing density of blended material blended with micronized sand with different fineness is calculated by using the continuous description of LPM. The PSD of micronized sand and the cement implemented in eq. 6.2 can be found in figure 6.3 (mentioned in chapter 4).

In an earlier study (De Vries 2008), the packing density of binary mixed material was studied. The material was made with cement with one of M6, M300 or M600. The packing density of the mixtures was calculated and shown in figure 6.4. The curves indicate that the fine micronized sand, M600, and the coarse one, M6, have bigger influence on the particle packing than the medium one, M300.

M600 is much finer and M6 is coarser than the cement. The wider PSD, which possibly results in a higher packing density, can be obtained by adding M600 or M6 in the mixture systems. M300 has the distribution that is similar to cement. It has less influence on the system packing.

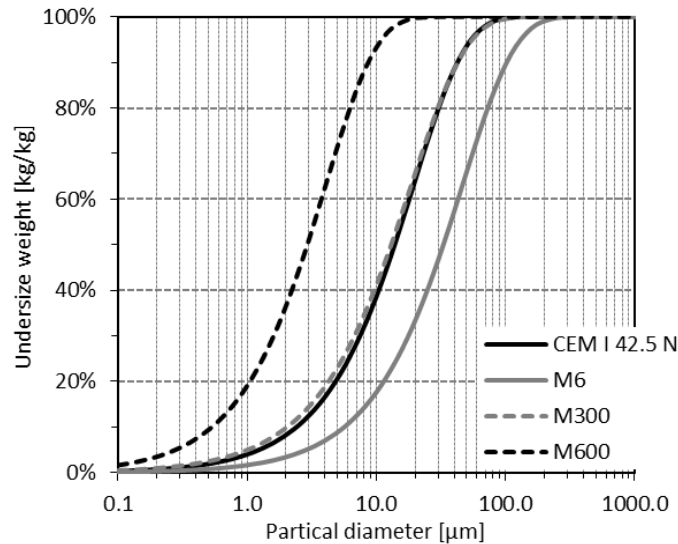


Figure 6.3. Particle size distribution of OPC and micronized sand

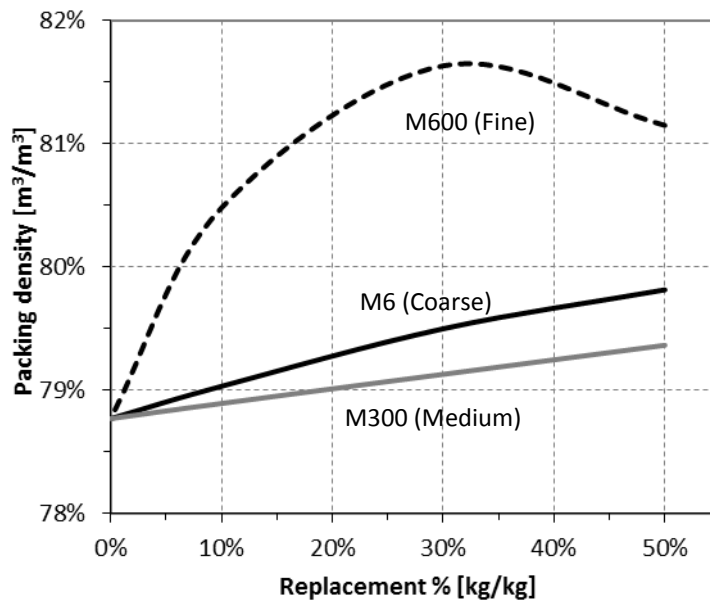


Figure 6.4. Packing density of mixtures blended with micronized sand with different fineness and different replacement levels (De Vries 2008).

Ternary mixed material

The mixed replacement material is made with M6, M300 and M600. The packing density of the mixtures was calculated by the continuous description of LPM and the results are shown in figure 6.5. The diagram shows that the packing density increases when the fraction of M300 is decreasing in the ternary mixed material. Maximum packing density appears where there is hardly M300 in the system.

In the cement-based ternary mixed material, M6 and M600 are selected as the replacement material. The packing density of the mixtures is presented in figure 6.6. Figure 6.6 shows that the packing density

increases with the increasing replacement percentage of micronized sand in the ternary mixed material. The area with blue indicates higher packing density of the mixtures. The highest packing density in this area locates in the mixtures in which the proportion of M600 is around 25%. To get the optimum packing of the ternary mixtures, the proportion of M600 in the system should be controlled around 25%.

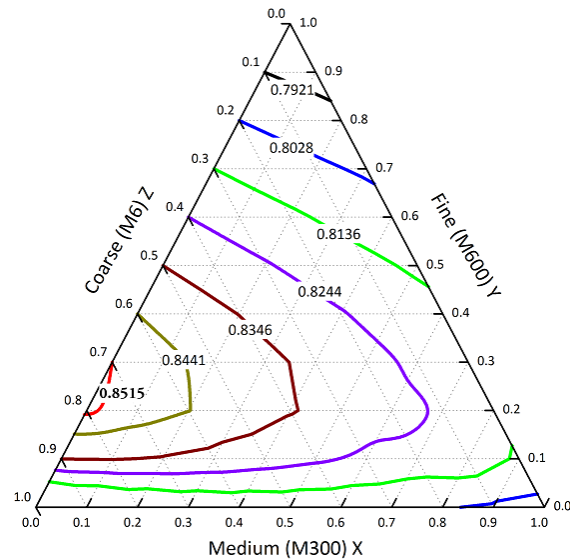


Figure 6.5. Packing density of the ternary mixed material (micronized sand with different fineness).

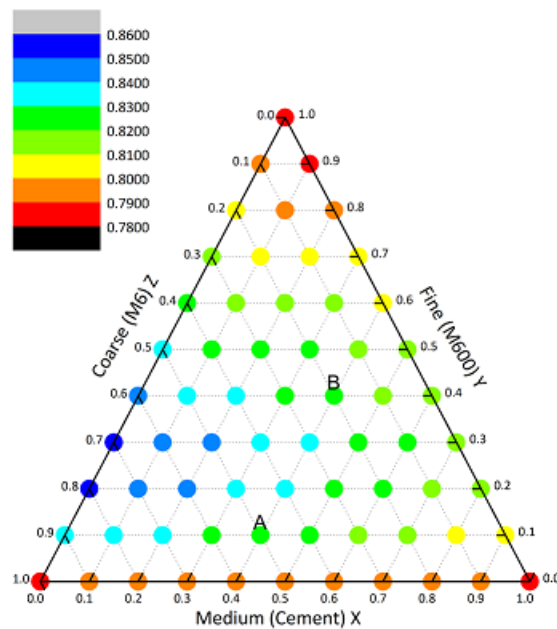


Figure 6.6. Packing density of the ternary mixtures (cement: OPC, M6: coarse, M600: fine).

Furthermore, the figure 6.6 gives the information that the mixtures with the same packing density can be got from different mixture designs. For

instance, under the 60% replacement of micronized sand, sample A and sample B in the diagram show the same packing density. Clearly, sample A is preferred from the economic point of view.

6.3 Properties of Ternary Mixtures from Simulation

The packing density of ternary mixtures has been discussed in the previous section. In this section, microstructures, porosity and water permeability of ternary mixtures will be investigated by means of numerical simulation, which has been described in chapter 5. Several mixture designs were selected from figure 6.6. In table 6.1, it gives the mixture composition and the corresponding packing density. The simulated results of porosity and permeability coefficient of the mixtures are presented in table 6.1 as well.

Table 6.1. Mixture composition and the simulated results of porosity and water permeability coefficients at the age of 28 days of ternary mixtures.

<i>Mixtures</i>	<i>Cement</i>	<i>M6</i>	<i>M600</i>	<i>Packing Density</i>	<i>Porosity</i>	<i>k_w</i> <i>(E-12 m/s)</i>
REF	1	0	0	0.7877	10.62%	3.73
Mixture 1	0.9	0.1	0	0.7903	8.28%	3.77
Mixture 2	0.8	0	0.2	0.8137	10.80%	4.05
Mixture 3	0.8	0.05	0.15	0.8124	9.40%	2.77
Mixture 4	0.8	0.2	0	0.7929	12.90%	4.80
Mixture 5	0.7	0.1	0.2	0.8185	10.27%	3.06
Mixture 6	0.7	0.3	0	0.7950	17.84%	8.59
Mixture 7	0.6	0.2	0.2	0.8232	20.78%	9.21
Mixture 8	0.5	0	0.50	0.8115	28.93%	12.53
Mixture 9	0.5	0.3	0.2	0.8281	23.64%	10.46
Mixture 10	0.5	0.45	0.05	0.8115	24.73%	10.94

6.3.1 Binary mixed materials

Table 6.1 shows that in the binary mixed materials (i.e. mixture 1, 2, 4, 6 and 8) the porosity is increasing with replacement percentages, which is in good agreement with experimental results presented in chapter 3. The dilution effect of micronized sand can not be compensated by a higher degree of hydration of cement when the replacement percentage is higher than 10%.

6.3.2 Ternary mixed materials

Table 6.1 also reveals that with the same replacement percentage, ternary mixtures have lower porosity than the binary mixtures (mixture 3

compared with mixture 4; mixture 5 compared with mixture 6.). Ternary mixture 5, with 30% replacement of micronized sand, shows lower porosity than sample 4, which has even lower replacement percentage, 20%. It indicated that with better packed mixture system, material can have denser developed microstructure. With high replacement percentage, i.e. 50%, binary mixture sample 8 and ternary mixture sample 10 have the same packing density. However, sample 8 has higher porosity than sample 10. Fine micronized sand M600 is replaced by coarse one, M6.

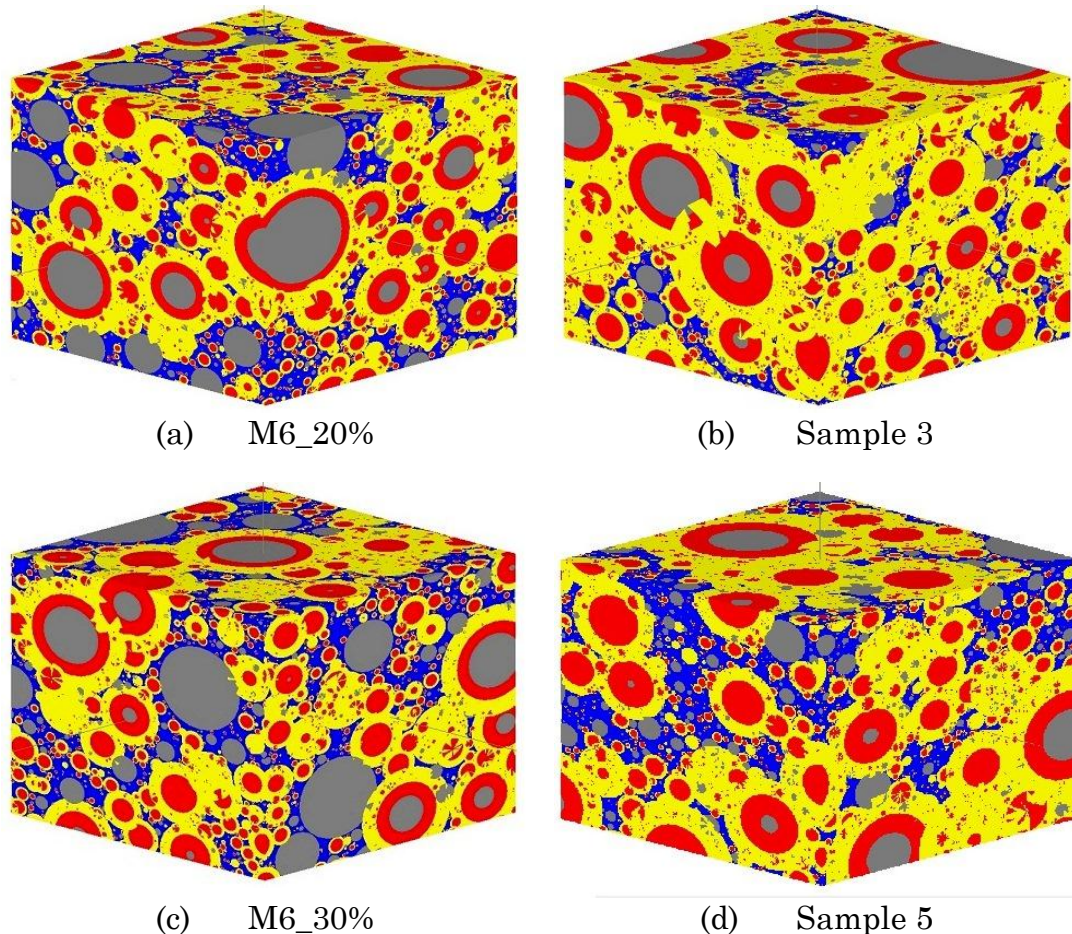


Figure 6.7. Microstructure of cement pastes at the age of 28 days ($w/b=0.40$).

In figure 6.7, the 28-day microstructures paste are compared between the binary mixture paste and ternary mixture paste. It shows that with the same replacement percentage (a and b, c and d), the microstructures of the ternary mixtures are denser than that in the sample which is mixed with M6.

6.4 Experiments Validation

In this section the numerical simulated properties from simulation of ternary mixtures were validated by the pore structure and water

permeability tests. Two mixture designs, sample 3 and 5 from table 6.1, were selected. The mixture compositions are presented in table 6.2. Sample preparation was the same as mentioned in chapter 3 and 4. Results of the porosity and water permeability of sample 3 and 5 at the age of 28 days are presented in table 6.3. The experimental results of ternary mixtures show the lower porosity and permeability coefficients compared to those of the reference sample. The trend is in a good agreement with the simulated results in table 6.1.

Table 6.2. Material composition of ternary mixtures.

	<i>Cement</i>	<i>M6</i>	<i>M600</i>	<i>Water</i>	<i>w/p</i>	<i>w/c</i>
Mixture 3	0.8	0.05	0.15	0.4	0.4	0.5
Mixture 5	0.7	0.1	0.2	0.4	0.4	0.57

Table 6.3. Porosity and water permeability coefficients of ternary mixed samples compared with reference sample (at the age of 28 days).

<i>Mixture</i>	<i>Porosity</i>	<i>k_w (E-12)</i>
Ref	22.89%	2.190
Mixture 3	20.07%	1.356
Mixture 5	22.07%	2.105

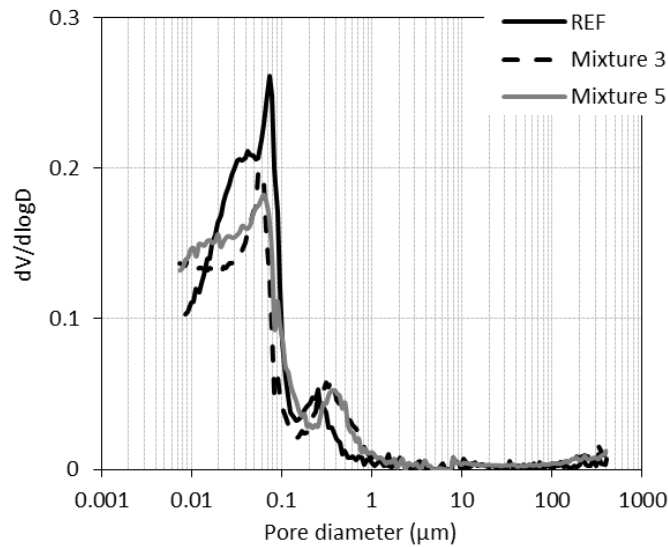


Figure 6.8. Pore size distribution of mixture 3 and 5 at the age of 28 days.

Pore size distributions of these two ternary mixtures were compared with the reference, which are shown in figure 6.8. The figure shows that the ternary mixtures have similar pore size distributions but the lower value on every range of pore size, in comparison with the value of reference sample. The pore structures have been refined by mixing micronized sand with different fineness. The microstructures become less permeable as a result.

6.5 Summary

In this chapter, the optimization of the cement-based mixtures incorporating micronized sand was studied. The results from the numerical and experimental work have been discussed. Several summary remarks can be drawn:

- M300, which has similar particle size distribution as cement, has less effect on improving the packing density than the coarse sand (M6) and the fine sand (M600) in the mixture system.
- In the cement-based ternary mixtures, the proportion of M600 in the system should be controlled around 25% to reach the optimum packing.
- Simulated results of microstructure and permeability coefficients shown the same trend as those from the experiments. The pore structures have been refined by mixing micronized sand with different fineness. The microstructures become less permeable as a result.
- The evaluation gives useful information of using micronized sand with different fineness.

Chapter 7

Service Life Prediction of Concrete Structures Blended with Micronized Sand

7.1 Introduction

Cement blended with micronized sand is a promising material for use in massive structures like residential houses, offices and industrial buildings. There are also possibilities for structures facing more severe environments, for instance a marine environment, submerged environment, etc.. It has been found that transport properties of blended concrete are slightly different from those of OPC concrete. Since the transport properties play an important role in the durability of concrete, it is important to figure out whether the presence of micronized sand will influence the durability and service life of concrete structures made with blended cement.

In the Dutch standards for concrete structures a service life of 50 years is implicitly assumed. However, in practice the required service life of some works can be 80, 100 or even up to 200 years (Webster 2000; Tang 2006; van der Wegen, Polder et al. 2012). The service life is defined as the period during which the structure's resistance $R(t)$ is high enough to withstand the environmental load $S(t)$. During that period, it can deliver a particular performance, which ensures that the structure can meet the requirements of the design (Siemes, Vrouwenvelder et al. 1985; Siemes, Schiessl et al. 2000; Polder and De Rooij 2005). The concept is schematically shown in figure 7.1.

With respect to service life of reinforced concrete structures it is noticed that chloride ingress in concrete is one of the most important issues (Tang 2006). In addition, in the prevailing Dutch concrete standards (NEN 6720, NEN-EN 206-1/NEN 8005 and NEN 6722), chloride ingress mechanisms dominate the service life.

Colleparidi (Colleparidi, Marcialis et al. 1972) was one of the first researchers who analysed chloride penetration can be modelled as diffusion by using Fick's 2nd law (eq. 7.1) in the early 1970's. A probabilistic methodology for service life design was conceived in the 1980's (Siemes, Vrouwenvelder et al. 1985). In the 1990's, the DuraCrete methodology was developed in a European research project.

$$\frac{\partial C_x}{\partial t} = -\frac{\partial}{\partial x} \left[-D \frac{\partial C_x}{\partial x} \right] = D \frac{\partial^2 C_x}{\partial x^2} \quad (7.1)$$

where C_x = the concentration at a distance x from the reference point (concrete surface) (mol/m^3);

t = time (s);

D = the diffusion coefficient of the material (m^2/s).

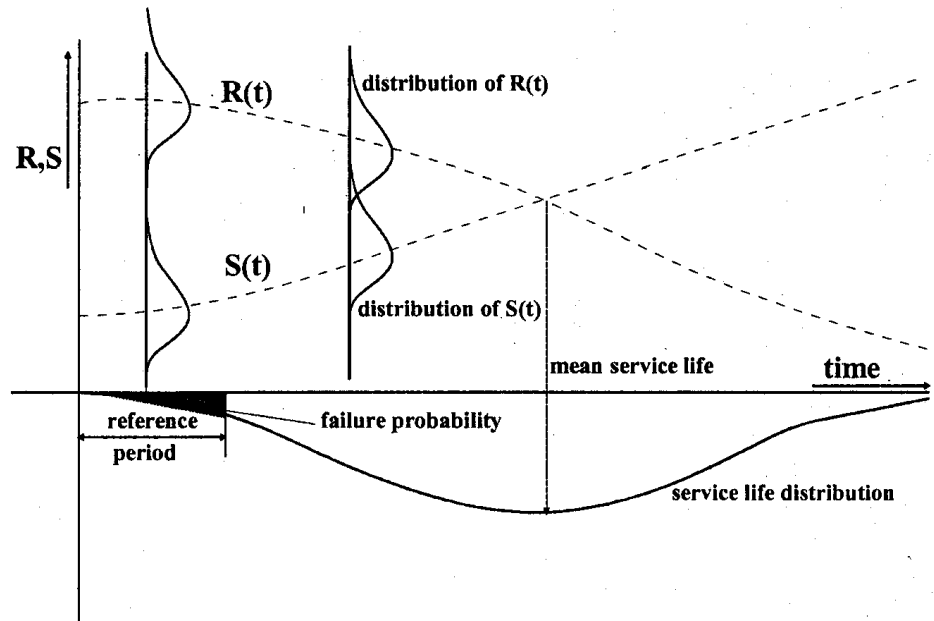


Figure 7.1. Schematic representation of probabilistic durability design (Siemes, Vrouwenvelder et al. 1985; Siemes, Schiessl et al. 2000; Polder and De Rooij 2005).

The guideline for durability design is based on the LRFD approach (Load Resistance Factor Design). The LRFD approach is an approach where all variables are represented by deterministic values and where the reliability of the structure with respect to a given event is assured by applying partial safety factors for the load and resistance variables (DuraCrete. 2000).

The guide is to a large extent based on probabilistic analysis because this methodology offers a consistent basis for updating the reliability of the structure using information from inspections and measurements (DuraCrete. 2000)

7.2 Service Life Prediction according to DuraCrete

The aim of the DuraCrete project was to develop a durability design methodology, based on realistic and sufficiently accurate environmental and material models, capable to predict the behaviour of concrete

structures (DuraCrete. 2000). The service life is assumed to be limited to the initiation period, i.e. the period for aggressive substance to reach the reinforcement and induce depassivation of the steel. The initiation phase ends when the chloride concentration at the reinforcement reaches a critical threshold value or when the carbonation front reaches the reinforcement. Depassivation does not necessarily represent an alarming state. However, it is an early warning that corrosion will start.

In this chapter, the study is focused on the initiation of chloride-induced corrosion. Following the DuraCrete methodology, the chloride ion concentration in the concrete can be evaluated by using equation 7.2. This probability-based guideline for service life design has been developed based on initiation of corrosion due to chloride penetration for exposure class XS (marine environment) and class XD (de-icing salts) (DuraCrete. 2000; De Schutter 2011; van der Wegen, Polder et al. 2012).

$$C(x,t) = C_s^d - (C_s^d - C_i) \cdot \left(1 - \operatorname{erf} \left[\frac{x}{\sqrt{\left\{ 4kD_0 \left(\frac{t_0}{t} \right)^n t \right\}}} \right] \right) \quad (7.2)$$

- where $C(x,t)$ = the chloride content at depth x at time t ;
 C_s^d = the design value of surface chloride content, in % by mass of binder;
 C_i = the initial chloride content, in % by mass of binder;
 k = a correction factor;
 n = the aging coefficient;
 D_0 = the reference diffusivity at reference time t_0 , (m^2/s);
 t_0 = the reference time, in this study t_0 is 28 days, (s);
 erf = Gauss error function.

7.3 Value Determination of Parameters in DuraCrete Model

The DuraCrete model can be used to calculate the chloride concentration over the cover depth of concrete structures. Parameters, including the design cover depth, the expected/empirical surface chloride content and experimentally determined chloride diffusion coefficients, need to be determined.

7.3.1 Chloride content C_s^d and C_i

The design value surface chloride content, C_s^d , is determined from eq. 7.3 (DuraCrete. 2000).

$$C_s^d = A_{C_s} \cdot (w/b) \cdot \gamma_{C_s} \quad (7.3)$$

where A_{C_s} = a regression parameter describing the relation between the chloride surface concentration and water to binder ratio, w/b

w/b = water to binder ratio.

γ_{C_s} = partial factor for the surface chloride concentration.

The structure is assumed to be exposed to the atmospheric zone of a marine environment (class XS). Referred to DuraCrete project report (DuraCrete. 2000), values of A_{C_s} and γ_{C_s} are 2.57 and 1.40, respectively.

Water to binder ratio is 0.40. The initial chloride content in concrete mix, C_i , is taken as 0.1%, the same as normally considered.

7.3.2 Correction factor k

The correction factor, k , depends on the type of the binder, the environment and the curing condition (eq. 7.4) (DuraCrete. 2000):

$$k = k_c \cdot k_e \cdot \gamma_{R_{cl}} \quad (7.4)$$

where k_c = the curing condition factor;

k_e = the environment factor;

$\gamma_{R_{cl}}$ = partial factor for the resistance with respect to chloride ingress.

The environment factor k_e is described by the environment factor $k_{e,0}$ and the factor $k_{e,c}$, which refers to the type of cement. It holds:

$$k_e = k_{e,0} \cdot k_{e,c} \quad (7.5)$$

For the correction factor, k , it then holds:

$$k = k_c \cdot (k_{e,0} \cdot k_{e,c}) \cdot \gamma_{R_{cl}} \quad (7.6)$$

In this thesis, concrete samples were cured for 28 days. The type of cement used in the concrete samples was ordinary Portland cement. The structure is assumed to be exposed to the atmospheric zone of a marine environment (class XS). Referred to DuraCrete project report (DuraCrete. 2000), characteristic values of k_c , $k_{e,0}$, $k_{e,c}$, and $\gamma_{R_{cl}}$ for determining correction factor k are shown in table 7.1.

Table 7.1. Characteristic values of the factors k (DuraCrete. 2000).

<i>Variable</i>	<i>Factor name</i>	<i>Condition</i>	<i>Characteristic value</i>	<i>Unit</i>
k_c	curing condition factor	28 day curing	0.79	---
$k_{e,0}$	environment factor	atmospheric zone	0.68	---
$k_{e,c}$	cement type factor	OPC	1.0	---
$\gamma_{R_{cl}}$	partial factor	Marine environment	2.35	---

7.3.3 Aging factor n

A decrease of the rate of chloride penetration can be described with a time-dependent diffusion coefficient, viz. (Maage, Helland et al. 1996), which can be modelled as:

$$D_{cl}(t) = D_0 \left(\frac{t_0}{t} \right)^n \quad (7.7)$$

where D_0 is the diffusion coefficient at reference hardening time t_0 (e.g. 28 days) and n is the aging coefficient. The aging factor n in eq. 7.2 is used to quantify the effect of aging of the material on the rate of chloride penetration for a given type of cement. This factor has a big influence on the outcome of a service life prediction.

Examples of the evolution of time-dependent diffusion coefficients are shown in figure 7.2 for different aging factors. In this figure the values of the aging factor n vary from 0.3 to 0.6. With the same initial diffusion coefficient, a higher aging factor indicates a more intensive densification of the microstructure, which results in a lower diffusion coefficient as function of time. For $n=0.6$, the diffusion coefficient reduces two orders of magnitude during a 100-year time span as a result of densification of the microstructure.

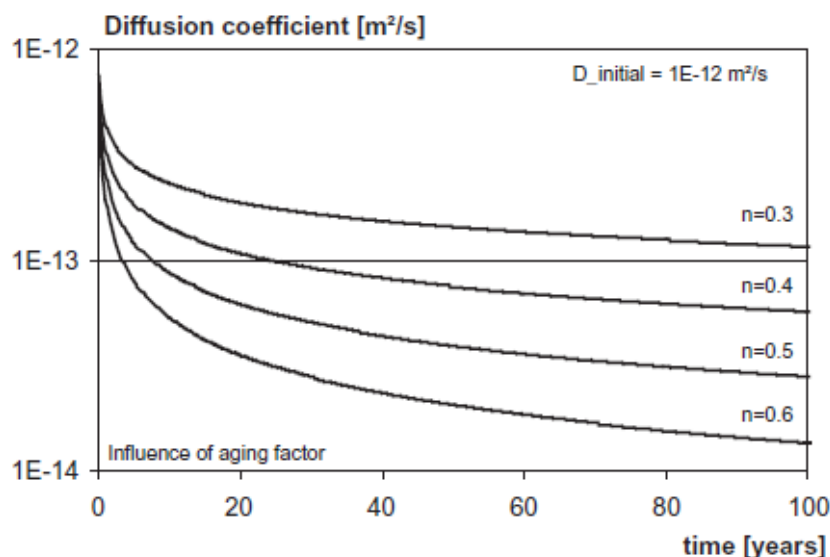


Figure 7.2. Diffusion coefficient for different aging values by using eq. 7.6 (Koenders, Ottel  et al. 2008).

Table 7.2. Aging factors n for different binders (van der Wegen, Polder et al. 2012).

Environmental classes	Underground, splash zone	Above ground, marine environment
NEN-EN 206	XD2, XS3	XD1, XD3, XS1
Type of binder		
CEM I	0.40	0.60
CEM I, 25-50% slag, II/B-S; or III/A, <50% slag	0.45	0.65
CEM III 50-80% slag	0.50	0.70
CEM I with 21-30 % FA	0.60	0.70
CEM V/A (25% slak en 25% vliegas)	0.60	0.70

Based on the values presented in table 7.2, in which values refer to Dutch concrete standard NEN-EN 206, the value of the aging factor adopted in this chapter is chosen as 0.60 for the OPC concrete, since the environment to which the concrete structures were exposed was assumed as the atmospheric zone in marine environment (XS1).

In chapter 4 it was found that after 90 days the water permeability coefficients and chloride diffusivity coefficients of blended samples were in the same order of magnitude as plain cement and reference concrete. It is assumed, therefore, that the microstructure of blended samples is similar to that of the reference sample after 90 days. In the following the aging factor of blended samples is estimated as 0.60, the same as reference OPC concrete.

7.3.4 Reference diffusivity D_0

The chloride diffusion coefficients D_{nssm} , obtained from the RCM test in chapter 4, will be used as the reference diffusivity, D_0 , in the model for

predicting the service life of concrete structures. The values of D_{nssm} , obtained in the RCM tests from chapter 4, are shown in table 7.3.

Table 7.3. Values of D_{nssm} obtained from RCM tests on concrete ($w/b=0.40$).

<i>Sample</i>	<i>Sand description</i>	<i>Replacement</i>	<i>D_{nssm} (*10^{-12} m²/s)</i>
OPC	---		13.40
M6_10%	coarse	10%	16.71
M6_20%	coarse	20%	18.06
M6_30%	coarse	30%	26.28
M300_20%	medium	20%	24.15
M600_20%	fine	20%	23.25

7.3.5 Design value of critical chloride content C_{cr}^d

In the DuraCrete model corrosion of the reinforcement is considered to be initiated when the chloride concentration around reinforcement exceeds a design critical threshold value C_{cr}^d . It holds:

$$C_{cr}^d = C_{cr} \cdot \frac{I}{\gamma_{C_{cr}}} \quad (7.8)$$

where C_{cr} = the critical chloride concentration, in % by mass of binder;

$\gamma_{C_{cr}}$ = partial factor of the critical chloride concentration;

The critical chloride content not only depends on the environment and the type of binder, but also on the water/binder ratio. At present, there is no generally accepted or standardized procedure for the determination of the critical chloride content. Following the environmental exposure conditions determined in section 7.3.2, the combinations of water/binder ratio and the type of binder, the critical chloride content C_{cr} is taken as 0.6% by mass of cement. The partial factor of critical chloride concentration is 1.06.

Table 7.4 summarizes the values of parameters and the chloride contents required in the DuraCrete model for predicting service life of concrete structures using blended cement paste.

Table 7.4. Values of factors and chloride contents required to run the DuraCrete model for predicting service life of concrete structures using plain and blended cement pastes.

<i>Items</i>	<i>Symbol</i>	<i>Value</i>
Design value of surface chloride content	C_s^d	1.44%
Initial chloride content	C_i	0.1%
Correction factor	k	$0.68 \times 0.79 \times 1.0 \times 2.35$
Result from RCM test (m ² /s)	D_o	D_{nssm} (determined in Chapter 4)
Reference time (sec)	t_o	$28 \times 24 \times 3600$
Aging factor	n	0.60
Design value of critical chloride content	C_{cr}^d	0.57%

7.4 Service Life Prediction by Using DuraCrete Model

7.4.1 Chloride penetration profiles

For the prediction of the service life of concrete structures made of different concrete mixtures, simulations of chloride penetration profiles are performed by using the DuraCrete model. Values of factors and chloride contents required in the model were determined in the last section (table 7.4). The structures are made of OPC concrete or concrete blended with micronized sand as partial replacement of cement (hereinafter called concrete blended with micronized sand). The mixture compositions are the same as mentioned in chapter 4. The required service life is assumed to be 80 years. The calculated chloride profiles in the concrete are presented in figure 7.3 and figure 7.4. The chloride content is plotted as function of the penetration depth. The critical chloride content, i.e. 0.6%, is indicated by a horizontal dashed line. In the reference concrete mixture with OPC, at the age of 80 years the chloride content is lower than 0.6% at a depth deeper than around 35mm from the surface of the concrete structures.

The commonly used values of the cover thickness are in the range of 30mm to 50mm. In this example, 35mm is assumed as cover thickness in the OPC concrete structure. Figures 7.3 and 7.4 show that in structures made of blended materials the chloride concentration at a depth of 35mm is higher than the critical chloride content, i.e. 0.6%. In other words, if the cover thickness is 35mm, the outer rebar is potentially at risk of corrosion before the indicated service life of 80 years.

In the following the DuraCrete model will be used to determine the required cover thickness of the concrete structures to ensure that structures made with blended cement have the required service life.

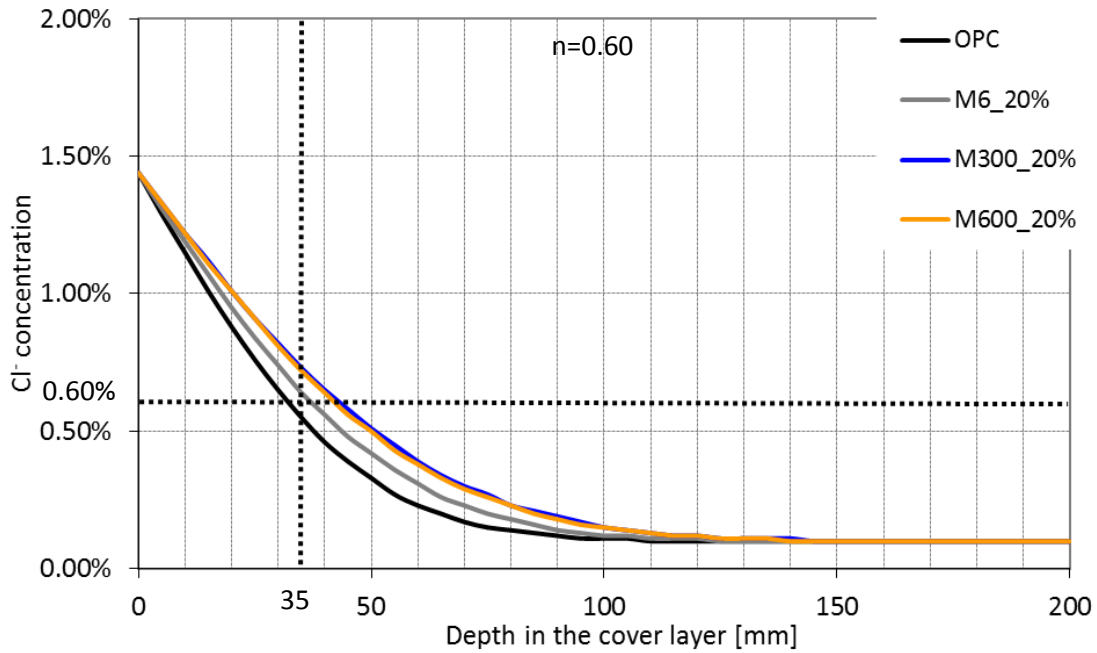


Figure 7.3. Calculated chloride profiles according to the DuraCrete model for concrete mixture made with OPC, M6_20%, M300_20% and M600_20% (time: 80 years).

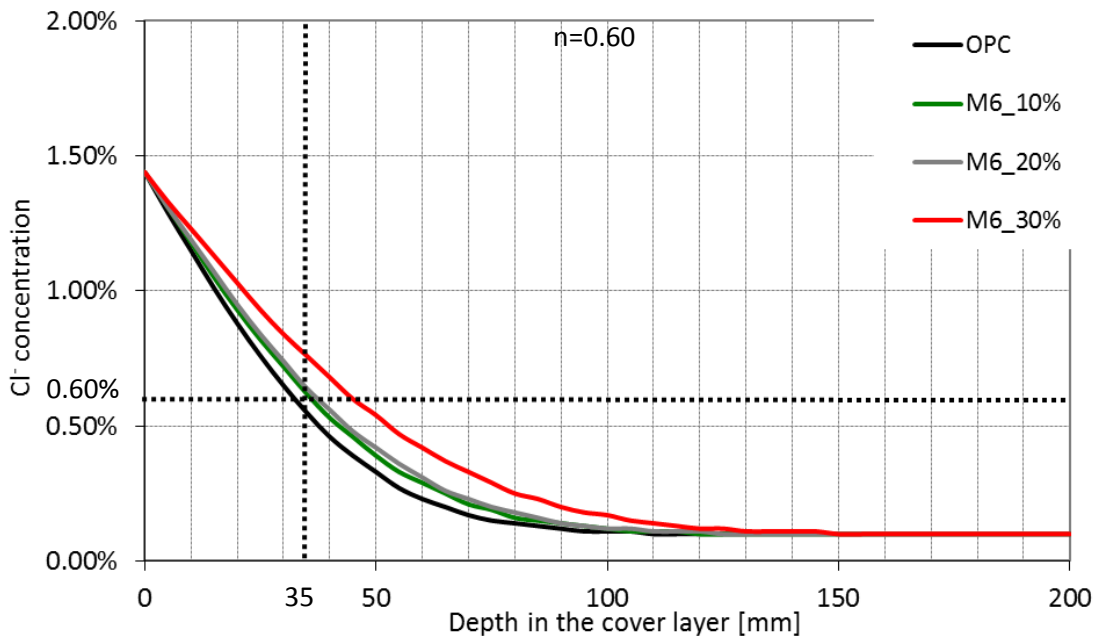


Figure 7.4. Calculated chloride profiles according to the DuraCrete model for concrete mixture made with OPC, M6_10%, M6_20% and M6_30% (time: 80 years).

7.4.2 Cover layer thickness modification

The required cover thickness, x_c , needed to ensure a certain predefined service life, t_{SL} , of a structure can be calculated with equation 7.9.

$$x_c = \operatorname{erf}^{-1} \left(\frac{C_s^d - C_{cr}^d}{C_s^d - C_i} \right) \cdot \sqrt{\left\{ 4kD_0 \left(\frac{t_0}{t_{SL}} \right)^n t_{SL} \right\}} \quad (7.9)$$

In figure 7.5 and figure 7.6 results are shown representing the relationship between the cover thickness and the designed service life for different concrete mixtures. The aging factor was considered as 0.60 and 0.40, respectively. The figures clearly show the sensitivity to the aging factor. For a higher aging factor, i.e. 0.60, substantially lower values for the cover thickness are required. Besides, they also indicate that the cover thickness of structures made of concrete blended micronized sand should be increased to meet the requirement of service life in comparison to the structure made with OPC concrete. For instance, the cover thickness of a structure made of M6_30% should be increased by about 15 mm in order to guarantee the service life of 80 years (figure 7.5). However, compared with the size of the structural elements, the increase in the cover thickness is relatively small.

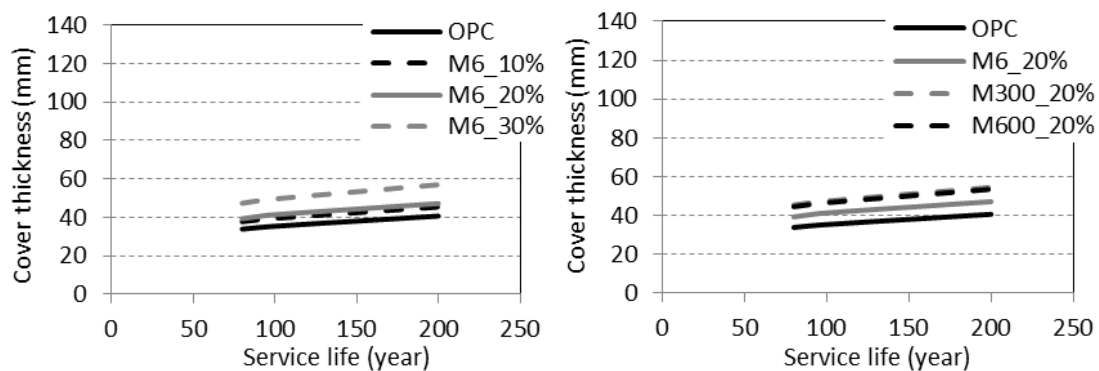


Figure 7.5. Design graph for the cover thickness versus the associating service life for different materials. (aging factor: 0.60)

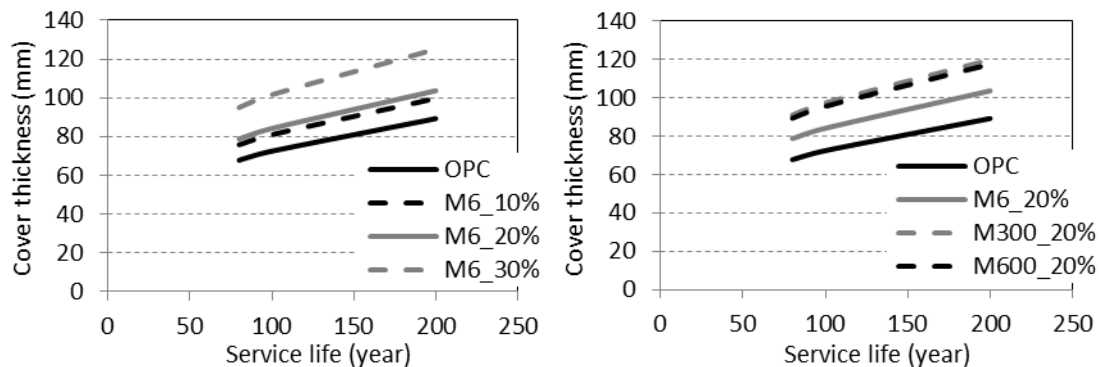


Figure 7.6. Design graph for the cover thickness versus the associating service life for different materials. (aging factor: 0.40)

7.5 Cost Evaluation

In the previous section it was found that in order to maintain the service life of 80 years, the cover thickness of structures made of concrete blended with micronized sand has to be increased. Therefore, the amount of the material is increased. In this section, the extra costs of concrete material required to meet the service life criteria will be evaluated.

The price of cement, micronized sand and aggregate sand, including sand and gravels, is shown in table 7.5. The coarse sand, M6 and medium one, M300, are cheaper and M600 is more expensive than cement. Table 7.6 shows the mixture design of the concrete. The price of the reference and the modified concrete is presented in table 7.7. Except M600_20%, the price of the modified concrete is lower than the reference OPC concrete. The price of the material per ton is reduced by about 5.5% if 30% of the cement is replaced by coarse micronized sand. Obviously, it is very promising to use concrete blended with micronized sand with economic profits. Figure 7.7 shows one-sided reinforced structural elements that are considered in this cost evaluation.

Table 7.5. The price per ton of cement, micronized sand and aggregates.

<i>Material</i>	<i>Price (€/ton)</i>
CEM I 42.5N	100
M6	60
M300	80
M600	250
Sand	31
Gravel	22

Table 7.6. Mix composition of the concrete. (kg/m³).

<i>Sample</i>	<i>OPC</i>	<i>Micronized sand</i>	<i>Water</i>	<i>Sand</i>	<i>Gravel</i>
Ref	390	0	156	498	1103
M6_10%	351	39 (M6)	156	498	1103
M6_20%	312	78 (M6)	156	498	1103
M6_30%	273	117 (M6)	156	498	1103
M300_20%	312	78 (M300)	156	498	1103
M600_20%	312	78 (M600)	156	498	1103

Table 7.7. The price of the reference OPC concrete and the concrete made with blended cement.

Sample	Price (€/ton)
Ref	39.53
M6_10%	38.75
M6_20%	37.96
M6_30%	37.18
M300_20%	38.75
M600_20%	45.41

The cost of the material by using reference OPC concrete, Pr_1 (€), is (figure 7.7a):

$$Pr_1 = Pr_{OPC} \cdot V_a \quad (7.10)$$

where Pr_{OPC} = the price of OPC concrete per m^3 ;

V_a = the amount of OPC concrete used in the structure.

If the structure is made of modified concrete (figure 7.7b), the cover thickness has to be increased in order to ensure the required service life. The cost of the material using modified concrete, Pr_2 (€), is:

$$Pr_2 = Pr_m \cdot V_b \quad (7.11)$$

where Pr_m = the price of the modified concrete, per m^3 .

V_b = the amount of modified concrete in the structure.

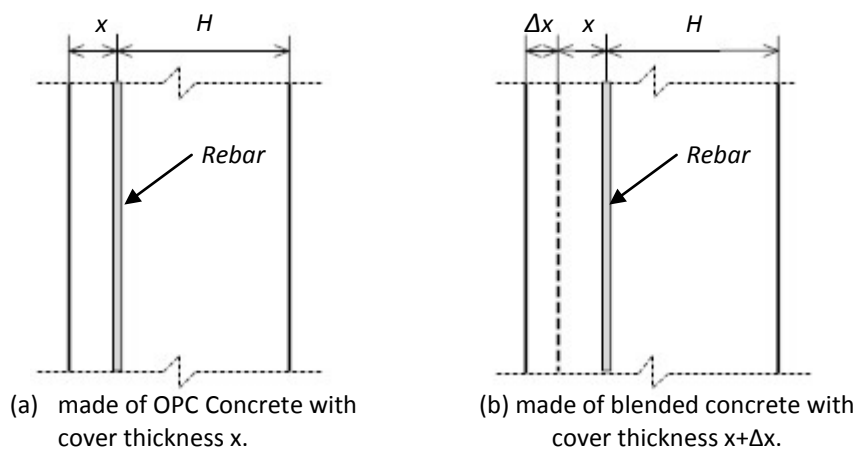


Figure 7.7. One-sided reinforced concrete elements used for cost evaluation.
 (a) element made of OPC concrete with cover thickness x ;
 (b) element made of concrete blended with micronized sand with cover thickness $x + \Delta x$.

Then it comes to:

$$Pr_2 = \frac{Pr_m}{Pr_{OPC}} \cdot \frac{V_b}{V_a} \cdot Pr_1$$

$$= \frac{Pr_m}{Pr_{OPC}} \cdot \frac{H+x+\Delta x}{H+x} \cdot Pr_1 \quad (7.12)$$

where $H+x$ = the size of structural element, m.

x = cover thickness in the structure made of OPC concrete, m.

Δx = increased cover thickness needed to meet the required service life, m.

Eq 7.10 indicates that the cost of material is not only related to the increase of the cover thickness, but also to the dimension of the structure. Figure 7.8 gives the material cost of concrete elements with different sizes made of modified concrete mixtures by using eq. 7.12. Then the costs are compared with the one of elements made of normal OPC concrete, which is given as the reference. Except for the modified concrete blended with M600, the use of concrete blended with micronized sand results in lower costs. The curves also show, as expected, that with increasing size of structural elements the costs are further reduced.

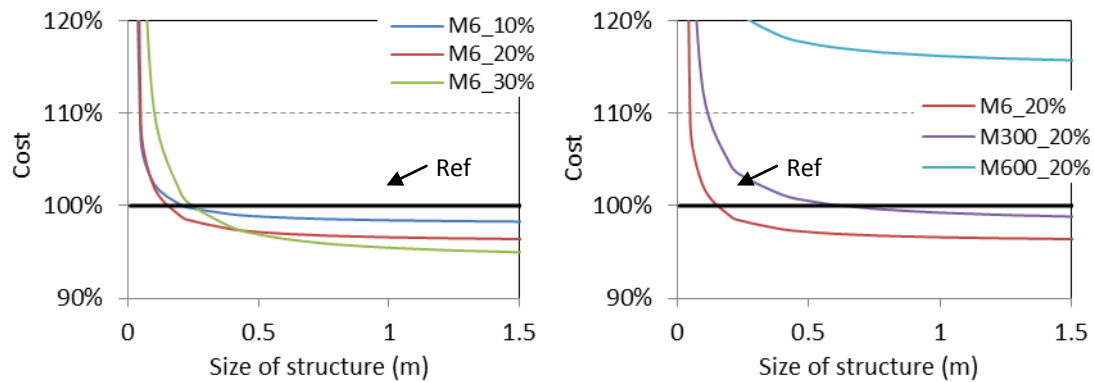


Figure 7.8. Costs of one-sided reinforced structural elements made of concrete blended with micronized sand as partial replacement of cement as function of the thickness of the structure compared with reference OPC concrete (with required service life of 80 years).

7.6 Summary

In this chapter, the service life of structures made of concrete blended with micronized sand as partial replacement of cement was evaluated by using the DuraCrete methodology in atmospheric marine environment (XS1). In this study the service life was assumed to be reached when the chloride concentration at the reinforcement has reached a critical threshold value. The calculated chloride profiles in concrete and the cover thickness were

evaluated for structures made of concrete blended with micronized sand. Conclusions that can be drawn from this chapter are the following.

- Because of the presence of micronized sand, the chloride ion concentration in structure made with blended concrete is a bit higher than in the reference OPC concrete.
- Structures made with concrete blended with micronized sand can meet the required service life by increasing the cover thickness. The increase of the cover thickness is relatively small compared to the size of the structural elements.
- Considering the increase in cover thickness, the cost evaluation of concrete material shows that the cost of concrete structures is reduced by using concrete blended with micronized sand.

Chapter 8

Sustainability Aspects of Cement-based Material Blended with Micronized Sand

8.1 Introduction

In previous chapters, the microstructure and the transport properties of cement-based material blended with micronized sand were studied. According to the experimental results, it can be concluded that the use of micronized sand is very promising and has good prospects as a replacement of cement. Using micronized sand as a replacement material reduces the total amount of cement required in concrete mixtures. This will result in a reduction of CO₂ emission and will be beneficial in view of sustainable development. It could be that, depending on the exposure condition, the service life of structures is reduced when a certain amount of cement is replaced by micronized sand. However, the advantage of micronized sand in view of mitigating the impact on the environment is the desired benefit in producing cement-based material.

Worldwide, the cement industry alone was estimated to be responsible for 5-10% of all anthropogenic CO₂ generated (Meyer 2009; Rodrigues and Joekes 2011; Van Den Heede and De Belie 2012). In literature (Gibbs, P. et al. ; Pade and Guimaraes 2007), it is reported that CO₂ emission from a cement plant can be divided into two source categories: the emission from combustion, which is responsible for about 40% of the CO₂ emission of a cement manufacturing facility, and the emission from calcination, which is responsible for about 60%. In other words, CO₂ is emitted mostly during cement production due to the calcination process, a chemical reaction from heating limestone. Calcination takes place when the raw materials (mostly limestone and clay) are heated to over 1400°C and CO₂ is liberated from the decomposed limestone. During this procedure, it releases huge amounts of other persistent organic pollutants, such as oxides and dioxides: CO, CO₂, NO_x and SO₂, heavy metals: zinc, lead and copper, and other particles: ferrous powder, fly ash and clay dust. Also these substances have impact on the environment, but, because of their smaller quantities, the environmental impact is lower. All the aspects, however, have to be evaluated in an integral assessment procedure from the sustainable point of view.

In general, sustainability means having no net negative impact on the environment (Struble and Godfrey 2004). It is a characteristic of a process or state that can be maintained at a certain level unlimitedly (www.concreteSDC.org 2008). Sustainable development policies

encompass three general policy areas: economic sustainability, environmental sustainability and social sustainability (Struble and Godfrey 2004).

- The environmental component has our attention now because deterioration of the environment is driving the current worldwide focus on sustainable development and is measured by a sustainability life cycle assessment (LCA).
- The economic component is given less attention than the other two policy areas in the developed countries of the world, but is still very important for sustainable development.
- The social component is also given less attention at the moment, but will hopefully be brought into balance in the ensuing decades and will be measured with a social LCA, which is now in its emerging stage (Struble and Godfrey 2004).

Sustainability is normally referred to as the balance of these three components, environmental stewardship, economic prosperity and social responsibility (figure 8.1). These three components of sustainable development are also called the "Triple Bottom Line", a concept that was first introduced by John Elkington in the book *Cannibal with Forks* (Elkington 1997). This is also known as the 3 Ps of sustainability - People, Planet, Profit (figure 8.2).

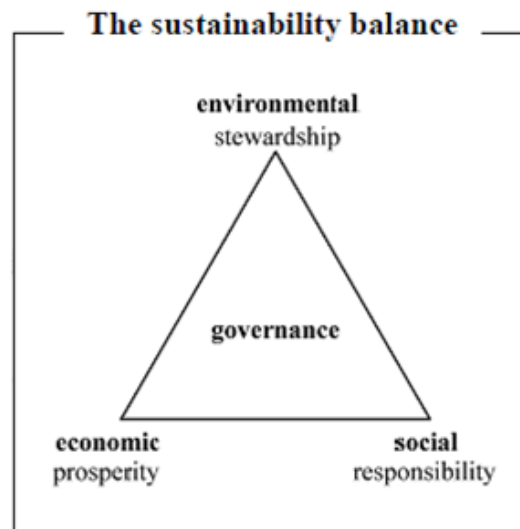


Figure 8.1. The sustainability balance based on three aspects (Struble and Godfrey 2004).

In this study, the environment is the focus from the sustainable point of view. That is not to say that economic and social issues are less important, but that they are outside the concern of this research. This chapter will focus mainly on the environmental impact resulting from the use of blended materials.

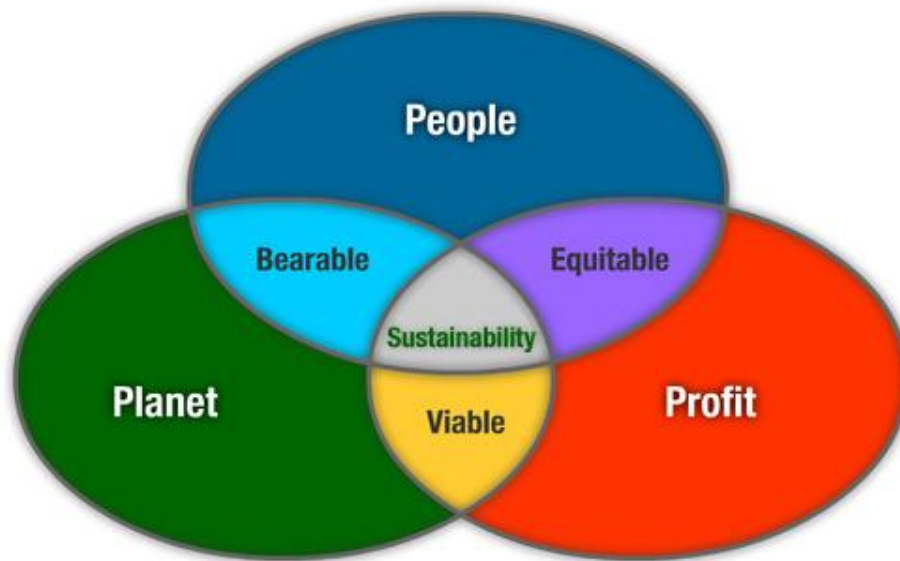


Figure 8.2. The the 3 Ps of sustainability - People, Planet, Profit (Elkington 1997).

8.2 Life Cycle Assessment

A life cycle assessment (LCA) is a technique to assess environmental impacts associated with all the stages of a product's life. According to the ISO standard (ISO 14040:2006 and 14044:2006), a LCA is carried out in four steps (NIBE 2012), as shown in the figure 8.3.

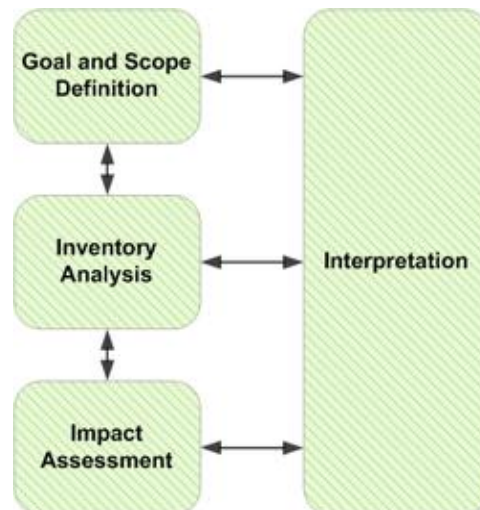


Figure 8.3. Illustration of LCA phases (NIBE 2012).

1. Goal and scope Determination

First, it is necessary to point out the subject, the central objective and the definition of the study and the system boundaries.

2. Inventory analysis of environmental data

The inventory analysis consists of defining all the inputs from the environment (raw material, fuels) and outputs to the environment (energy, emissions) (Cabal, Lechón et al. 2005).

3. Impact assessment

Impact assessment is aimed at evaluating the significance of potential environmental impacts.

4. Interpretation

Interpretation is the technique to identify, check and evaluate information from the results of the inventory analysis and the impact assessment. The results from the inventory analysis and impact assessment are summarized during this phase.

A set of impact categories and characterization methods for the impact assessment step was proposed in a new “operational guide to the ISO standards” (Guinée, Gorrée et al. 2001), led by a group of scientists in the Center of Environmental Science (CML) of Leiden University. The influence of a certain product on the environment is classified by a list of impact categories that are quantified by a number of characterization factors. In the impact assessment phases, the results of the inventory analysis are translated into contributions to relevant impact categories. Scientific background and guidelines can be found in the literature (Guinée, Gorrée et al. 2001).

In following sections, environmental impact of cement and micronized sand will be assessed by using LCA and will be explained in detail.

8.3 Step 1: Determination of Goal and Scope

8.3.1 Goal and scope

The research questions are what the difference is in environmental impact between normal concrete and concrete blended with micronized sand. Therefore, the goal of the LCA in this study is to make a comparison between using normal concrete and using concrete blended with micronized sand for a structure and to estimate the environmental benefits by using micronized sand as a replacement of cement in concrete.

8.3.2 Impact categories

The CML impact assessment method considers as sustainability consisting of several impact categories (Guinée, Gorrée et al. 2001; Cabal, Lechón et al. 2005; Frischknecht, Jungbluth et al. 2007):

Abiotic depletion refers to the exhaustion of natural resources such as iron ore or copper, which are regarded as non-living. Impacts considered are those derived from the extraction of minerals and fossil fuels.

Acidification is the result of acidifying pollutants emissions, such as SO₂ or NO_x, to the air. These emissions have negative impacts on soil, groundwater, surface waters, biological organisms, ecosystems and materials.

Eutrophication is the consequence of high levels of macronutrients, such as nitrogen and phosphorus, in the environment.

Fresh water aquatic Eco toxicity refers to the impact of toxic substances emitted to freshwater aquatic ecosystems.

Global warming potential (GWP) is the impact of greenhouse gases emissions on the atmosphere. These emissions have negative impacts on climate, human and ecosystem health.

Human toxicity includes the impacts on human health of toxic substances emitted to the environment.

Marine aquatic Eco toxicity refers to the impact of toxic substances emitted to marine aquatic ecosystems.

Ozone layer depletion (ODP) a steady decline of about 4% per decade in the total volume of ozone in Earth's stratosphere (the ozone layer), and a much larger springtime decrease in stratospheric ozone over Earth's polar regions.

Photochemical oxidation is the formation of reactive chemical compounds, such as ozone, by the action of sunlight on certain primary air pollutants. These compounds may injure health, ecosystems, materials and crops.

Terrestrial Eco toxicity refers to the impact of toxic substances emitted to terrestrial ecosystems.

The environmental load assigned qualitatively to one or more impact categories in the classification phase are quantified in terms of a common unit for that category by using characterization factors. The characterization factors and units used in the CML method are shown in table 8.1.

8.4 Step 2: Inventory Analysis

Inventory analysis involves creating inventory flows including inputs of water, energy and raw material. The flowchart for using cement and micronized sand is shown in figure 8.4. Two different materials will be analyzed based on 1 kg cement and 1 kg silica sand. Different fineness of micronized sand is not considered in this research. To some extent, it would underestimate the environmental impact of sand with high fineness. Since higher fineness requires longer grinding procedure, it would cause higher consume of energy. But the estimated results can still give an

indication of different environmental impact between cement and silica sand.

The emission values of these two materials on the environment came from the program SimaPro 7.1. It is the world's most widely used LCA software, which is developed by PRé Consultants. With the database of EcoInvent 2.1, the environmental impact of cement and micronized sand can be calculated. The method that is used for all values is CML 2 baseline 2000 v2.04 (Guinée, Gorrée et al. 2001).

Table 8.1. The characterization factors and units used in CML.

<i>Categories</i>	<i>Characterization Factors</i>	<i>Unit</i>
Abiotic depletion	the potential of abiotic depletion of the extraction of those minerals and fossil fuels.	kg of antimony (SB) equivalents per kg of extracted mineral. kg SB eq
Acidification	the acidification potential for each acidifying emission to the air.	kg of sulfur dioxide (SO ₂) equivalents per kg of emission. kg SO ₂ eq
Eutrophication	the potential of eutrophication of each eutrophying emission to the air, water and soil.	kg of phosphate ion (PO ₄ ⁻) equivalents per kg of emission. kg PO ₄ eq
Fresh water aquatic Eco toxicity.	the potential of fresh water aquatic toxicity of each substance emitted to the air, water or/and soil.	kg of 1.4-DB equivalents per kg of emission. kg 1.4-DB eq
Global warming potential (GWP)	the potential of global warming of each greenhouse gas emission to the air.	kg of carbon dioxide (CO ₂) equivalents per kg of emission. kg CO ₂ eq
Human toxicity	the potential of human toxicity of toxic substances emitted to the air, water or/and soil.	kg of 1.4-dichlorobenzene (1.4-DB) equivalents per kg of emission. kg 1.4-DB eq
Marine aquatic Eco toxicity	the potential of marine aquatic toxicity of each substance emitted to the air, water or/and soil.	kg of 1.4- DB equivalents per kg of emission. kg 1.4-DB eq
Ozone layer depletion (ODP)	the potential of ozone layer depleted by each substance emitted to the air.	kg CFC-11 eq
Photochemical oxidation	the potential of photochemical ozone formation of each substance emitted to the air.	kg of ethylene (C ₂ H ₄) equivalents per kg of emission. kg C ₂ H ₄ eq
Terrestrial Eco toxicity	the potential of terrestrial toxicity of each substance emitted to the air, water or/and soil.	kg of 1.4- DB equivalents per kg of emission. kg 1.4-DB eq

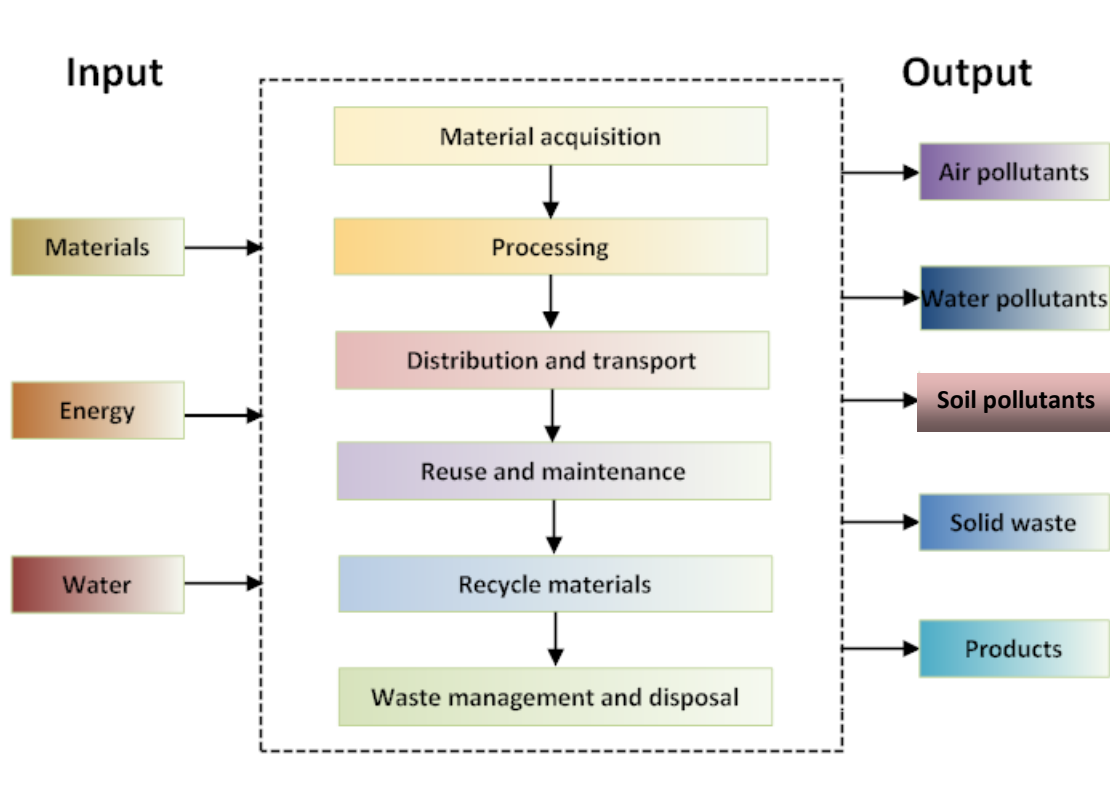


Figure 8.4. Flow chart of inventory analysis.

8.5 Step 3: Impact Assessment

The impact assessment is an important part in the LCA. The environmental impact of cement is compared with that of micronized sand. The emission values of impact categories are shown in table 8.2 and table 8.3, respectively. It can be seen that the impact values of cement on the environment are higher than those of micronized sand in all categories.

Table 8.2. The impact assessment of Portland cement CEM I.

<i>Impact category</i>	<i>Unit</i>	<i>Impact Assessment</i>
Abiotic depletion	kg SB eq	7.19E-04
Acidification	kg SO ₂ eq	9.09E-04
Eutrophication	kg PO ₄ eq	1.48E-04
Fresh water aquatic Eco toxicity.	kg 1.4-DB eq	4.61E-03
Global warming potential (GWP)	kg CO ₂ eq	7.35E-01
Human toxicity	kg 1.4-DB eq	3.19E-02
Marine aquatic Eco toxicity	kg 1.4-DB eq	8.69E-00
Ozone layer depletion (ODP)	kg CFC-11 eq	6.85E-10
Photochemical oxidation	kg C ₂ H ₄ eq	3.23E-05
Terrestrial Eco toxicity	kg 1.4-DB eq	1.02E-03

Table 8.3. The impact assessment of micronized sand.

<i>Impact category</i>	<i>Unit</i>	<i>Impact Assessment</i>
Abiotic depletion	kg SB eq	6.61E-06
Acidification	kg SO ₂ eq	1.15E-05
Eutrophication	kg PO ₄ eq	4.37E-06
Fresh water aquatic Eco toxicity.	kg 1.4-DB eq	4.94E-04
Global warming potential (GWP)	kg CO ₂ eq	2.13E-03
Human toxicity	kg 1.4-DB eq	2.60E-03
Marine aquatic Eco toxicity	kg 1.4-DB eq	1.32E-00
Ozone layer depletion (ODP)	kg CFC-11 eq	3.49E-11
Photochemical oxidation	kg C ₂ H ₄ eq	5.54E-07
Terrestrial Eco toxicity	kg 1.4-DB eq	1.51E-05

Table 8.4. The shadow prices of the impact categories (NIBE).

<i>Impact category</i>	<i>Unit</i>	<i>Shadow price (€/unit)</i>	<i>Source</i>
Abiotic depletion	kg SB eq	0.16	TNO
Acidification	kg SO ₂ eq	4	CE
Eutrophication	kg PO ₄ eq	9	CE
Fresh water aquatic Eco toxicity.	kg 1.4-DB eq	0.03	TNO
Global warming potential (GWP)	kg CO ₂ eq	0.05	CE
Human toxicity	kg 1.4-DB eq	0.09	TNO
Marine aquatic Eco toxicity	kg 1.4-DB eq	0.0001	TNO
Ozone layer depletion (ODP)	kg CFC-11 eq	30	CE
Photochemical oxidation	kg C ₂ H ₄ eq	2	CE
Terrestrial Eco toxicity	kg 1.4-DB eq	0.06	TNO

To weigh different environmental effect categories, the environmental load is monetized. The equivalent environmental effects are multiplied by the monetizing cost numbers per environmental effect. By adding up all environmental costs, a total price overview is created. This can be done with the shadow price method (de Bruyn, Korteland et al. 2010). These shadow prices represent the costs for preventive measures that must be taken to reduce the emissions to an acceptable level from sustainable point of view (NIBE 2012). These environmental costs can be seen as virtual costs because the measures are not taken in reality. Therefore, they are not integrated in the production processes and thus not integrated in the real cost. The costs of a kilo emission per impact category are shown in the table 8.4. The values are obtained from the NIBE material database (NIBE 2012). These shadow prices are not fixed, but are adjusted and updated due to new insights and methods. With the shadow price, the environmental impact from different categories can be monetized. A total shadow price of a material can be created to present the net impact on the environment.

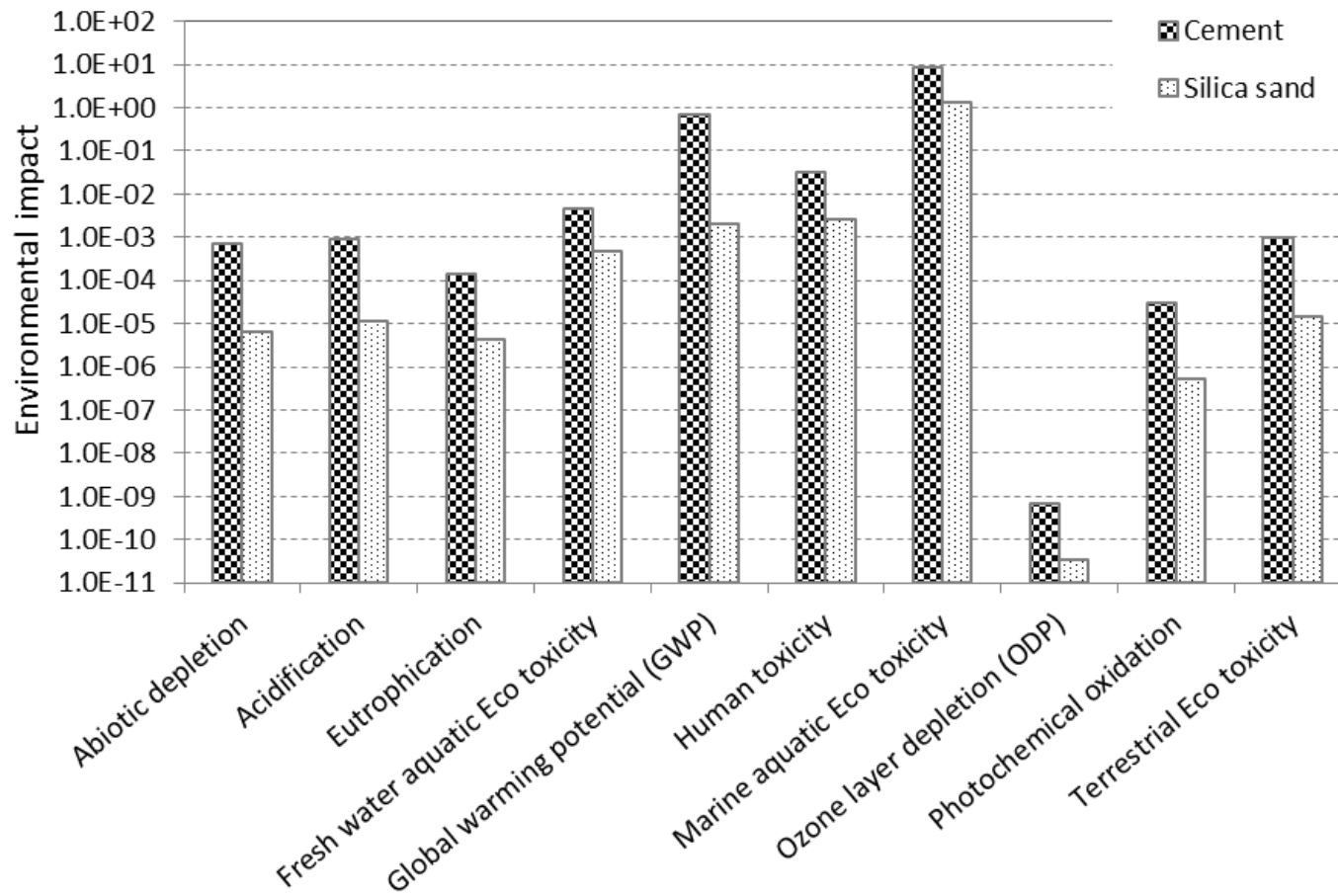


Figure 8.5. Environmental impact assessment of cement and silica sand.

8.6 Step 4: Interpretation

In figure 8.5, the results of the comparison of the environmental impact of cement and micronized sand are significantly different. Figure 8.6 shows that the shadow price of cement is two orders of magnitude higher than that of micronized sand, which means that the cost for cement to reduce the emission to a sustainable level is much higher than that for micronized sand. Figure 8.7 indicates the share of the shadow price per environmental effect in cement and micronized sand, respectively. Global warming and human toxicity are taken as the important categories. The pie diagrams show that global warming potential has the largest share in the shadow price of cement, i.e. 80%, whereas only 18% in micronized sand. The share of human toxicity is 41% of the total price in micronized sand, whereas 6% in cement. The environmental impact of Portland cement is mainly from global warming potential, i.e. CO₂ emission.

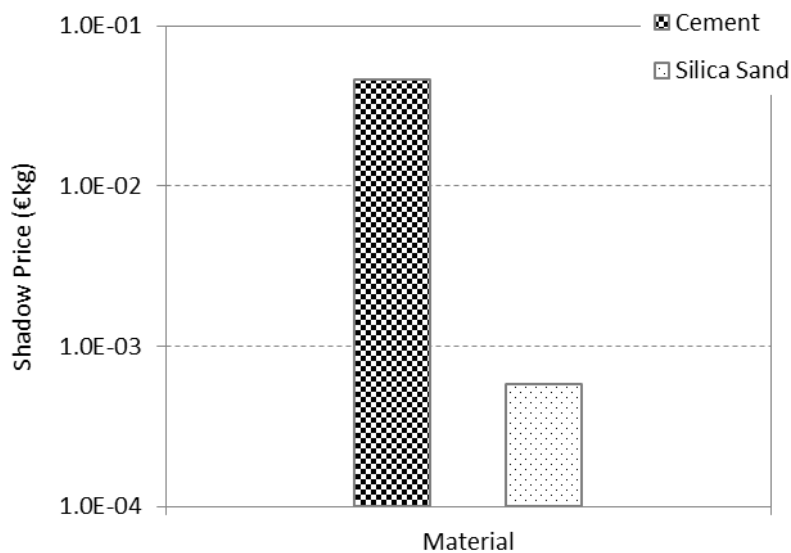


Figure 8.6. Shadow price of cement and silica sand.

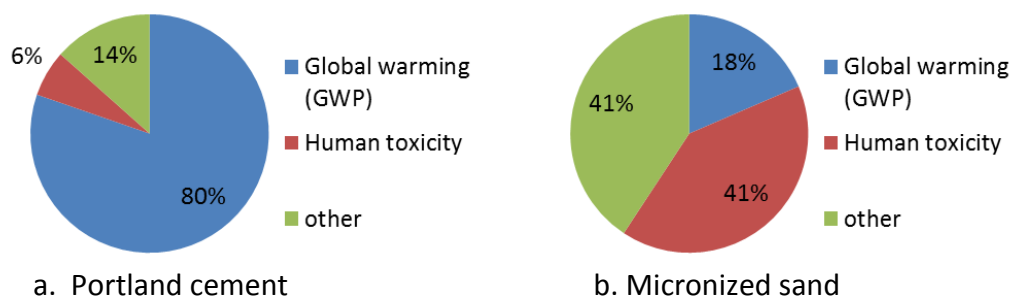


Figure 8.7. The share of shadow prices of categories in cement (a) and micronized sand (b).

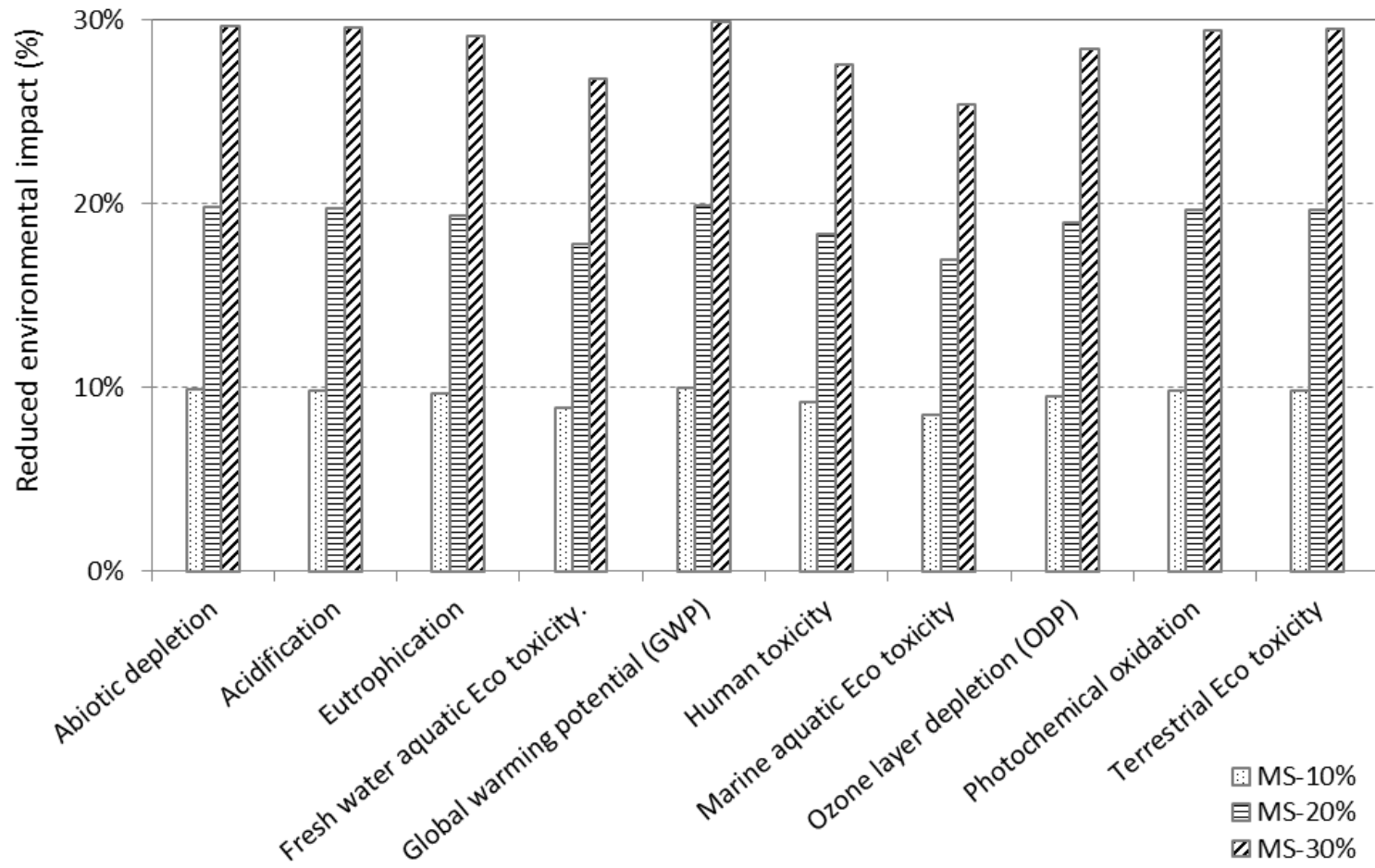


Figure 8.8. Reduced environmental impact of different mixtures.

The environmental impact and shadow price of cement paste under different replacement percentages of micronized sand were evaluated. The reduced environmental impact of blended material is shown in figure 8.8. The columns in figure 8.8 show that in every category the impact on the environment of the blended materials is reduced when the content of micronized sand increases. It also shows that a big improvement can be achieved on reducing CO₂ emission by using micronized sand.

In figure 8.9, the shadow prices of materials, mixtures of cement under different replacement percentage of micronized sand, are presented and compared to the shadow price of reference Portland cement. The shadow price of blended material decreases with the increasing replacement percentage of sand in the mixture. It indicates that blended materials are more environment-friendly and require lower cost for preventive measures to reduce the emissions to an acceptable level.

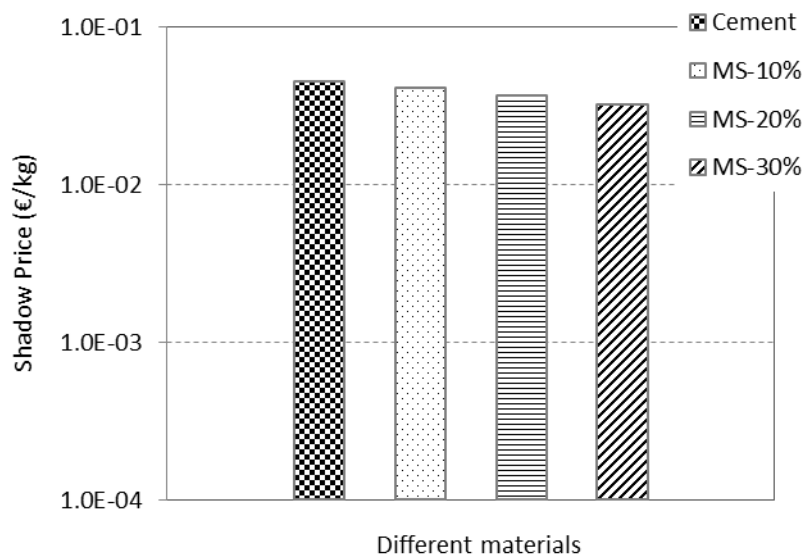


Figure 8.9. Shadow price of different materials: cement and mixtures of cement under different replacement percentage of micronized sand (MS).

8.7 Summary

In this chapter, micronized sand as the replacement of cement was analyzed from the sustainability point of view. Environmental impact of cement and micronized sand was studied. Blended concrete was compared with the normal concrete based on the life cycle assessment analysis. The following remarks can be made.

- The sustainability is a complex issue. In this study, sustainability was quantified by several impact categories and shadow price of the material was used to evaluate the costs for preventive measures.

- In all categories of sustainability, the assessed values of micronized sand were lower than the values of cement, about 2 orders of magnitude less, which indicates that micronized sand has less impact on the environment than cement.
- The use of micronized sand as cement replacement gave the biggest contribution in the category of reduction of global warming, i.e. CO₂ emission.
- Mixtures of cement blended with micronized sand have lower shadow price and less impact on the environment in comparison with plain cement. Blended materials are more environment-friendly, which is good from sustainable point of view.

Chapter 9

Mixture Design, Service Life and CO₂ Footprint

9.1 Mixture Design, Cost and Sustainability Aspect

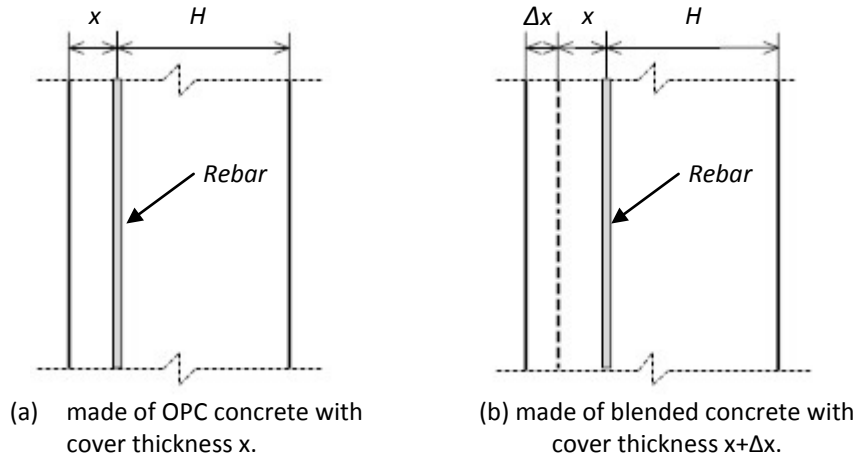
In chapter 6, cement-based mixtures were optimized by blending cement with micronized sand with different fineness. Ten mixture compositions are listed in table 9.1. Porosity and water permeability coefficients of plain and blended paste samples of simulations and experimental tests are shown. The cost of blended mixtures and the environmental impact represented by their shadow prices are also presented in table 9.1. The table shows that blended mixtures have a decreasing shadow price when the replacement percentage increases. Less impact of the mixed material on the environment can compensate for the relatively high cost of micronized sand in comparison with normal concrete.

Table 9.1 also gives useful information and advices for applying modified concrete in structures. Mixture 6 and mixture 10 are cheaper than plain cement paste (reference). Using these two mixtures for concrete structures is economically attractive and also results in a lower impact on the environment. Some properties of mixtures 6 and 10 are not as good as that of the reference, but they might be good enough for structures needed for temporary use. On the other hand, two blended materials, mixture 3 and mixture 5, are denser and less permeable compared to the reference OPC. The cost of these materials is a bit higher than the reference, however, structures made of these materials will require less maintenance because of the denser and less permeable microstructure. This will save lots of money for repair. In addition, the shadow price gives promising outcomes from the sustainability point of view.

9.2 Service Life and CO₂ Footprint

In section 8.6 it has been concluded that using micronized sand as replacement of cement can result in a reduction of CO₂ emission. In chapter 7 it has been discussed that the cover thickness needs to be increased to maintain a required service life for structures made of concrete blended with micronized sand as partial replacement of cement (hereinafter called concrete blended with micronized sand). It means that the amount of material (cement and micronized sand) used for these structures, has to be increased. This will, however, have a negative effect on the footprint of the structure elements. In this section, the CO₂ footprint of structures will be discussed in more detail. Parameters,

including the size of structural elements, replacement percentage of micronized sand used in concrete mixtures and required service life, will be taken into account. The one-sided reinforced structural elements are schematically shown in figure 9.1.



*Figure 9.1. One-sided reinforced concrete elements used for evaluation.
 (a) element made of OPC concrete with cover thickness x ;
 (b) element made of concrete blended with micronized sand with cover thickness $x + \Delta x$.*

The thickness of structural elements considered in this study is 25cm, 50cm and 100cm, the same as used in chapter 7. The replacement percentage of cement was varied from 10% to 30%, the same replacement percentage as used in previous chapters. The service life of structural elements was considered as 50, 80, 100 and 200 years. The DuraCrete model was used to design the cover thickness of structural elements with the required service life. The values of factors in the DuraCrete model have been determined in chapter 7.

In figure 9.2, the CO_2 footprints of structural elements are presented as a function of the required service life for mixtures with different micronized sand replacement percentages. These three charts show that with a required service life of 50, 80, 100 and 200 years the reduced CO_2 footprints are not influenced significantly by increasing service life. Furthermore, the CO_2 footprint of the structural elements is reduced with increasing replacement percentage of the micronized sand. For larger structural elements a reduction of the CO_2 footprint can be achieved up to 30% for mixtures with a replacement percentage of 30%.

Table 9.1. Evaluation of the material from different aspects.

<i>Mixtures</i>	<i>Proportion (%)</i>			<i>Packing Density</i>	<i>Porosity</i>		<i>Water Permeability</i>		<i>D_{nssm}</i> <i>RCM test</i>	<i>Cost</i> <i>(€/ton)</i>	<i>Shadow Price (€/ton)</i>
	<i>Cement</i>	<i>M6</i>	<i>M600</i>		<i>Simulation</i>	<i>Experiment</i>	<i>Simulation</i>	<i>Experiment</i>			
REF	1	0	0	0.7877	10.62%	23.68%	3.73	2.19	1.340E-11	39.53	9.43
Mixture 1	0.9	0.1	0	0.7903	8.28%	21.24%	3.77	1.43	1.671E-11	38.74	8.55
Mixture 2	0.8	0	0.2	0.8137	10.80%	25.00%	4.05	3.05	2.325E-11	45.4	7.66
Mixture 3	0.8	0.05	0.15	0.8124	9.40%	20.07%	2.77	1.36	---	43.54	7.66
Mixture 4	0.8	0.2	0	0.7929	12.90%	27.11%	4.8	2.77	1.806E-11	37.96	7.66
Mixture 5	0.7	0.1	0.2	0.8185	10.27%	22.07%	3.06	2.11	---	44.62	6.78
Mixture 6	0.7	0.3	0	0.795	17.84%	28.15%	8.59	4.29	2.628E-11	37.18	6.78
Mixture 7	0.6	0.2	0.2	0.8232	20.78%	---	9.21	---	---	43.84	5.89
Mixture 8	0.5	0	0.5	0.8115	38.93%	---	12.53	---	---	54.22	5.01
Mixture 9	0.5	0.3	0.2	0.8281	23.64%	---	10.46	---	---	43.05	5.01
Mixture 10	0.5	0.45	0.05	0.8115	24.73%	---	10.94	---	---	37.47	5.01

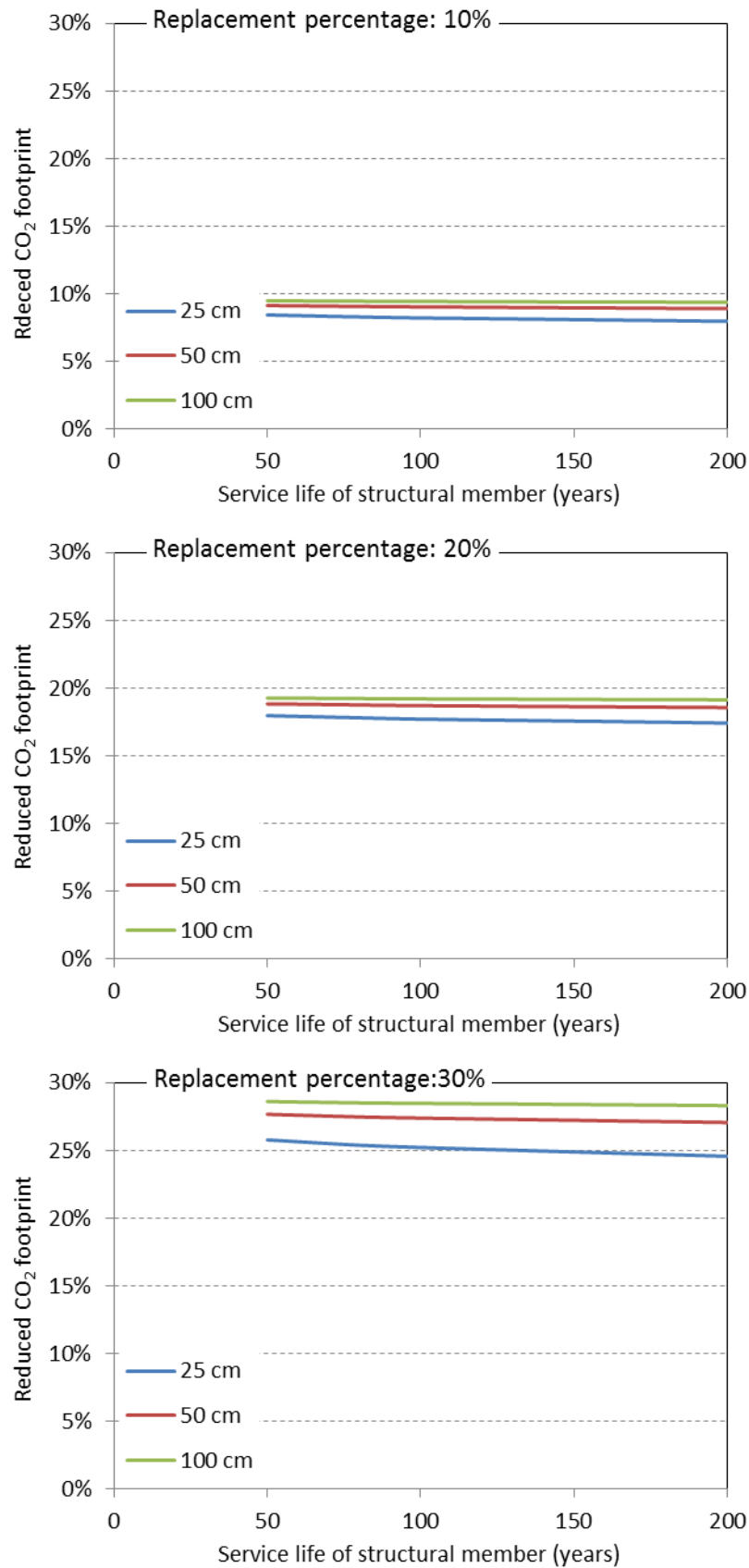


Figure 9.2. Reduced CO₂ footprint of structural elements with different sizes and different designed service life: 50, 80, 100 and 200 years (percentage of cement replacement is 10%, 20% and 30%).

9.3 Cost and Service Life

In the previous section it has been shown that the CO₂ footprint of structural elements made of concrete blended with micronized sand is reduced. In this section, structural elements made of concrete blended with micronized sand will be evaluated from the economic point of view.

Normally, the material costs of structures are strongly related to the size and the required service life. Figure 9.3 shows the reduced material cost of structural elements made of concrete blended with micronized sand. The material cost of the structural element made of OPC concrete was used as the reference. Figure 9.3 shows that the material cost can be substantially reduced when the cement is partially replaced by micronized sand.

The graphs in figure 9.3 show that for higher values of the required service life the savings will become less. For a structural element made of concrete blended with micronized sand, the cover thickness has to be increased in order to protect the steel rebar and meet the required service life (see in figure 7.5). Increasing cover thickness indicates a higher amount of material used in structural elements and results in a higher cost. With increasing size of structural element (represented by $x+H$ in figure 9.1), a higher reduction of material cost is achieved. The economic benefits of using concrete blended with micronized sand increases with the increasing size of a structure. This is in agreement with the discussion in section 7.5. Figure 9.3 shows that, with different replacement percentages of cement, i.e. from 10% to 30%, the material cost are as a function of the replacement percentage. The higher the replacement percentage of micronized sand used in concrete mixture, the lower the material cost of the structural element is. The saving of material cost can reach around 5% for mixtures with 30% of cement replacement.

From figures 9.2 and 9.3, it can be inferred that with increasing required service life, both the CO₂ footprint and the material cost of the structural element are reduced. The saving of the CO₂ footprint and the material cost is getting smaller with increasing required service life. For a required service life less than 100 years, which is the value normally used in service life design, using concrete blended with micronized sand for structures can be beneficial from both the economic and sustainability points of view.

It has to be noticed that the micronized sand used in this study is relatively expensive. The material cost can be reduced further if cheaper resources of quartz sand are available. There are possible ways to lower the cost of sand. Since for practical purpose, the sand does not need to meet the high purity of SiO₂ or extremely high fineness, the milling and cleaning processes of producing micronized sand can be shortened and less intensive. Therefore, the cost of sand can be cheaper.

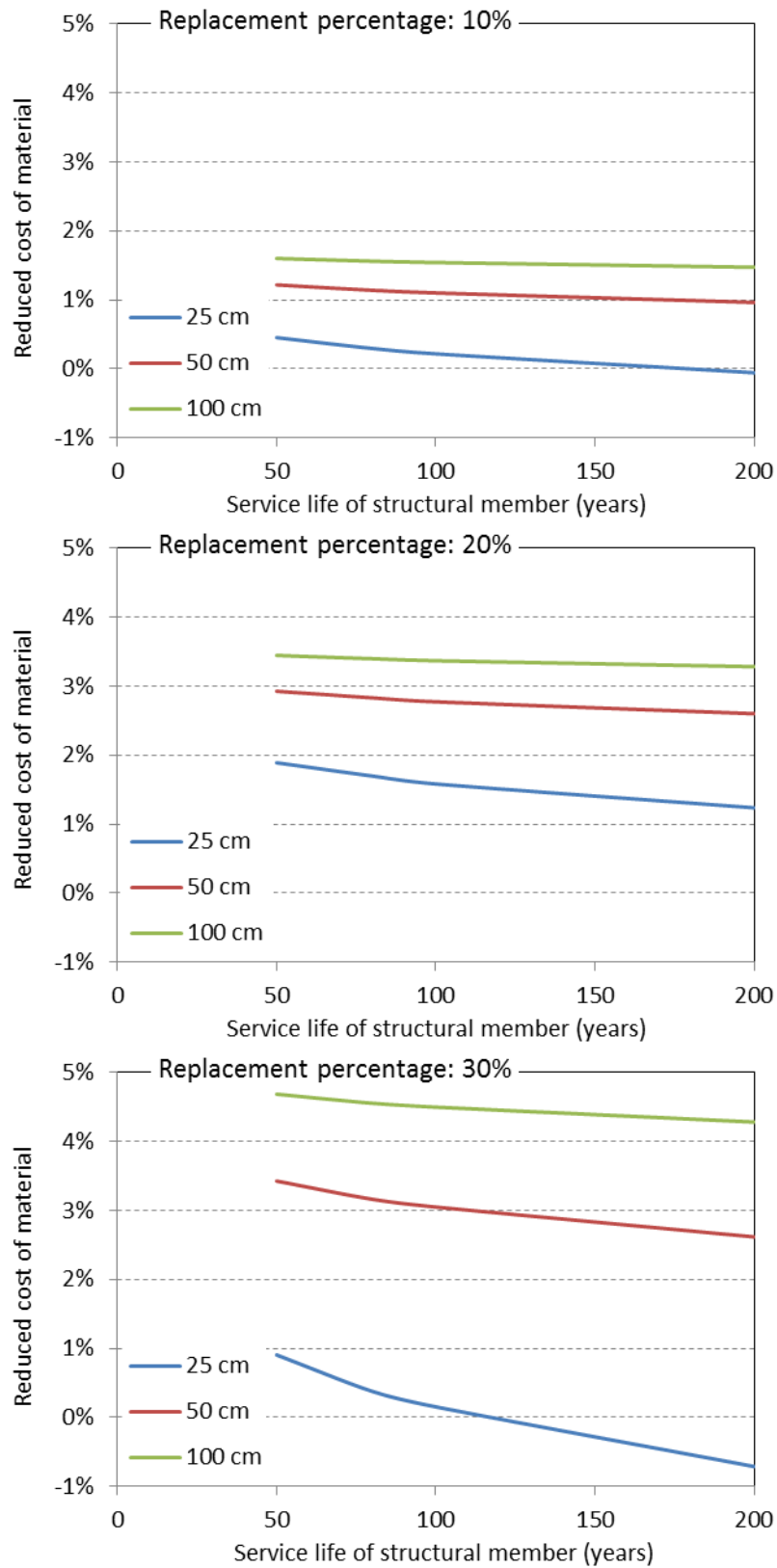


Figure 9.3. Reduced material cost of structural elements with different sizes and different designed service life: 50, 80, 100 and 200 years (percentage of cement replacement is 10%, 20% and 30%).

9.4 Summary

In this chapter, CO₂ footprints and material costs of structural elements made of concrete blended with micronized sand have been evaluated. Service lives from 50 to 200 years and replacement percentages of cement from 10% to 30% were taken into account. The results for structural elements made of concrete blended with micronized sand were very promising. Several remarks can be made:

- Using concrete blended with micronized sand for structures is economically attractive and also results in less impact on the environment.
- With a required service life of 50, 80, 100 and 200 years the reduction of the CO₂ footprints was not significantly influenced by the required service life. The CO₂ footprint of structural elements decreases with increasing amount of micronized sand in the concrete.
- The material costs are directly related to the replacement percentage of cement. The savings of material cost can reach up around 5% for mixtures with 30% of cement replacement. The higher the replacement percentage of micronized sand used in concrete mixture, the lower the material cost of the structural element was.
- With increasing required service life, both CO₂ footprint and material cost were reduced for structural elements made of concrete blended with micronized sand. The saving of CO₂ footprint and material cost was getting smaller with increasing service life. For a required service life less than 100 years, which is the value normally used in service life design, using concrete blended with micronized sand for structures can be beneficial from both economic and sustainability points of view.

Chapter 10

Retrospection, Conclusions and Further Research

10.1 Retrospection

Concrete is one of the most important construction materials in the world. However, Portland cement, one of the constituents of concrete, is responsible for about 5-10% of global CO₂ emission. From sustainability point of view, it is important, therefore, to search for materials which can be used to reduce or to replace Portland cement in concrete. Among the mineral admixtures, micronized sand, with high purity SiO₂, has been selected as cement replacement in this study. The objective of this research is to investigate the possibility of using micronized sand to partially replace Portland cement in concrete. The performance of cement-based material blended with micronized sand was evaluated with respect to the microstructure, durability and sustainability, both experimentally and by numerical simulations.

In the literature review, the effects of fillers on cement-based material were discussed. A further review of the effects of fillers on microstructure development as well as durability aspects was presented.

In the experimental program, micronized sand, M6, M300 and M600 indicating increasing fineness, were used. The cement was replaced by 10%, 20% and 30% micronized sand, respectively. The results of experimental studies showed that, although micronized sand is considered as an inert material, it affects the hydration process and microstructure development, especially the pore structure of blended cement paste. The effects of micronized sand on blended cement paste were assigned to dilution effect and heterogeneous nucleation effect. It was also found that there is an interfacial zone between micronized sand and hydration products. It is one of the most important factors regarding transport properties of the blended material.

The transport properties of cement-based material blended with micronized sand were investigated in chapter 4. Water permeability measurements on paste and rapid chloride migration tests on concrete were used to evaluate water permeability and chloride diffusivity. Results showed that the water permeability coefficients and chloride diffusivity coefficients of cement-based material blended with micronized sand were in the same order of magnitude as reference samples. Micronized sand as cement replacement in mixtures in which the replacement percentage was

up of 30% did not alter the transport properties very much. The interfacial zone between micronized sand and hydration products influences the connectivity of capillary pores, which was discussed in chapter 4. The connectivity of capillary pores, represented by the volume of the interfacial zone in the blended samples was an important factor determining the permeability.

Numerical simulation is very useful for understanding the effect of micronized sand on the hydration process and microstructure development of cement paste. The HYMOSTRUC3D model was adapted to simulate the cement hydration and microstructure development of cement blended with micronized sand. The simulated microstructures were used to trace the connectivity of capillary pores. The water permeability coefficients of materials were predicted based on the simulated microstructures. Simulated results were in good agreement with experimental results. Numerical simulation turned out to be useful for designing cement-based material blended with micronized sand.

To find an optimal mixture design, micronized sands with different fineness were mixed with Portland cement. The Linear Packing Model with continuous description (see chapter 6.2.1) was used to calculate the packing density of material blended with micronized sand with different fineness. Simulation results showed that the pore structure of optimized mixtures was finer by mixing coarse sand M6 and fine sand M600 with cement. The microstructure of optimized mixtures resulted in lower permeability.

The service life prediction of structures made of concrete blended with micronized sand was evaluated by using the DuraCrete model in chapter 7. In this model the end of service life was assumed to be reached when the chloride concentration at the reinforcement had reached a critical threshold value for initiation of corrosion. The chloride profiles and the cover thickness were evaluated for structures made of concrete blended with micronized sand as partial replacement of cement. To meet the required service life, the cover thickness of structures made with concrete blended with micronized sand was evaluated.

In chapter 8, the environmental impact of micronized sand was evaluated and compared with Portland cement. The footprints showed that environmental impact of micronized sand was much lower than that of Portland cement. The use of micronized sand as cement replacement gave a large contribution of reducing CO₂ emission.

In the last chapter, the CO₂ footprints and the material costs of structural elements have been evaluated. Different required service lives and different percentages of cement replacement were taken into account. Results for structural elements made of concrete blended with micronized sand were very promising. With increasing required service life, i.e. 50,

100, 150 and 200 years as considered in this study, both the CO₂ footprint and the material cost of the structural elements decreased.

10.2 Conclusions

In this thesis, the performance of cement-based material blended with micronized sand was evaluated both experimentally and by numerical simulations. Blended materials were evaluated with respect to not only transport properties regarding durability, but also sustainability aspects. The general conclusions of this research are given as follows:

- Up to the age of 28 days, the degree of hydration of cement in cement pastes blended with micronized sand increases by using micronized sand. Therefore, in a blended system the Portland cement is used more efficiently than in plain paste.
- The pore structure of cement paste is influenced by the presence of micronized sand. A different pore size distribution in the range from 0.1 μm -0.5 μm appears in the blended samples in comparison with OPC paste. Pores in this range are defined as large capillary pores in chapter 3, which significantly influence the permeability.
- There is a clear interfacial zone between micronized sand and hydration products. Its thickness is hardly influenced by the fineness or replacement level (up to 30%) of the micronized sand. This interfacial zone is caused by the surface energy of micronized sand to prevent hydration products precipitating on the surface of sand particles. The interfacial zone is considered as an important factor for the transport properties of cement pastes blended with micronized sand.
- At the ages of 28 days and 90 days, with water to binder ratio of 0.4, results of samples showed that the water permeability coefficients and chloride diffusivity coefficients of cement-based material blended with micronized sand were in the same order of magnitude as reference sample (OPC paste in water permeability measurement, OPC concrete in chloride diffusivity tests). The presence of micronized sand in the mixture, up to replacement percentages of 30%, does not change the long-term transport properties very much.
- The connectivity of the pores, represented by the volume of the interfacial zone in the blended pastes, strongly influences the permeability of material.
- The microstructure of cement paste blended with micronized sand can be simulated by the modified and extended HYMOSTRUC3D simulation model. The connectivity of pores can be determined and the water permeability coefficients can be predicted based on the

simulated microstructure. Numerical simulation is a very important approach to design cement-based materials blended with micronized sand.

- By mixing micronized sand with different fineness the pore structure can be manipulated, i.e. refined. A microstructure with lower connectivity results in a lower permeability. There is a maximum amount of M600 that can be used effectively in the mixtures. Beyond the maximum amount of M600, any additional amount of M600 does not contribute to a denser packing system and a denser microstructure.
- Structures made of concrete blended with micronized sand can meet the required service life criteria by adjusting the cover thickness. The increase of the cover thickness is relatively small compared to the size of the structural elements.
- The environmental impact of micronized sand was lower than the values for cement for all the sustainability categories, about 2 orders of magnitude less. This indicates that micronized sand has less impact on the environment than cement. Micronized sand as an environment-friendly replacement of cement gave the biggest contribution in the category of reduction of global warming, i.e. CO₂ emission.
- With increasing required service life, both CO₂ footprint and material cost of a structural element are reduced by using concrete blended with micronized sand as partial replacement of cement. Concrete blended with micronized sand is recommended for use in structures of which the required service life is less than 100 years. The benefit can be received from both economic and sustainability points of view.

10.3 Further Research

This thesis presents promising results for the use of micronized sand as replacement of cement in cement-based materials. Further research can focus on different aspects of the material properties as well as other durability aspects to further improve and optimize the use of micronized sand as replacement of cement in cement-based materials. Several aspects are recommended for further research:

- 1). More durability properties research in details.

The durability of concrete structures made of blended with blended cement needs to be evaluated in more detail. In this study, only chloride-induced corrosion was studied. Besides chloride ingress also other aspects need to be investigated, such as carbonation, alkali-silica reaction of the material and freeze-thaw action.

2). Interfacial zone properties.

In chapter 3, an interfacial zone was observed between micronized sand and hydration products. It was found that this interfacial zone has a big effect on permeability of blended cement pastes and determines the transport properties significantly. In future research, it will be important and necessary to investigate this zone in more detail. For instance, from the mechanical point of view how the adhesion strength of the paste matrix with micronized sand will influence the bulk matrix. The porosity and permeability of this zone need to be figured out: how much does it differ from the bulk matrix and affect the blended material? Furthermore, in concrete there is the interfacial transition zone between aggregate and hydration products. It is also important to figure out if micronized sand can influence this interfacial transition zone.

3). Mechanical properties.

In this study, only the relation between microstructure and transport properties was studied, as well as sustainability aspects. The mechanical properties were not considered. For an integral judgment of the potential of micronized sand as cement replacement, it is necessary to take all the properties into account. Compressive strength, tensile strength and ductility are, of course, relevant properties for the use of concrete blended with micronized sand in practice.

4). Combination of other mineral admixtures.

Some mechanical and transport properties of cement-based materials are influenced by micronized sand, since it is inert and does not have pozzolanic effect. It is possible to use a combination of micronized sand with pozzolanic mineral admixtures such as rice husk ash, fly ash or slag to replace cement. The combination of several mineral admixtures may have a positive effect on the properties of material. This aspect should be investigated in the future.

5). Searching for cheaper sand filler

The micronized sand used in this study is quite expensive. There are several ways to lower the cost of sand. Since for practical purpose, the sand does not need to meet the high purity of SiO_2 or extremely high fineness, the milling and cleaning processes of producing micronized sand can be shortened and less intensive. Therefore, the cost of sand can be cheaper.

Bibliography

- Aligizaki, K. K. (2006). Pore structure of cement-based materials, Taylor & Francis.
- Banthia, N. and S. Mindess (1989). "Water permeability of cement paste." Cement and Concrete Research **19**(5): 727-736.
- Basheer, L., J. Kropp, et al. (2001). "Assessment of the durability of concrete from its permeation properties: A review." Construction and Building Materials **15**(2-3): 93-103.
- Bentz, D. P. (2008). "Virtual pervious concrete: microstructure, percolation, and permeability." ACI MATERIALS JOURNAL **105**(3).
- Bentz, D. P. and J. T. Conway (2001). "Computer modeling of the replacement of "coarse" cement particles by inert fillers in low w/c ratio concretes Hydration and strength." Cement and Concrete Research **31**(3): 503-506.
- Bentz, D. P. and E. J. Garboczi (1991). "A Digitized Simulation Model for Microstructural Development." Advances in Cementitious Materials **16**: 221-226.
- Bentz, D. P. and E. J. Garboczi (1991). "Percolation of phases in a three-dimensional cement paste microstructural model." Cement and Concrete Research **21**(2-3): 325-344.
- Bentz, D. P., E. J. Garboczi, et al. (1999). "Effects of cement particle size distribution on performance properties of Portland cement-based materials." Cement and Concrete Research **29**(10): 1663-1671.
- Bentz, D. P. and P. E. Stutzman (1994). SEM analysis and computer modelling of hydration of portland cement particles. Philadelphia.
- Bertolini, L., B. Elsener, et al. (2004). Corrosion of steel in concrete: prevention diagnosis, repair. Weinheim, Wiley-VCH Verlag GmbH & Co. KGaA.
- Boel, V., K. Audenaert, et al. (2007). "Transport properties of self compacting concrete with limestone filler or fly ash." Materials and Structures/Materiaux et Constructions **40**(5): 507-516.
- Bonavetti, V., H. Donza, et al. (2003). "Limestone filler cement in low w/c concrete: A rational use of energy." Cement and Concrete Research **33**(6): 865-871.
- Cabal, H., Y. Lechón, et al. (2005). European sustainable electricity; comprehensive analysis of future European demand and generation of European electricity and its security of supply.
- Collepari, M., A. Marcialis, et al. (1972). "Penetration of chloride ions into cement pastes and concretes." Journal of the American Ceramic Society **55**(10): 534-535.
- Cook, R. A. and K. C. Hover (1991). "Experiments on the contact angle between mercury and hardened cement paste." Cement and Concrete Research **21**(6): 1165-1175.

Cook, R. A. and K. C. Hover (1999). "Mercury porosimetry of hardened cement pastes." Cement and Concrete Research **29**(6): 933-943.

Copeland, L. E. and J. C. Hayes (1953). "The determination of non-evaporable water in hardened Portland cement pastes." ASTM Bulletin **194**: 70-74.

Cui, L. a. C., J. H.. (2001). "Permeability and pore structure of OPC paste." CEMENT and CONCRETE RESEARCH **31**(2): 277-282.

Cyr, M., P. Lawrence, et al. (2005). "Mineral admixtures in mortars: Quantification of the physical effects of inert materials on short-term hydration." Cement and Concrete Research **35**(4): 719-730.

Cyr, M., P. Lawrence, et al. (2006). "Efficiency of mineral admixtures in mortars: Quantification of the physical and chemical effects of fine admixtures in relation with compressive strength." Cement and Concrete Research **36**(2): 264-277.

de Bruyn, S., M. Korteland, et al. (2010). Valuation and weighting of emissions and environmental impacts. Delft, CE Delft.

de Larrard, F. (1989). "Ultrafine particles for the making of very high strength concretes." Cement and Concrete Research **19**(2): 161-172.

de Larrard, F. and T. Sedran (1994). "Optimization of ultra-high-performance concrete by the use of a packing model." Cement and Concrete Research **24**(6): 997-1009.

De Schutter, G. Limestone filler based self-compacting concrete: from microstructure to engineering properties.

De Schutter, G. (2011). Effect of Limestone Filler as Mineral Addition in Self-compacting Concrete. 36th Conference on Our World in Concrete & Structures. Singapore.

De Vries , W. (2008). The use of micronized sand as cement replacement. Delft, Delft University of Technology. **Master**.

Diamond, S. (2000). "Mercury porosimetry: An inappropriate method for the measurement of pore size distributions in cement-based materials." Cement and Concrete Research **30**(10): 1517-1525.

Diamond, S. (2001). "Considerations in image analysis as applied to investigations of the ITZ in concrete." Cement and Concrete Composites **23**(2-3): 171-178.

Diamond, S. and J. Huang (2001). "The ITZ in concrete - a different view based on image analysis and SEM observations." Cement and Concrete Composites **23**(2-3): 179-188.

Diamond, S. and M. E. Leeman (1994). Pore size xistributions in hardened cement paste by SEM image analysis. Microstructure of Cement-Based Systems/Bonding and Interfaces in Cement-Based Materials.

DuraCrete. (2000). DuraCrete Final Technical Report R17. Gouda, The European Union – Brite EuRam III, DuraCrete – Probabilistic Performance based Durability Design of Concrete Structures, CUR, .

Elfgren, L. and J.-E. Jonasson (2000). Enegetically modified cement (EMC) and Ordinary Portland cement (OPC) - A comparison, Center of High Performance Cement, LuLeå University of Technology.

Elkington, J. (1997). Cannibals with forks: The triple bottom line of 21st century business. Oxford, Capstone.

Francy, O. and R. François (1998). "Measuring chloride diffusion coefficients from non-steady state diffusion tests." Cement and Concrete Research **28**(7): 947-953.

Frischknecht, R., N. Jungbluth, et al. (2007). Implementation of life cycle impact assessment methods. ecoinvent report No. 3. R. Frischknecht and N. Jungbluth. Dübendorf, Swiss Centre for Life Cycle Inventories.

Gallé, C. (2001). "Effect of drying on cement-based materials pore structure as identified by mercury intrusion porosimetry - A comparative study between oven-, vacuum-, and freeze-drying." Cement and Concrete Research **31**(10): 1467-1477.

Garboczi, E. J. (1990). "Permeability, diffusivity, and microstructural parameters: A critical review." Cement and Concrete Research **20**(4): 591-601.

Geoffrey, G. (1999). Percolation (2. ed), Springer Verlag.

Gibbs, M. J., S. P., et al. CO₂ emission from cement production. Good Practice Guidance and Uncertainty Management in National Greenhouse Gas Inventories.

Guinée, J. B., M. Gorrée, et al. (2001). Life cycle assessment An operational guide to the ISO standards; Characterisation and Normalisation Factors. G. J. B.

Halamickova, P., R. J. Detwiler, et al. (1995). "Water permeability and chloride ion diffusion in portland cement mortars: Relationship to sand content and critical pore diameter." CEMENT and CONCRETE RESEARCH **25**(4): 790-802.

He, H. (2012). Computational modelling of particle packing in concrete Delft, Delft University of Technology. **Doctor**.

<http://en.wikipedia.org/wiki/Nucleation>.

Hu, J. and P. Stroeven (2003). "Application of image analysis to assessing critical pore size for permeability prediction of cement paste." Image Anal Stereol **22**: 97-103.

Jennings, H. M. and S. K. Johnson (1986). "SIMULATION OF MICROSTRUCTURE DEVELOPMENT DURING THE HYDRATION OF A CEMENT COMPOUND." Journal of the American Ceramic Society **69**(11): 790-795.

Johansson, K., C. Larsson, et al. (1999). "Kinetics of the hydration reactions in the cement paste with mechanochemically modified cement 29Si magic-angle-spinning NMR study." Cem. Concr. Res **29**: 1575-1581.

Jonasson, J.-E., V. Ronin, et al. (1996). High strength concretes with energetically modified cement and modeling of shrinkage caused by self-desiccation. Proceedings of the 4th International Symposium on the Utilization of High Strength/High Performance Concrete. R. L. E. F. de Larrard. Paris, France, Presses Pont et Chaussées (ISBN 2-85978-258-3). **vol. 2**.

Jones, M., L. Zheng, et al. (2002). "Comparison of particle packing models for proportioning concrete constituents for minimum voids ratio." Materials and Structures **35**(5): 301-309.

Justnes, H., P. A. Dahl, et al. (2007). "Microstructure and performance of energetically modified cement (EMC) with high filler content." Cement & Concrete Composites **29**.

Justnes, H., L. Elfgren, et al. (2005). "Mechanism for performance of energetically modified cement versus corresponding blended cement." Cement and Concrete Research **35**(2): 315-323.

Katz, A. J. a. T. A. H. (1986). "Quantitative prediction of permeability in porous rock." The American Physical Society **34**(11): 8179-8181.

Khatri, R. P. and V. Sirivivatnanon (1997). "Methods for the determination of water permeability of concrete." ACI MATERIALS JOURNAL **94**(3): 257-261.

Koenders, E. (1997). Simulation of volume changes in hardening cement-based materials. Delft, Delft University of Technology. **PhD**.

Koenders, E. A. B., M. Ottel , et al. (2008). A spreadsheet model for service-life predictions, the Second International Conference on Concrete Repair, Rehabilitation and Retrofitting (ICCRRR 2008), Cape Town, South Africa, Taylor & Francis Group, London.

Kutay, M. E., A. H. Aydilek, et al. (2006). "Laboratory validation of lattice Boltzmann method for modeling pore-scale flow in granular materials." Computers and Geotechnics **33**(8): 381-395.

Lange, D. A., H. M. Jennings, et al. (1994). "Image analysis techniques for characterization of pore structure of cement-based materials." Cement and Concrete Research **24**(5): 841-853.

Lange, F., H. M rtel, et al. (1997). "Dense packing of cement pastes and resulting consequences on mortar properties." Cement and Concrete Research **27**(10): 1481-1488.

Larson, A. (2011). Sustainability, Innovation, and Entrepreneurship.

Lawrence, P., M. Cyr, et al. (2003). "Mineral admixtures in mortars: Effect of inert materials on short-term hydration." Cement and Concrete Research **33**(12): 1939-1947.

Lawrence, P., M. Cyr, et al. (2005). "Mineral admixtures in mortars effect of type, amount and fineness of fine constituents on compressive strength." Cement and Concrete Research **35**(6): 1092-1105.

Maage, M., S. Helland, et al. (1996). "Service life prediction of existing concrete structures exposed to marine environment." ACI Materials Journal **93**(6): 602-608.

McGrath, P. F. and R. D. Hooton (1996). "Influence of voltage on chloride diffusion coefficients from chloride migration tests." Cement and concrete research **26**(8): 1239-1244.

McNally, C., M. G. Richardson, et al. (2005). Chloride diffusion coefficient determination for specifications. Proceedings of the 6th International Congress on Global Construction Thomas Telford.

Meyer, C. (2009). "The greening of the concrete industry." Cement and Concrete Composites **31**(8): 601-605.

Mindess, S., J. F. Young, et al. (2002). Concrete 2nd Edition, Prentice Hall, Englewood Cliffs, NJ.

Molina, L. (1992). On predicting the influence of curing conditions on the degree of hydration. CBI Report Stockholm, Swedish Cement and Concrete Research Institute. **5**.

Moosberg-Bustnes, H., B. Lagerblad, et al. (2004). "The function of fillers in concrete." Materials and Structures **37**.

Moro, F. and H. Böhni (2002). "Ink-bottle effect in mercury intrusion porosimetry of cement-based materials." Journal of Colloid and Interface Science **246**(1): 135-149.

Muskat, M. (1937). The flow of homogeneous fluids through porous media. New York, McGraw-Hill Book Company Inc.

Navi, P. and C. Pignat (1996). "Simulation of cement hydration and the connectivity of the capillary pore space." Advanced Cement Based Materials **4**(2): 58-67.

Neville, A. M. (2006). Properties of concrete, Pearson Education Limited.

NGUYỄN, V. T. (2011). Rice husk ash as a mineral admixture for ultra high performance concrete. Faculty of Civil Engineering and Geosciences. Delft, Delft University of Technology. **PhD**.

NIBE (2012). "Omschrijving methode milieuclassificatie bouwproducten.TWIN2011-MODEL. Retrieved from <http://www.nibe.org>."

NT BUILD 492 (1999). Concrete migration coefficient from non-steady-state migration experiments.

Olivier, J. G. J., G. Janssens-Maenhout, et al. (2011). Long-term trend in global CO₂ emissions. Julian PBL Netherlands Environmental Assessment Agency.

Ollivier, J. P. and M. Massat (1992). "Permeability and microstructure of concrete: a review of modelling." CEMENT and CONCRETE RESEARCH **22**: 503-514.

Pade, C. and M. Guimaraes (2007). "The CO₂ uptake of concrete in a 100 year perspective." Cement and Concrete Research **37**(9): 1348-1356.

Polder, R. B. and M. R. De Rooij (2005). "Durability of marine concrete structures - Field investigations and modelling." Heron **50**(3): 133-154.

Poppe, A. M. and G. de Schutter (2005). "Cement hydration in the presence of high filler contents." Cement and concrete research **35**: 2290-2299.

Powers, T. C., L. E. Copeland, et al. (1955). "Permeability of portland cement paste." ACI Journal Proceeding **51**: 285-298.

Rehan, R. and M. Nehdi (2005). "Carbon dioxide emissions and climate change: policy implications for the cement industry." Environmental Science & Policy **8**: 105-114.

Richardson, M. G. (2002). Fundamentals of durable reinforced concrete., London and New York: Modern Concrete Technology.

Rodrigues, F. and I. Joeke (2011). "Cement industry: sustainability, challenges and perspectives." Environmental Chemistry Letters **9**(2): 151-166.

Ronin, V. and L. Elfgren (2009). "High volume Pozzolan concrete : three years of industrial experience in Texas with CemPozz." Concrete in Focus **8**(2): 22-27.

Ronin, V., J. E. Jonasson, et al. (1997). Advanced modification technologies of the Portland cement based binders for different high performance applications. 10th International Congress on the Chemistry of Cement. Gothenburg, Sweden, Amarkai. **2**: 8.

Samir E, C. (2009). "Sustainability of civil engineering structures – Durability of concrete." Cement and Concrete Composites **31**(8): 513-514.

Scrivener, K. L. (2004). "Backscattered electron imaging of cementitious microstructures: understanding and quantification." Cement and Concrete Composites **26**(8): 935-945.

Siemes, T., P. Schiessl, et al. (2000). Future developments of service life design of concrete structures on the basis of DuraCrete. Service life prediction and ageing management of Concrete Structures, RILEM Publications SARL.

Siemes, T., T. Vrouwenvelder, et al. (1985). "Durability of buildings: a reliability analysis." HERON **30**(3): 2-48.

Stovall, T., F. de Larrard, et al. (1986). "Linear packing density model of grain mixtures." Powder Technology **48**(1): 1-12.

Struble, L. and J. Godfrey (2004). How sustainable is concrete? International Workshop on Sustainable Development and Concrete Technology. Beijing.

Stumm, W. (1992). Chemistry of the Solid-Water Interface: Processes at the Mineral-Water and Particle-Water Interface in Natural Systems, John Wiley & Sons, Inc.

Stutzman, P. E. and J. R. Clifton (1999). Specimen preparation for Scanning Electron Microscopy. twenty-First international conference on cement microscopy., Las vegas, Nevada.

Tang, L. P. (2006). Chloride induced corrosion in concrete structures testing and modelling. Bridge and Infrastructure Research in Ireland: Symposium. Ireland.

Tang, L. P. (2006). Service-life prediction based on the rapid migration test and the ClinConc model. Intl. RILEM Workshop on Performance Based Evaluation and Indicators for Concrete Durability. Madrid, Spain.

van Breugel, K. (1991). Simulation of hydration and formation of structure in hardening cement-based materials. Delft, Delft University of Technology. **PhD**.

Van Den Heede, P. and N. De Belie (2012). "Environmental impact and life cycle assessment (LCA) of traditional and 'green' concretes: Literature review and theoretical calculations." Cement and Concrete Composites **34**(4): 431-442.

van der Wegen, G., R. B. Polder, et al. (2012). "Guideline for service life design of structural concrete-a performance based approach with regard to chloride induced corrosion." Heron in press.

Wang, Y., G. Ye, et al. (2008). Microstructure characteristics in the cement paste containing micronized sand filler. International Conference on Microstructure Related Durability of Cementitious Composites. Nanjing, China.

Washburn, E. W. (1921). "Note on a method of determining the distribution of pore sizes in a porous material." Proc. Natl. Acad. Sci USA **7**: 115-116.

Webster, M. P. (2000). The Assessment of Corrosion-damaged Concrete Structures. School of Civil Engineering, University of Birmingham. **PhD**.

Winslow, D. N. (1968). The pore size distribution of Portland cement paste, Lafayette, IN: Purdue University.

Wong, H. S., M. K. Head, et al. (2006). "Pore segmentation of cement-based materials from backscattered electron images." Cement and Concrete Research **36**(6): 1083-1090.

www.concreteSDC.org (2008). Concrete sustainability: A vision for sustainable construction with concrete in north America.

www.sibelco.be.

Ye, G. (2003). Experimental study and numerical simulation of the development of the microstructure and permeability of cementitious materials. Delft, Delft University of Technology. **PhD**.

Ye, G. and K. van Breugel (2009). "Simulation of connectivity of capillary porosity in hardening cement-based systems made of blended materials." HERON **54**(2/3).

Zhang, M., Y. He, et al. (2011). "Computational investigation on mass diffusivity in Portland cement paste based on X-ray computed microtomography (μ CT) image." Construction and Building Materials(0).

Zhang, M., G. Ye, et al. (2011). Lattice Boltzmann simulation of the ionic diffusivity of cement paste. International Conference on Advances in Construction Materials through Science and Engineering. Hong Kong.

Zhang, T., Q. Yu, et al. (2011). "A gap-graded particle size distribution for blended cements: Analytical approach and experimental validation." Powder Technology **214**(2): 259-268.

Zhou, J., G. Ye, et al. (2010). "Characterization of pore structure in cement-based materials using pressurization-depressurization cycling mercury intrusion porosimetry (PDC-MIP)." Cement and Concrete Research **40**(7): 1120-1128.

Summary

Concrete is one of the most important construction materials in the world. However, Portland cement which is one of the constituents of concrete is responsible for about 5-10% of global CO₂ emission. From sustainability point of view, therefore, it is important to search for materials which can be used to reduce or to replace Portland cement in concrete. Among the mineral admixtures micronized sand with high purity SiO₂ has been selected as cement replacement. Micronized sand is produced by grinding of quartz sand, which is the most abundant mineral in the earth's crust. Therefore, the use of this material will not cause a depletion of resources. The objective of this research is to investigate the possibility of using micronized sand to partially replacement cement in concrete. The performance of cement-based material with micronized sand as partial replacement of cement was evaluated with respect to the microstructure, durability and sustainability both experimentally and by numerical simulations.

In the literature review the effects of fillers on cement-based material were discussed. A further review of the effects of fillers on the microstructure development as well as the durability aspects was presented. Using micronized sand as cement replacement was found to be very promising.

In the experimental program micronized sands M6 (coarse), M300 (medium) and M600 (fine) were used. The cement was replaced by 10%, 20% and 30% micronized sand, respectively. The results of experimental studies showed that although micronized sand is considered as an inert material, it affects the hydration process, microstructure development and especially the pore structure of blended cement paste. The effects of micronized sand on blended cement paste were assigned to a dilution effect and a heterogeneous nucleation effect. The degree of hydration of cement in the blended pastes was increased by adding micronized sand. Thus Portland cement is used more efficiently in the blended mixtures. It was also found that there is an interfacial zone between micronized sand and hydration products. The results of image analysis showed that the thickness of this interfacial zone was hardly influenced by the fineness or replacement level of micronized sand in the material. The interfacial zone was caused by the surface energy of micronized sand that prevents hydration products precipitating on the surface of sand particles. The porous interfacial zone is a very important factor that influences the transport properties of the blended material.

The transport properties of cement-based material with micronized sand as partial replacement of cement were investigated experimentally, i.e. by water permeability measurements and chloride diffusivity tests. Results of samples at the age of 90 days showed that the water permeability coefficients and chloride diffusivity coefficients of material with micronized sand as partial replacement of cement were in the same order of magnitude as reference sample (OPC paste in water permeability measurement, OPC concrete in chloride diffusivity tests). Micronized sand as cement replacement in mixtures, in which the replacement percentage was up of 30%, did not alter the transport properties very much.

Numerical simulation is very useful for understanding the effect of micronized sand on the hydration process and microstructure development of cement paste. The HYMOSTRUC3D model was adapted to simulate the hydration and microstructures development of cement past blended with micronized sand. Based on the simulated microstructures, the connectivity of capillary pores was evaluated, and the water permeability coefficients of materials were predicted. Simulated results were in good agreement with experimental results. Numerical simulation turned out to be very instrumental for designing cement-based material blended with micronized sand.

To find an optimal mixture design, micronized sands with different fineness were mixed with Portland cement. The simulation results show that there is a maximum amount of M600 that can be used in the mixtures. Beyond the maximum amount of M600, any additional amount of M600 does not contribute to a denser packing and a denser microstructure. Simulation results showed that the pore structure of optimized mixtures was refined by mixing coarse sand M6 and fine sand M600 with cement. The microstructures of optimized mixtures were less permeable.

The service life of structures made of concrete blended with micronized sand was evaluated by using the DuraCrete model. In this model the end of service life was assumed to be reached when the chloride concentration at the reinforcement had reached a critical threshold value. The chloride profiles in concrete structure and the cover thickness of structures were evaluated for structures made of concrete blended with micronized sand as partial replacement of cement. For a required service life of 80 years, the chloride ion concentration over the cover depth of structures made with blended concrete was a bit higher than in reference OPC concrete. To ensure the required service life, the cover thickness of structures made with concrete blended with micronized sand has to be increased. The increase of the cover thickness was relatively small compared to the size of the structural elements.

Environmental impact of micronized sand was evaluated and compared with Portland cement. The footprints showed that micronized sand has much less impact than cement on environment. In all categories of sustainability the environmental impact of sand was 2 orders of

magnitude lower than that of Portland cement. It was found that the use of micronized sand as cement replacement gave a big contribution in the category “global warming”, i.e. reducing CO₂ emission.

The CO₂ footprints and the material costs of structural elements have been evaluated. Different required service life and different percentages of cement replacement were taken into account. Results for structural elements made of concrete blended with micronized sand were very promising. With an increasing service time, which was 50, 100, 150 and 200 years in chapter 9, both the CO₂ footprint and the material cost of the structural elements decreased. The achievable savings were getting smaller with increasing service life. Concrete blended with micronized sand is recommended for use in structures of which the required service life is less than 100 years. The benefit can be received from both economic and sustainability points of view.

Samenvatting

Beton is een van de meest belangrijke bouwmaterialen in de wereld. Echter, Portland cement, dat een van de bestanddelen van beton is, is verantwoordelijk voor ongeveer 5-10% van de wereldwijde CO₂-uitstoot. Vanuit het oogpunt van duurzaamheid, dus, is het belangrijk om te zoeken naar materialen die gebruikt kunnen worden om Portland cement in beton te verminderen of vervangen. Onder de minerale toeslagstoffen, was gemicroniseerd zand met hoge zuiverheid SiO₂ geselecteerd als cement vervanger. Gemicroniseerd zand wordt geproduceerd door het malen van kwartszand, dat een van de meest voorkomende mineralen in de aardkorst is. Vandaar, het gebruik van dit materiaal zal niet zorgen voor een uitputting van bronnen. De doestelling van dit onderzoek is om de mogelijkheid te onderzoeken om gemicroniseerd zand te gebruiken om cement in beton gedeeltelijk te vervangen. De prestaties van een cement-gebaseerd materiaal met gemicroniseerd zand als gedeeltelijke vervanger van cement was geëvalueerd met betrekking tot de microstructuur en duurzaamheid, zowel experimenteel als door numerieke simulaties.

In de literatuurstudie waren de effecten van vulstoffen op cement-gebaseerde materialen besproken. Een verder onderzoek naar de effecten van vulstoffen op de ontwikkeling van de microstructuur en ook de duurzaamheidsaspecten werd gepresenteerd. Het gebruik van gemicroniseerd zand als cementvervanger leek veelbelovend.

In het experimentele programma werden gemicroniseerde zanden gebruikt; M6 (grof), M300 (gemiddeld) en M600 (fijn). Het cement werd vervangen door 10%, 20% en 30% gemicroniseerd zand, respectievelijk. De resultaten van de experimentele studies lieten zien dat, hoewel gemicroniseerd zand beschouwd wordt als een inert materiaal, het hydratatieproces, ontwikkeling van microstructuur en voornamelijk de poriestructuur van de gemengde cementpasta beïnvloed worden. De effecten van gemicroniseerd zand op gemengde cementpasta werden toegewezen aan een verdunningseffect en een heterogeen nucleatie effect. De mate van cementshydratatie in de gemengde pasta's werd vergroot door toevoeging gemicroniseerd zand. Aldus, Portlandcement wordt meer efficiënt gebruikt in de gemengde mengsels. Er werd ook vastgesteld dat er een grensvlakzone tussen het gemicroniseerde zand en hydratatieproducten aanwezig is. De resultaten van beeldanalyse lieten zien dat de dikte van deze grensvlakzone nauwelijks beïnvloed werd door de fijnheid of vervangingsgehalte van gemicroniseerd zand in het materiaal. De grensvlakzone werd veroorzaakt door de oppervlakte-energie van gemicroniseerd zand, dat het neerslaan van

hydratatieproducten op de oppervlakte van de zanddeeltjes voorkomt. De poreuze grensvlakzone is een belangrijke factor dat de transporteigenschappen van het gemengde materiaal beïnvloed.

De transporteigenschappen van cement-gebaseerd materiaal met gemicroniseerd zand als gedeeltelijke vervanger van cement werden experimenteel onderzocht, namelijk door waterdoorlatendheidsmetingen en chloride diffusiviteitstests. Resultaten op monsters op de leeftijd van 90 dagen lieten zien dat de waterdoorlatendheidscoëfficiënt en chloride diffusiviteitscoëfficiënt van het materiaal met gemicroniseerd zand als gedeeltelijke vervanging van cement in dezelfde orde van grootte lagen als referentiemonster (OPC pasta in waterdoorlatendheidsmeting, OPC beton in chloride diffusiviteitstest). Gemicroniseerd zand als cementvervanger in mengsels, waarin het vervangingspercentage tot 30% lag, had de transporteigenschappen niet veel veranderd.

Numerieke simulatie is zeer nuttig voor het begrijpen van het effect van gemicroniseerd zand op het hydratatieproces en de ontwikkeling van de microstructuur van cementpasta. Het HYMOSTRUC3D model was aangepast om hydratatie en ontwikkeling van microstructuur te simuleren van cementpasta vermengd met gemicroniseerd zand. Gebaseerd op de gesimuleerde microstructuren, werd de connectiviteit van capillaire poriën geëvalueerd, en de waterpermeabiliteitscoëfficiënten voorspeld. Gesimuleerde resultaten waren in goede overeenstemming met de experimentele resultaten. Numerieke simulatie bleek zeer nuttig voor ontwerp van cement-gebaseerde materialen gemengd met gemicroniseerd zand.

Om een optimaal mengselontwerp te vinden, werden gemicroniseerde zanden met verschillende fijnheden gemengd met Portlandcement. De simulatieresultaten laten zien dat er een maximale hoeveelheid M600 is dat kan worden gebruikt in de mengsels. Boven de maximale hoeveelheid van M600, draagt geen een extra toevoeging van M600 bij aan een dichtere pakking en een dichtere microstructuur. Simulatieresultaten lieten zien dat de poriestructuur van geoptimaliseerde mengsels verfijnd werden door het mengen van grof zand M6 en fijn zand M600 met cement. De microstructuren van geoptimaliseerde mengsels waren minder doorlaatbaar.

De levensduur van constructies gemaakt met beton gemengd met gemicroniseerd zand werd geëvalueerd gebruikmakend van het DuraCrete model. In dit model werd uitgegaan dat het einde van de levensduur bereikt werd wanneer de chloride concentratie bij de wapening een kritische drempelwaarde had bereikt. De chloride profielen in betonnen constructies en de betondekking van constructies werden geëvalueerd voor constructies gemaakt met beton vermengd met gemicroniseerd zand als gedeeltelijke vervanger van cement. Voor een vereiste levensduur van 80 jaar, was de chloride ionenconcentratie over de dekkingslaagdikte iets hoger voor constructies gemaakt met gemengd beton dan bij het

referentiebeton met OPC. Om de vereiste levensduur te verzekeren, zou de dekkingslaagdikte vergroot dienen te worden bij constructies gemaakt met beton vermengd met gemicroniseerd zand. De toename van de dekkingslaagdikte was relatief klein vergeleken met de afmeting van de constructieve elementen.

Milieugevolgen van gemicroniseerd zand werd geëvalueerd en vergeleken met Portlandcement. De voetafdrukken lieten zien dat gemicroniseerd zand veel minder invloed heeft op het milieu dan cement. In alle duurzaamheidscategorieën was de invloed van zand op het milieu twee orden van grootte lager dan dat van Portlandcement. Er werd gevonden dat het gebruik van gemicroniseerd zand als cementvervanger grote bijdrage gaf in de categorie “opwarming van de aarde”, dat wil zeggen het verminderen van CO₂-uitstoot.

De CO₂ voetafdrukken en de materiaalkosten van constructie elementen zijn geëvalueerd. Verschillende vereiste levensduren en verschillende percentages van cementvervanging werden in acht genomen. Resultaten voor constructie elementen gemaakt van beton vermengd met gemicroniseerd zand waren veelbelovend. Met een toenemende dienstduren, warden 50, 100, 150 en 200 jaar in hoofdstuk 9, namen zowel de CO₂ voetafdruk als de materiaalkosten van de constructie elementen af. De haalbare besparingen werden kleiner met toenemende levensduur. Beton vermengd met gemicroniseerd zand wordt aanbevolen voor gebruik in constructies waarvan de vereiste levensduur minder is dan 100 jaar. Het voordeel kan worden ontvangen uit het oogpunt van zowel economie als duurzaamheid.

Acknowledgements

The research project reported in this thesis was sponsored by China Scholarship Council (CSC) and Delft University Technology (TU Delft). The research was conducted in the TU Delft. CSC and TU Delft are gratefully acknowledged for the financial support and the opportunity offered to me for pursuing Ph.D. degree.

Working as a Ph.D. candidate has been an exciting, unique and unforgettable journey. My life has been enriched and completed not only by the cheerful moments but also by the difficult times in these 5 years. It would be impossible for me to reach this wonderful point without the help and support of the amazing people around me.

I would like to express my greatest gratitude to my promotor Prof. Klaas van Breugel. I feel deeply honored to work with him and I highly respect his knowledge, experience, and enthusiasm in research. I was always inspired by his excellent guidance, sparkling ideas and constructive suggestions throughout my PhD period. I also want to deliver my special and sincere thanks to Prof. Michiel Haas for his kind guidance and helpful advice in my study.

I would like to give my sincerest acknowledgement to my co-promotor Assoc. Prof. Guang Ye for his excellent supervision. His suggestions, patience, encouragement, and understanding helped me through my study. I will always hold the appreciation for the lessons I learned from him during the inspiring discussions.

I also want to thank my supervisor, Dr. Zhanqi Guo, for his useful guidance and generous support during the first two years.

The committee members are very appreciated for their great insights and constructive comments, which are really important and helpful for improving the quality of my thesis.

My cordial acknowledge goes to Ms. Franca Post, assistant project coordinator, at the Center for International Cooperation and Appropriate Technology (CICAT) of TU Delft, for the consideration and support she provided during my stay in Delft.

My thanks go to all the friendly colleagues in the Microlab. They left me with many delighted memories, which are not only the direct or indirect help on my research but also the smart talks every day. It is really my pleasure to meet these wonderful people in the Netherlands.

I want to thank the helpful technicians: Arjan Thijssen, Gerrit Nagtegaal and Jon van der Weg, for giving me their practical experience and brilliant solutions for my laboratory problems.

I would like to thank secretaries, Claudia Baltussen, Melanie Holtzapffel and Ingrid van Wingerden, who helped me arrange numerous things during my Ph.D. study.

My special appreciation goes to my dearest friends for their support and help. Particularly, I want to thank Virginie Wiktor for her friendship, kindness and sharing positive attitudes with me. I feel very grateful for Lupita Sierra Beltran and Dennis Waterman. They are so nice and always make me feel warm. Jie Zhao, a nice colleague turned out to be a good friend, gave me lots of interesting ideas and helped me get through many difficulties. Thank Jure Zlopasa, Damian Palin, Renee Mors and all colleagues for memorable lunch and coffee breaks. Thank Dennis and Renee for helping me translate the summary and propositions to Dutch. Zhuqing Yu, Ning Li, Peipei Dong and Liang Li are incredible friends. I will always remember the enjoyable moments we spent together. Thank Xiaohua Lian and Jos Wubbeling for offering their help and kind hospitality. A special word goes to Xiaohua, who shared the ups and downs of my life in the Netherlands while keep inspiring and supporting me in the best way possible.

I want to express my deepest love, respect and gratitude to my parents. They always believe in me. They support me and encourage me all the time, even when I was frustrated and about to give up. Their love is the priceless thing I ever have to get through the path with flowers and thorns.

Ying Wang

May, 2013.

Delft, the Netherlands.

Curriculum Vitae

Name Ying Wang
Date of birth 2 July 1981
Place of birth Tianjin, P. R. China
Email y_wang@live.com



2000.9-2004.7 Bsc. Degree in Civil Engineering, Beijing Jiaotong University, Beijing, P. R. China.
2004.9-2007.7 Master of Science (MSc.) in Building Engineering, Beijing Jiaotong University, Beijing, P. R. China.
2007.10-2013.3 Ph.D. candidate, Microlab, Section of Materials and Environment, Faculty of Civil and Geosciences, Delft University of Technology, Delft, the Netherlands.